Università degli Studi di Napoli “Federico II”

Dottorato di Ricerca

Ingegneria Aerospaziale, Navale e della Qualità

XXVI Ciclo

Computational Fluid Dynamics in support to Flight Test Experiments using Optimization Techniques

Relatori Ch.mi
Prof. Carlo de Nicola
Prof.ssa Lina Mallozzi

Candidato
Alessandro d’Argenio

Anno Accademico 2014-2015

Non possiamo pretendere che le cose cambino, se continuiamo a fare le stesse cose. La crisi è la più grande benedizione per le persone e le nazioni, perché la crisi porta progressi. La creatività nasce dall'angoscia. come il giorno nasce dalla notte oscura. È nella crisi che sorge l'inventiva, le scoperte e le grandi strategie. Chi supera la crisi supera se stesso senza essere "Superato". Chi attribuisce alla crisi i suoi fallimenti e difficoltà, violenta il suo stesso talento e da più valore ai problemi che alle soluzioni. La vera crisi, è la crisi delle'incompetenza. L'inconveniente delle persone e delle Nazioni è la pigrizia nel cercare soluzioni e vie d'uscita. Senza la crisi non ci sono sfide, senza sfide la vita è una routine, una lenta agonia. Senza crisi non c'è merito. È nella crisi che emerge il meglio di ognuno, perché senza crisi tutti i venti sono solo lieve brezze. Parlare di crisi significa incrementarla e tacere nella crisi è esaltare il conformismo, invece, lavoriamo duro. Finiamola una volta per tutte con l'unica crisi pericolosa, che è la tragedia di non voler lottare per superarla.

(*A. Einstein*)

CONTENTS

INTRODUCTION

Flight testing continues to remain an essential step in the development or modification of an aircraft. Modern fixed wing aircrafts, especially mitary jet aircrafts, are highly complex systems that push the edges of aerodynamic, propulsion, and control system technologies. The ever-increasing complexity of the aircrafts presents new challenges to those who are involved in the flight testing of those vehicles.

Over the last 40 years, simulation has played a vital role in increasing the safety and the efficiency of flight testing. Modeling and Simulation (M&S) is a tool to support testing and its use has improved flight test planning, execution and safety. The incredible growth in computational capabilities has created also new possibilities on how M&S can be used to support flight testing.

Even with improved computers, high-fidelity simulations still depend on the ability of the engineering team to create models that accurately represent the aircraft or the environment that they are testing. Simulation is a tool that greatly improves the efficiency and the effectiveness of a flight test program, but it must be used in conjunction and in coordination with the actual testing.

As the aircrafts continue to evolve in complexity, the role of simulation continues to grow. Every major aircraft developer, whether they are commercial or military, depends on the use of simulation to some degree. The application of these simulations to flight testing is an important aspect of the aircraft's development. Many of the technical disciplines involved with the aircraft development make use of simulation.

In flight testing, simulation is especially used to support structures and flutter tests, stores separation tests, as well as total weapon system's effectiveness tests. Simulation in support of flight testing is here to stay, and there is a growing to demand to further increase its use.

The purpose of this thesis is to illustrate how simulation can be effectively used to support flight testing of fixed-wing military aircrafts and what should be considered when developing a simulation that is used to support flight test. In particular, the contribution of M/S in support to store integration and separation activities will be carried out.

In chapter 1 is briefly described the role of M/S in flight test activity. Chapter 2 points out the typical store integration and separation flight test phases and describe the use of Computation Fluid Dynamics in these activities. Chapter 3 illustrates the techniques used in this thesis to support flight testing and finally chapter 4 describes the results. In chapter 5, the use of optimization techniques in DoE is described.

CHAPTER 1

1 THE ROLE OF SIMULATION IN FLIGHT TESTING

The role of simulation in support to flight testing has been evolving almost since the beginning of manned flight. As the aircraft continue to evolve in complexity, the role of simulation continues to grow.

The use of simulation in flight testing is increasing. Nowadays the question is how much testing can really be replaced by simulation. Of course, simulation is not a panacea for all test problems, but a valuable tool that must be used cautiously and wisely in order to reduce cost and risk.

In this chapter, the use of M&S in support of flight testing will be briefly described. In particular, will be explained the different kinds of M/S that could be used in support to flight test and the main technical areas where simulation could be efficiently used. In particular, [1] was the main reference about the use of M&S in military flight test program.

1.1 Definition of M&S

First of all, in order to discuss the use of M&S is necessary to provide a definition of terms.

Modeling is the process of producing a model; a model is a representation of the construction and working of some system of interest. A model is similar to but simpler than the system it represents. One purpose of a model is to enable the analyst to predict the effect of changes to the system. On the one hand, a model should be a close approximation to the real system and incorporate most of its salient features. On the other hand, it should not be so complex that it is

impossible to understand and experiment with it. A good model is a judicious tradeoff between realism and simplicity. An important issue in modeling is model validity. Model validation techniques include simulating the model under known input conditions and comparing model output with system output. Generally, a model intended for a simulation study is a mathematical model developed with the help of simulation software. Mathematical model classifications include deterministic (input and output variables are fixed values) or stochastic (at least one of the input or output variables is probabilistic); static (time is not taken into account) or dynamic (time-varying interactions among variables are taken into account). Typically, simulation models are stochastic and dynamic.

A simulation of a system is the operation of a model of the system. The model can be reconfigured and experimented with; usually, this is impossible, too expensive or impractical to do in the system it represents. The operation of the model can be studied, and hence, properties concerning the behaviour of the actual system or its subsystem can be inferred. In its broadest sense, simulation is a tool to evaluate the performance of a system, existing or proposed, under different configurations of interest and over long periods of real time. Simulation is used before an existing system is altered or a new system built, to reduce the chances of failure to meet specifications, to eliminate unforeseen bottlenecks, to prevent under or over-utilization of resources, and to optimize system performance. For instance, simulation can be used to answer questions like: What is the best design for a new telecommunications network? What are the associated resource requirements? How will a telecommunication network perform when the traffic load increases by 50%? How will a new routing algorithm affect its performance? Which network protocol optimizes network performance? What will be the impact of a link failure?

1.2 Brief history of simulation in Aeronautics

The use of mathematical models as a means to represents the aircraft first came into being with the advent of digital computers in 1950's. After the sound barrier was broken, advances in aviation proceeded at an ever increasing pace. Engineers realized that they needed new tools to help them understand complicated aerodynamic phenomenon and to increase the safety of these hazardous test missions.

A real time simulation first appeared at the current National Aeronautics and Space Administration (NASA) Dryden Flight Test Center (DFRC) in 1957 with an analogue simulation of the X-1B aircraft. The first simulation at the United States Air Force Flight Test Center (AFFTC) was built in 1958 to support the testing of the X-2 aircraft.

Early simulations had definite limitations because of the computer's inability to support complex, non-linear models. Still, these early simulations played a major simulation role until the advent of relatively inexpensive micro-computers in the 1970's. These computers greatly improved the ability to model the aircraft in such areas as high angle-of-attack (AOA), as well as complex flight control systems (FCS).

With the advent of the personal computers (PC), a new wave of simulation advances has been made. Simulations that once required a room full of computers are now done on a PC at the engineer's desk. This has allowed simulation costs to be drastically reduced at the same time increasing the utility of simulation.

1.3 Benefits of Simulation

There are many benefits from using simulation to support flight testing. In this section we provide a brief overview of some of those benefits such as cost savings, increased safety and life cycle support.

1.3.1 Cost savings

One of the most noted factors in the defence of using simulation is the cost savings that can be realized. These cost savings can be elusive to document, and often hard to prove. This lack of firm proof will often lead an airplane development manager to question the cost of a high-fidelity simulation.

For example, a modern military aircraft may cost over $50M per copy, yet the flight test simulation generally costs an order of magnitude less to build and validate. The prevention of an accident in flight test often justifies the costs of a simulation. Moreover, also the substantial delay in being able to sell the aircraft has a direct impact on profit.

Still, prevention is a cost avoided and not a cost saver. [2] points out that *"Simulation offers the prospect of potential cost savings to be realized through reductions*

in development hardware, instrumentation, test facilities, and test programmes. By cost savings I do of course mean better value for money rather than simply reduced costs". This better value is obtained by being able to test more complex systems.

During a recent United States spin test program, it was possible to save $1M reducing the number of test points using simulation.

Simulation is a tool, cost savings are indirectly realized because of the efficiencies resulting from using that tool.

1.3.2 Safety increasing

By far the most significant benefit from using simulation to support flight testing is increased flight safety. Improving flight safety has always been the main object of simulation.

Simulation allows the flight envelope to be investigated and understood prior to flight testing. Early use of simulation, even in the design stages can highlight safety concerns that can be designed out. Predictions of aircraft characteristics are gathered prior to testing and then used as a basis for comparison during actual testing. If significant excursions from predicted value occur during the tests, the test engineer is able to make an intelligent assessment as to whether to continue with the tests, or to quit and analyze the differences.

Maximized the safety gained from simulation requires a disciplined process. The complete test team must be involved in gathering simulation data. A sufficient number of simulation runs must be accomplished in order to predict trends or find anomalous conditions. As mentioned earlier, a thorough understanding of the models being used is necessary in order interpret the data. If anomalies are predicted, then the test team must seek to understand whether the model has been implemented correctly, or whether some assumptions were incorrect. If the model or implementation have caused a problem, then these must be fixed prior to continuing to gather data. Likewise, if the actual test data diverges from predicted, the test team must endeavour to understand the causes.

Overall, increasing safety is one of the primary uses of flight test simulation. In the rush of getting the test program done, spending time on simulation often becomes a second priority. Yet the time and money invested are well spent if an accident or an incident can be avoided. The use of simulation to increase safety should be a part of every test program's safety reviews and safety planning.

1.3.3 *Life Cycle*

The use of simulation can also play a major role in the life cycle of an aircraft. If the simulation is kept current during the test program and updated with actual test data, it will accurately represent the aircraft characteristics.

These simulations will form the basis from which future upgrades to the aircraft or its systems can be evaluated in virtual environment before deciding to proceed with development. Simulation should be viewed as assets in the aircraft program and not just as one time occurrences.

1.4 Types of Simulation

There are different types of simulations that can be used in support of flight testing; each of these is better suited to some tests than others. It is fundamental that the test engineer understands the strength and the weaknesses of each type of simulation in order to determine the optimal tool to apply to the test.

Understanding the level of fidelity of the models used in the simulation is critical to comprehending the meaning of the results. The result of a simulation is only as accurate as the lowest fidelity model used. It therefore does not make sense to use a high fidelity representation.

Obviously there are a lot of factors to consider when building a simulation. Defining the requirements for the simulation is the first step. If a simulation is required to support high AOA tests, then the test plan should contain structured test that will allow the data to be used in validating simulation.

The issue of simulation validity is an important aspect if the benefits of using simulation are to be realized.

In the following paragraphs, the different types of simulation will be described.

1.4.1 *Analytic Simulation (Non Real-Time)*

Analytic simulation (non real-time) are used to conduct a multitude of engineering tasks including design tradeoffs, system performance characterization, operational limitations, safety analysis, test planning and test predictions. The term non real-time means that simulated time does not operate at the same rate as actual time, either faster or slower than real-time.

In general, the hallmark of analytic simulations is that they run very high fidelity models. The models are the most accurate representation of the system being developed and tested. These models may have been derived from Computer Aided Design (CAD) drawings in order to support structures analysis, or very fine grids for Computation Fluid Dynamics (CFD) analysis of the aircraft wing or engine characteristics. The complexity of the models is the primary reason why these simulations often do not run in real-time.

Analytic simulation play an important role in flight testing, in particular they are used for test planning and test manoeuvre definition. Essentially these simulations enable the test engineer to investigate flight test issues early on in the development of a program. The main challenge is to develop a simulation that has appropriately matched fidelity models.

An example of application of analytic simulations is in the planning of in-flight structures testing. This type of simulation requires a detailed representation of the aircraft's structural response to an input. Typically these high fidelity models are limited to aerodynamics, flight controls and equation of motion models.

Simulations run to explore the potential matrix of test points can best use the power of analytic simulations. The test engineer can then plot out the results of the runs in order to visualize the potential fight envelope. This enables the engineer to look for area of non-linearities or inconsistencies. These interest areas can then serve as the basis for early flight test plans and safety of flight planning exercises.

Analytic simulations are often complex and the ability to predict aircraft flutter and structure characteristics in enhanced by a complete aero model.

The computer resources required are a trade-off between cost and simulation performance. The faster the computer, the more simulation runs that can be made in less time; however the faster the computer, the more expensive it is. Complex visualization tools require expensive graphical devices and drive the cost of the machine up. Obviously, the benefit of these visualization tools must be weighted against the cost of the software and hardware.

1.4.2 Engineering or Man-in-the-Loop (Real-Time)

Engineering or Man-in-the-Loop (MITL) simulations are the most common types of simulations used to support flight dynamic testing. These simulations provide the most benefit to the test team and are used in virtually every

application in support to flight testing. However, putting together a high-fidelity MITL simulation is very expensive and requires significant expertise.

MITL simulators consist of three basic components: tactile, visual and mathematical. The tactile refers to the pilot's control of the aircraft such as the stick and the throttle. The visual refers to the visual information presented to the pilot including cockpit displays and out-the-window visual scenes. Mathematical refers to the validity of the models being used in the simulation to include aircraft, environment and even the visual scene models.

MITL simulations are generally used for test planning/envelope clearance, test manoeuvre definition, flight test anomaly investigation, test scenario development and flight crew training.

One of the most important benefits of using manned flight simulation is the increase in flight test safety. Manned simulation has provided the pilot and the engineers an opportunity to understand the flight characteristics of the aircraft before flying it.

However, the most limiting factor in using MITL simulations for these kind of investigation is the quality of the aerodynamic data within the simulation. Very often the data at high AOAs is non-linear and not easily measured with wind tunnel testing or CFD. Data gathered from simulations is critical when doing these kind of hazardous flight tests. Not only does the simulator provide the pilot with a familiarity of the aircraft's handling characteristics at high AOA, but it also provides the engineer with data to measure flight test against. This data will be used for comparison; if there is significant deviation from the predicted, the tests will stopped until the difference can be explained and the safety of the aircraft is assured.

Overall, the development of a MITL simulator is very complex and costly to develop and maintain.

1.4.3 Hardware-in-the-Loop

Hardware-in-the-Loop (HWIL) simulations take MITL simulations one step further. Instead of computers running digital models of the aircraft, the aircraft's avionics, FCS and maybe the engine, the actual components are laid out and connected on a spreadbench.

The primary uses of HWIL simulations are for pilot training, flight control system software validation and FMET.

1.4.4 Iron Bird

Iron bird simulations consist of all of the components that make up an aircraft except the skin. The term "Iron bird" is used since most of the aircraft's mechanical/electrical components are mounted against a rigid frame sometimes made of steel, and they are arranged just as if they were in the actual aircraft. The intent of an iron bird simulator is to verify and validate that all of the mechanical/electrical components will function together as an integrated system. The Iron Bird simulator is the tool used to test for Limit Cycle Oscillations (LCO).

Because of the extensive investment, Iron Bird simulators tend to remain for the life of the aircraft. Upgrades to airplane's hydromechanical systems, electrical or control systems, can then be conducted in the simulator and tests such as LCO, rerun to verify the aircraft's characteristics.

1.4.5 In-Flight simulation

The last type of simulation is in-flight simulation. This is the only method that allows the pilot to actually fly a simulated version of the aircraft. The type of aircraft that can be simulated by a flying simulator really depends on the simulator platform.

In-flight simulation introduces the pilot's sensory perceptions into the task. This often results in driving up the pilot's gain and can highlight undesiderable flying qualities such as Pilot Involved Oscillations (PIO) tendencies.

The best use of in-flight simulation is for well-defined, closed loop tasks.

A challenge with in-flight simulation is to make the baseline aircraft behave like the test aircraft.

1.5 Simulation based test program

Integrating simulation into a test program requires forethought and planning. Figure 1 provides a generic flow of the steps to use simulation in support of flight testing.

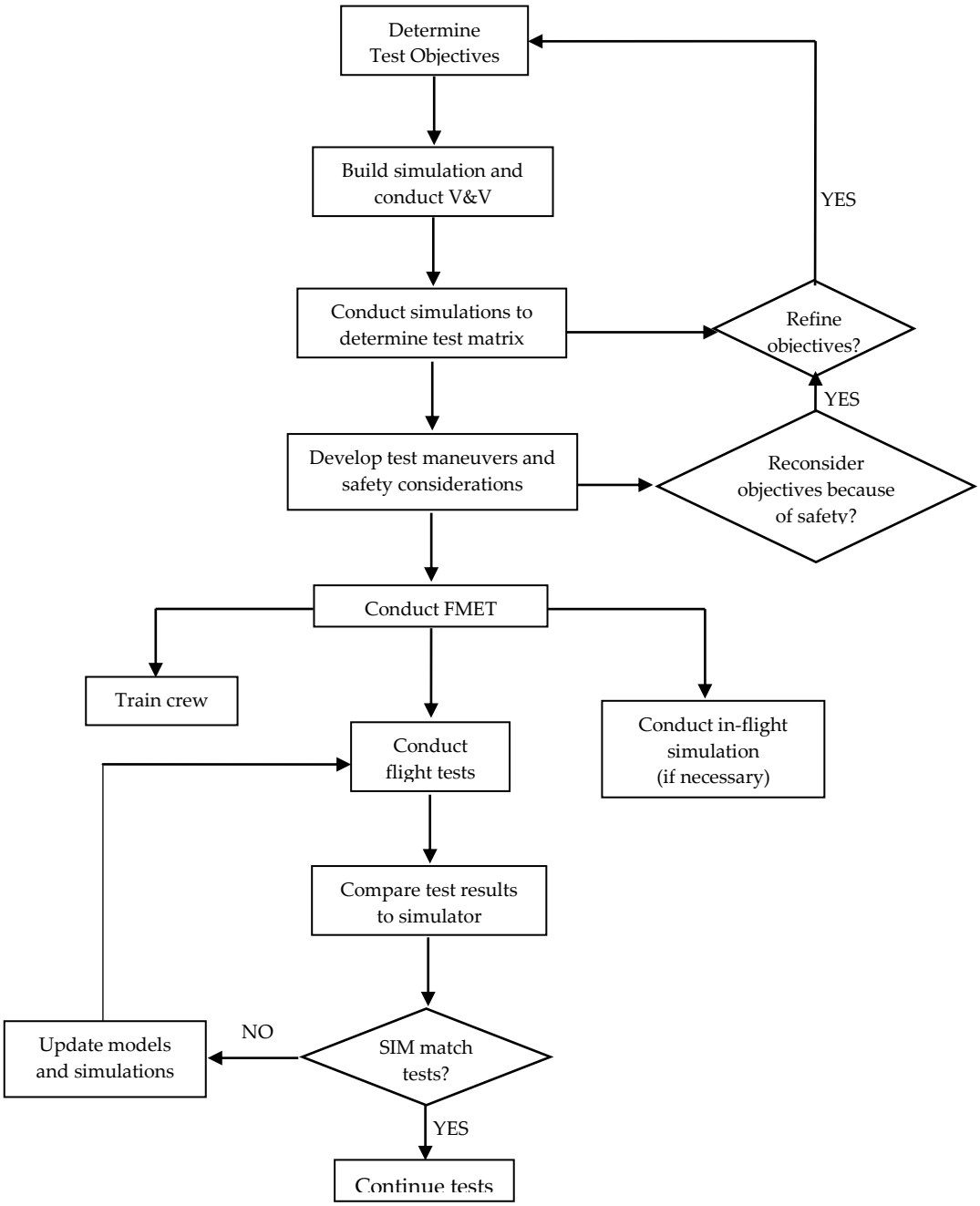

Figure 1: Generic flow to use simulation in support of flight testing

Determining what to test and then applying that to the simulator is the first step in the process. Not all flight testing activities requires a dedicated simulation.

However, there are some type of tests where a simulation capability is a major asset. Major changes to the aircraft's basic structure or the addition of a new weapon that is so radical in shape that it causes the flight characteristics to change dramatically. In these cases, a dedicated flight test simulation is fundamental. The minimum required is an analytic, non real-time simulation. This provide the test engineer a tool to help define the test conditions and obtain some predictions that will minimize the safety considerations.

The strength of analytic simulations is the ability to examine a broad spectrum of flight conditions very rapidly and without a lot of assistance. What the engineer is looking for are trends or anomalies that could indicate areas of particular interest that may need to be pursued during flight testing.

Of course, additional test points are not just automatically added if an anomaly is identified during simulation test planning runs, but this is where the test engineer can make a valuable contribution to the success of the whole program. Moreover, the test engineer uses the simulations to optimize the test program across the flight envelope.

Prior to the first test flight, the test engineer must have developed a comprehensive set of predicted results that can be used to compare against the aircraft actual performance. The important point is that the engineer is prepared to compare actual test results against the simulator predictions. Being able to do this comparison in real-time during the actual testing is a great advantage in terms of flight safety and speed of testing.

After each flight, the test engineer should do an analysis of the simulator data versus the actual test data. The engineer is looking for obvious discrepancies between the data or trends in the data, or other signs that may indicate that it is not safe to continue until the predicted data matches the actual test data.

This method, that involves the use of simulation to make predictions in order to make comparisons with flight test results, permit also to validate the model in order to have predictions for following tests and increase a lot the flight tests safety. This method is known as predict-test-validate and is the new flight test philosophy that has supplanted the old fly-fix-fly method.

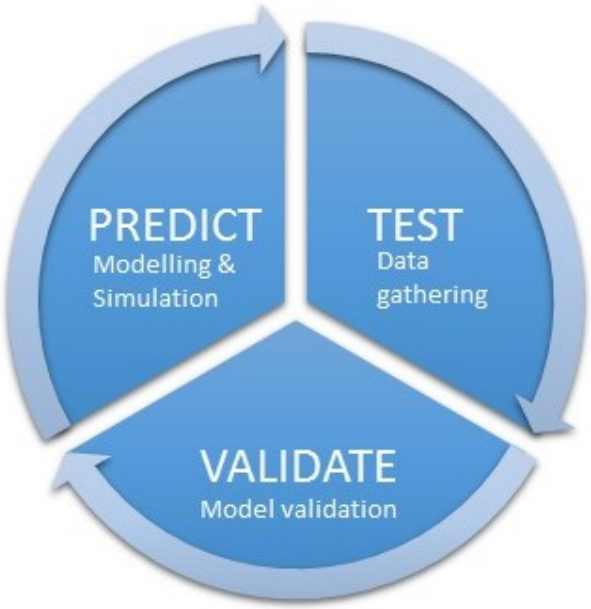

Figure 2: Predict-test-validate workflow

CHAPTER 2

2 AIRCRAFT/STORE COMPATIBILITY, INTEGRATION AND SEPARATION

Aircraft Store capability is of major importance to the aircraft and weapon designer and armed forces. Weapon system capability and aircraft performance are directly affected by the problems associated with store integration and separation. Improved weapon integration can improve the air vehicle effectiveness by orders of magnitude.

The aerodynamic problems associated with the carriage of stores and their release from military aircrafts are numerous and very complex, making this one of the most difficult tasks for the aircraft designers. Improvements in the integration process can lead to significant reductions in the air vehicle development costs.

However, the general understanding about the modern warfare is accustomed to focus on the missile and its capabilities mostly, considering that the weapon is a substantive system; people involved in integration business are profoundly aware that the weapon and the launch aircraft forms a complex system together in which the performance of each individual component depends on the performance of the other one. The weapon can only achieve its designated performance, if the transactions on the launch aircraft required for the integration are done accurately.

The integration of weapons on aircraft requires evaluation of multiple topics related to different disciplines such as aerodynamics, structures, avionics/software maintenance, electro-magnetic interactions, flight test instrumentation, ground and flight tests. In addition to compatibility concerns, the release of a weapon creates issues such as the ability of the specific store to achieve safe separation and the ability of the aircraft structure to withstand the imparted loads during the ejection of store from pylon or launching phase in the presence of aircraft flow

field. The number of subjects to cover is increased when the requirements for all the phases of integration process are considered. The execution of integration activities in a correct and complete manner is the solution of these concerns.

Analyses and simulations are used for a variety of purposes including program reviews, airworthiness release, safety-of-flight, and full integration activities. The selection of analyses and simulation requirements is highly tailorable to the nature, complexity and risk of the new or modified weapon.

2.1 Background and history

During World War I small air-to-ground bombs were dropped over the side of planes by the pilots and ground distribution patterns were quite scattered. Moreover, these operations were more effective from a morale standpoint than in terms of casualties produced or damage to enemy installation. In the interim, between World War I and World War II, a variety of weapons were perfected for aircraft usage. During World War I, the military employment of such weapons was extended to include various bombs and rockets.

At the start of the World War II, a typical bomb fell up to 3 miles from target and up to 5 miles away at night. At the end of World War II, the Circle of Error Probable had been reduced to about 1000 yards and at the same time great advances had been made in flight speed and ability to operate at high altitude. Thus the utility of the planes was greatly extended.

But still, destroying a single given military target required destroying a whole square mile of city to be certain of hitting the target, i.e. carpet bombing which requires huge bomber strings of 1000 – 2000 bombers. The atomic bomb was an incomparably more efficient weapon, i.e. a single aircraft capable of immense destruction. Instead of carpet bombing, a single atomic bomb was enough for destroying a huge city and hence the military target. On the contrary, smart bombs was a new and different approach compared to old approaches and this new approach made planes capable of hitting individual building, i.e. radar infrastructure or moving target with single bomb and the advantage of minimum collateral damage was gained. In addition to improvements in successful target hitting, there had been big improvements about bomb carriage and as a result, internal bomb carriage had begun. Internal bomb carriage had several advantages such as minimum effect on aircraft performance except for weight and minimum

effect on stability or control except center of gravity effects. Internal bomb carriage had also added new problems especially about release and separation. These improvements in both airplane and store performances have created additional problems concerning the design and employment of weapons.

In 1950's, Bomb Bay Nuclear Deterrent begun and planes B-47, B-52, Vulcan, Victor and Bear came into action with special properties such as internal bomb carriage, minimum effect on performance and stability, high altitude flight capability, one 'g' release, low dynamic pressure and finally dropping of importance of gravity from bomb carriage.

In the 1960's Limited Conventional War begun and fighter/bomber kind planes came into action with external store carriage. External store carriage introduced several problems which can be listed as:

- gross effects on performance;
- degraded flying qualities;
- serious effects of aerodynamics on stores;
- aeroelastic effects;
- separation problems;
- flow field effects on trajectories;
- steep dive angle/ high g/ high-speed deliveries;
- serious problems with accuracy.

In USA, starting with 1966 USAF recognized that aircraft/stores compatibility is a separate requirement. So, scientists had to endeavour to reduce possible loading configurations such as:

- compile data on stores and aircraft;
- define a procedure for store certification;
- use of extensive analytical techniques;
- use of low-cost wind tunnels when required;
- minimize flight test time in certification;
- update and verify trajectory by analytical methods;
- develop testing methods for computerized weapon delivery systems.

In the early stages of air warfare, aircraft/stores compatibility was not a significant consideration except to ensure that weapons would fit onto and function with a carrier aircraft. During the Vietnam War, aircraft that entered the inventory were large and powerful enough to carry significant amount of weapons. Also, many new weapons were being developed. The management of

the resulting integration projects of stores to different aircrafts resulted in a huge matrix of combinations that had to be identified, prioritized, analyzed and certified in a timely manner.

Moreover, in the 1970's other countries started to make large inventory of munitions, and these munitions needed to be flown on all fighter/bombers. Therefore, Triple Ejector Racks and Multiple Ejector Racks developed to carry as many bombs as possible and this resulted in about 6,000,000 possible loadings. And this result naturally led to:

- confusion for ground crews;
- many unauthorized configurations;
- seriously degraded performance and flying qualities;
- huge store certification flight test programs.

At the end of the Vietnam War, the McDonnell Douglas F-4 Phantom was the USAF's main tactical combat aircraft. Virtually every store in existence was certified for use on the F-4. In the late 1970s, the USAF decided to replace the F-4 with the General Dynamics F-16 Fighting Falcon. The F-16 exhibited many more incompatibilities with weapons than the F-4 did. As the F-4 was phased out, the F-16 combat users found they were not getting the quantity and quality of combat capability they were expecting and used to before. Their mounting frustration culminated in 1986 when the Commander of the Tactical Air Command challenged USAF Head Quarter to fix the problem. Head Quarter directed the SEEK EAGLE revitalization study. That study resulted in the establishment of the Air Force Seek Eagle Office in December 1987, when the office was chartered by the Secretary of the Air Force. After establishment of AFSEO the office has been taking care of all the aircraft/stores compatibility issues.

For economic efficiency, for both organizational and operational reasons, most military platforms are designed as multi-role platforms. Each specific mission profile requires weapon pairing or the assignment of optimal weaponry for the given mission. Weapon pairing involves the delivery of a particular load of a particular store or a specific combination of different store types and loads. The wide range of mission profiles required from modern military flying platform necessitates the option of carrying a variety of stores and loads.

2.2 Aero-mechanical and structural integration

In this thesis, we will focus our attention on the aero-mechanical and structural integration part of the aircraft/store integration and separation problem.

Figure 3 represents the typical process followed during a weapon integration and separation activity. At the beginning of the project, engineers use simulation to predict aerodynamic and structural behaviour. During ground and flight tests, the data gathered are compared to predictions in order to decrease the risk related to the test activity and validate the model.

In the following sections, we will briefly explain the different phases of aircraft/store integration and separation activity focusing our attention on the aero-mechanical part ([4], [5]).

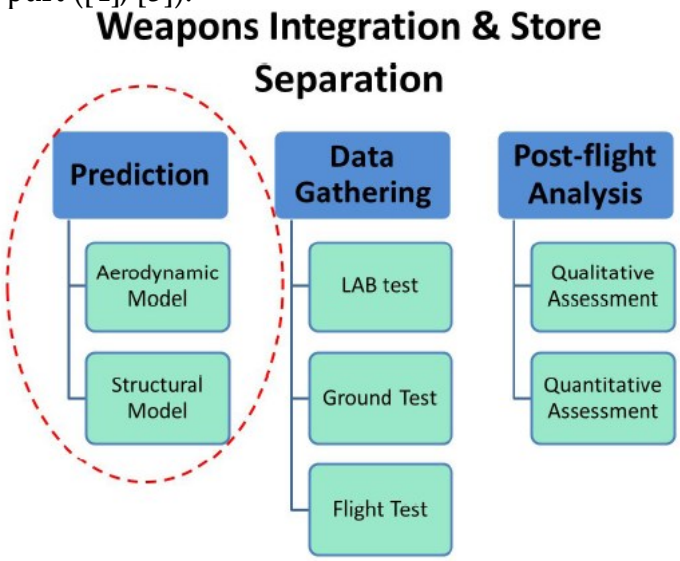

Figure 3: Aircraft/Store Integration and Separation activity process

2.2.1 Aero-mechanical integration

Physical shape and mechanical interfaces of stores should be designed according to the limitations and requirements of the carrying platforms. Hence, the limits of the physical parameters such as length, width, wing span, chord and diameter of the store should be determined during the preliminary design stages of the development projects. For this purpose 3D models of aircraft that have the

capability of simulating the moving parts should be prepared and limits of the design space should be determined by using this model. This model may also be used to determine mechanical interface requirements and limitations.

Platform/store compatibility studies cannot be realized with the lack of computational analyses in a budget optimized development project. According to computational analysis results, critical flight and release conditions can be determined and wind tunnel test program can be shortened. In this way, the wind tunnel testing is used only for accurate predictions of flight clearances which are considered as critical according to analysis results. With the coupling of these two methods flight test matrix can be minimized too.

Starting with the 1960's, some of CFD codes were started to provide trajectory solutions for the stores in the effect of carrier platform flow field. However, at that time, since the computational power was not sufficient for such large problems, techniques were limited to some linear theories and panel methods. With the advancements in the computational power, the capabilities and accuracy of the codes were also advancing. Higher order panel methods, Euler solvers and finally fully unsteady Navier-Stokes solvers were developed and applied to separation problems with the advancements in the computation power. Today, a separation problem may be solved with a fully unsteady N-S solver in couple of hours with the help of high-performance parallel computing facilities.

Nowadays, drag index, aerodynamic flight loads and its effect on aircraft performance and separation characteristics of stores can be analyzed by computational fluid dynamics analysis tools.

Aerodynamic loads on a store during carriage stage differ from free flight loads. Moreover, these loads may result in a performance defect in carrying platform. Hence, change in the aerodynamic characteristics of store should be analyzed and effect of aerodynamic loads on the platform performance should be considered for the carriage envelope. At the end of these analyses, carriage envelope of platform for the analyzed specific loading conditions should be clearly defined.

Determination of Drag index is of critical importance and is one of the measures of store effect on fuel consumption for the given loading configuration of carrying platform. Increase in the total drag of the carrying platform with a new integration shall be calculated and non-dimensionalized for the most flown conditions for accurate mission planning. Calculation methodology of drag index

value of a store for different platforms may vary according to platform cruise Mach number, angle of attack and other platform related physical reference values.

2.2.2 *Structural integration*

Aircraft structures are generally extremely flexible compared to ground structures. Therefore, they undergo large deformations and distortions under loads. When these loads are caused by aerodynamic forces, which themselves depend on the geometry of the structure and the orientation of the various structural components to the surrounding airflow, then structural distortion results in changes in aerodynamic load, leading to further distortion. The interaction of aerodynamic and elastic forces is known as aeroelasticity. Two distinct types of aeroelastic problems occur.

One involves the interaction of aerodynamic and elastic forces of the type described above. Such interactions may exhibit divergent tendencies in a too flexible structure, leading to failure, or, in an adequately stiff structure, converge until a condition of stable equilibrium is reached. In this type of problem static or steady state systems of aerodynamic and elastic forces produce such aeroelastic phenomena as divergence and control reversal.

The second class of problem involves the inertia of the structure as well as aerodynamic and elastic forces. Dynamic loading systems, of which gusts are of primary importance, induce oscillations of structural components. If the natural or resonant frequency of the component is in the region of the frequency of the applied loads, then the amplitude of the oscillations may diverge and cause a failure. The various aeroelastic problems may be conveniently summarized in the Collar's Triangle (Figure 4).

Aeroelastic behaviour of a mechanical system is mainly determined by its dynamic properties. Natural frequencies, mode shapes and damping characteristics have an important effect on the aeroelastic behaviour. Therefore, any additional mass, stiffness or damping could change systems aeroelastic behaviour.

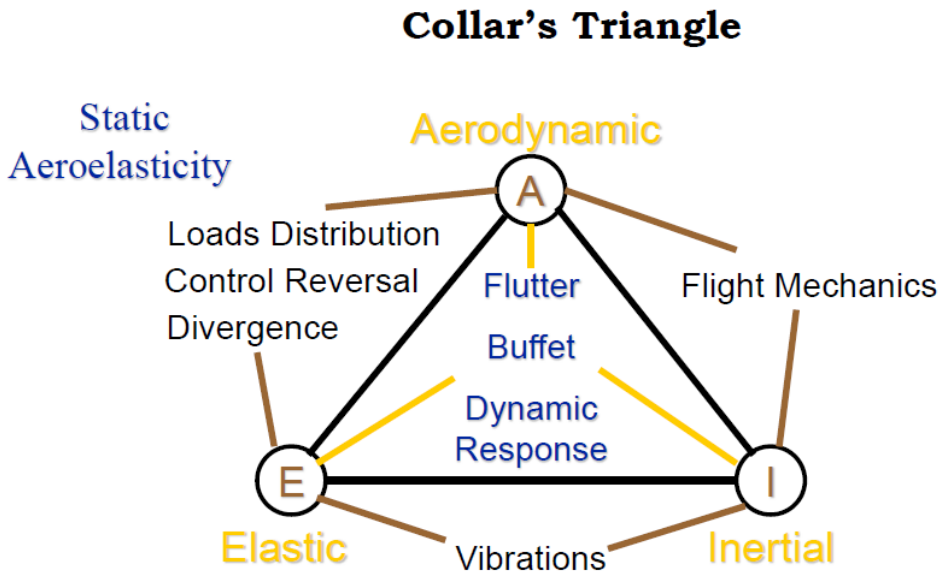

Figure 4: Collar's Triangle

For the aircraft and store compatibility, aircraft should not change its aeroelastic behaviour within its flight envelope while captive carry of stores. In order to be sure about aeroelastic behaviour stability following examinations should be performed:

- dynamic behaviour of the aircraft/stores system should be determined by modal analysis or modal testing;
- aeroelastic failure modes should be examined within the flight envelope;
- aeroelastic aircraft/stores system compatibility should be tested and verified with flight tests.

Ground Vibration Testing (GVT) is an essential preliminary ground test that must be conducted prior to the beginning of flight testing. The objective of the GVT is to obtain aircraft structural mode characteristics such as frequencies, mode shapes and damping. It is done to verify and update the aircraft analytical flutter model as well as provide a means of identifying modes from the frequencies found in flight test data. A GVT is not only required for new aircraft designs but also when extensive changes are made to existing aircraft or when new store configurations are added.

A basic GVT consists of vibrating the aircraft at a number of different frequencies and measuring the response at various locations on the aircraft. Usually several hundred response stations are monitored in order to fully define

the aircraft's modal characteristics. The response signals are processed through signal conditioning amplifiers and passed on to high-speed computers for data manipulation and analysis. The structural responses are most often sensed with accelerometers attached to the surface of the aircraft. The accelerometers are generally evenly distributed over one side of each aerodynamic surface (i.e. wings, horizontal and vertical tails, and control surfaces), and are also located at critical stations on the fuselage, engine nacelles, and pylon or stores.

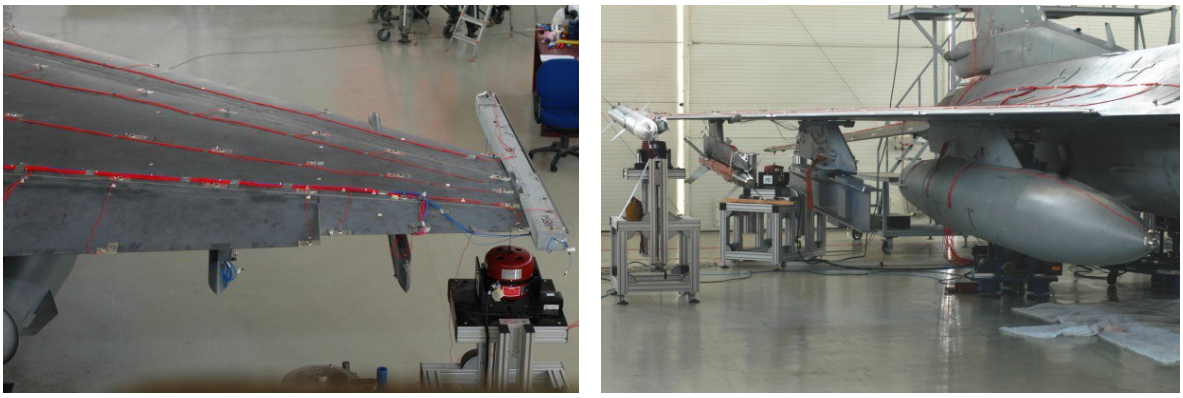

Figure 5: Example of GVT

The excitation of the aircraft is generally produced by electro-mechanical shakers. These are essentially electric motors which cause a center armature to translate up and down as a function of applied current. The armature of the shaker is attached to the structure of the aircraft by a sting. A force link is usually attached to the sting to measure input vibration force data for use in transfer function analysis. Generally more than one shaker is used and they are attached to the aircraft at its extremities such as the wing tips, vertical and horizontal tail tips and on the fuselage nose or tail. The shakers can be operated in and out of phase with each other to generate symmetric and anti-symmetric inputs, respectively, using either random or sinusoidal wave forms.

The products produced from GVT's include structural response frequencies, mode shapes and damping values. The data is presented in the form of frequency response plots (amplitude and phase versus frequency), animated mode shapes and a listing of damping values for each mode. Information as to the validity of the modal data is also presented in the form of orthogonality and reciprocity checks and coherency plots. This data is used to update the vibration, flutter and aeroservoelastic predictions necessary to support flight testing.

GVT is mainly "big" size modal testing performed on an aircraft structure. However, the practice of modal testing is more of an art than a science in many respects. There is no single right way to perform a modal test. The supporting systems, excitation sources or the transducers will influence the dynamic behavior of the structure. The "magic" of modal testing is to obtain results that are close to the "correct" answer. There is no recipe for a successful modal test.

2.2.3 Store separation predictions

The analysis of the separation behaviour of a store represents one of the most outstanding task throughout all engineering efforts associated to the operational role equipment of a fighter aircraft. The demand for a perfect weapon performance in order to achieve a high degree of target accuracy, requires a predictable, repeatable, controllable and reliable separation behaviour. Pragmatically considered, this ambitious scope also requires a realistic physical understanding and accurate description of a dynamical event with a duration of hardly more than one second. Within this short period of time, strong aerodynamic interactions may occur between the aircraft and the released or jettisoned store, depending on the flight conditions. In certain cases unfavourable release disturbances may cause some risks for collisions or may completely degrade the release accuracy of the weapon and end up with an operational loss. According to [3], store separation problems fall into three distinct areas: store-to-pylon/rack collisions, store-to-aircraft collisions, and store-to-store collisions.

When a store is ejected or released, the most likely problem that could occur is that the store might pitch, yaw, or roll more rapidly than it displaces away from the aircraft. If this occurs, the store will usually collide with the closest part of the adjacent structure, the pylon or rack from which it was released. Store-to-pylon/rack collisions usually occur within 200 milliseconds from release and may result in some bending or breakage of portions of the store or pylon rack. Aside from the fact that any such collision is undesirable and unacceptable, store-to-pylon/rack collisions are not usually dangerous or serious.

Store-to-aircraft collisions involve an impact after the release of the store with other parts of the aircraft such as wings, fuselage, or empennage. This type of collisions are the most serious from an aircraft safety standpoint. Since they occur at some time and distance from the initial point of release, the stores are moving

rapidly, and their mass, impacting the aircraft at high energy and high speeds, can cause serious aircraft damage (Figure 6).

Figure 6: An Example of store-to-aircraft collision

Ideally, when a store is separated it should pass through the aircraft's aerodynamic flowfield into undisturbed air as quickly as possible. If this does not occur, and the store remains in the aircraft flowfield, the flowfield forces begin to dominate the store's movements. When this happens, a store/aircraft collision is highly likely.

However, when the collision is between stores which have already been released, several things may occur: one or both could explode, one or both could sustain damage, or one or both could be knocked into an unstable trajectory thereby affecting accuracy. Of the three, the least likely to occur is explosion, particularly if the collision is immediately after release. Generally, the store fuze will not have had time to arm (normal setting is several seconds after release) and a side-to-side collision will not be of sufficient force to cause explosion or fuze

function. While not desirable, side-to-side collision of stores immediately, or shortly after, release is sometimes inevitable and must be expected, particularly when large numbers of stores are released simultaneously or in a short interval ripple release mode.

As soon as either a weapon, pod or tank starts to move relative to the carrier, aerodynamic loads become a dominant factor in their equations of motion. The mathematical complexity of the aerodynamical approach is an important factor which not only determines the computing power requirement, but also the turnaround time for one complete trajectory.

Strategies involving complex CFD-solutions with a high level of confidence, are slow and expensive, but once qualified, request a minimum amount of experimental certification and validation. Especially considering an appropriate flight test programme, considerable cost savings can be performed by downsizing flight test hours and trials by selecting a more expensive simulation strategy. This fact justifies nowadays even the use of NS-codes.

An envelope for both operational and jettison releases should be predicted accurately to determine safe separation region and to support and decrease wind tunnel tests. A computational fluid dynamics solver, 6 Degrees Of Freedom (6-DOF) solver and mesh movement technique is combined to model separation phenomena. Separation analysis examples are shown in Figure 7.

There are several methods used for mesh movement during the analysis. Most used examples are Chimera Method and Spring Analogy with re-meshing.

In the chimera method, domain is modelled with separate zones, which interconnects the solutions at the mesh interface areas. On the other hand, for the second method, mesh is deformed by spring analogy and quality is increased by re-meshing during the trajectory simulation.

A store separated from the aircraft defines a rigid body with 6-DOF. Therefore, it is possible to determine the track of the store by solving the rigid body motion in time by 6-DOF rigid body motion solver, provided that forces and moments acting on the body is known at any point in the solution domain. Motion of the store can be considered in two distinct phases. First is the motion under the ejector forces and second is the free motion where store is moving with aerodynamic forces. It is often assumed that ejector forces are high enough that the variation of the aerodynamic forces can be neglected. The motion in the first phase, between the moment of release and until the End-Of-Stroke (EOS) position can be

simulated with a 6-DOF solver considering only free-stream aerodynamic forces and moments and ejector forces, or with a simple use of charts provided by ejector/aircraft manufacturer. In this approach, free motion of the store is started using EOS linear and angular speeds as initial conditions. Then 6-DOF simulation is performed by using aerodynamic and gravity forces and proximity of the store and the aircraft is checked until the time where proximity is critical or safe. By use of these methods, the limits of safe separation envelope should be determined.

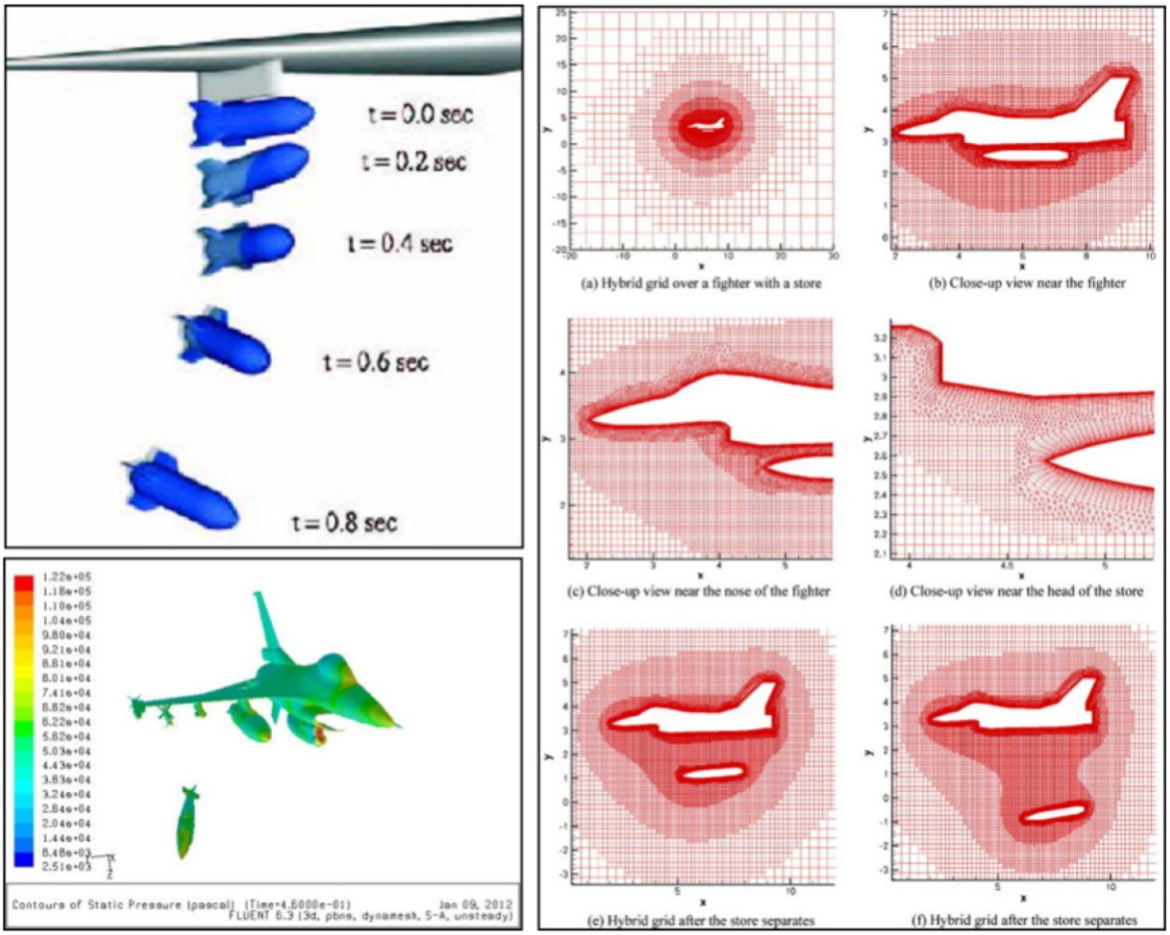

Figure 7: Separation analysis example

2.2.4 Static Ejection Test

Static ejection is one of the essential pre-flight test procedures that allow monitoring functionality of lanyard, separation characteristics and arming system. This type of testing, allows engineers to evaluate how:

- aircraft is physically affected by release of store;
- store on-board computer works;
- store components are affected by mechanical shock loads.

Especially following data are very important for evaluating airborne ejections:

- ejection force;
- ejection velocity;
- acceleration;
- pitch, yaw and roll rates.

These data could be collected by accelerometers, strain gauges or photographic records. This test basically consists of two different observation areas. First one is more mechanical interfaces that interested in forces on aircraft, pylon, store and store acceleration rates. These measurements could be essential for airborne separation analysis. Of course, differences due to external flow, outside temperature should be considered.

Second area is much more related with electrical (in some manner electronics) interfaces. When trigger signal is send, how long it does hold, how much time it takes for store to allow separation (mostly depends on rise time of store internal power sources), and time of separation are critical parameters to identify and understand separation. Also voltage levels might be measured to identify and clarify the future problem sources.

As a kind remainder, to use big and soft enough pillows for store landing would be very helpful, if reuse is considered or store is valuable. Some test pictures are shown in Figure 8.

Flight tests, where safe separation is evaluated, are the most critical stage for a new expandable external store certification. Understanding of how a store reacts when released from a flying platform provides engineers, the ability to identify the safety issues which may cause risks for the aircraft and the pilot. Moreover, understanding how a released store reacts also provides the knowledge required to develop accurate and safer systems.

Figure 8: Static Ejection Test

2.2.5 Store separation testing

One of the methods to verify the store-vehicle compatibility is recording of separation using on-board high-speed video cameras. It is important to choose proper air-borne high-speed cameras which may overcome high g loads and high vibrations. Generally high-speed cameras have random memories, and permanent memories. Once powered up the camera begin to record images and store them in a circular buffer to internal random memory. To store the recorded images permanently in cameras internal memory or any other storage, high-speed camera needs to be triggered. This mechanism allows the user to store the images recorded a specified time before triggering, to the random memory. The time gap should be designated so that the stored film covers the whole separation process. Connections of the high-speed cameras should be made depending on test requirements. Arranging the proper connections, high-speed cameras can be triggered by jettison or release signals generated by the aircraft/flying platform.

Stamping time data on the recorded images is also important to match the images and other flight test data on a common time base in means of post-flight analyses. IRIG-B may be used as a common time reference, if available. The high-speed camera should synchronize each frame to this reference time.

High-speed camera locations should be chosen where the separation can be observed clearly. To provide the clear line of sight, high-speed cameras can be located in other external stores, in the fuselage, under the wing or fuselage in direct free air stream.

To carry the high-speed cameras in other external loads, the external load should be modified, or a new external load should be produced which is dimensionally and inertialy an exact copy of a certified load. In Figure 9 a camera pod used in flight tests is shown.

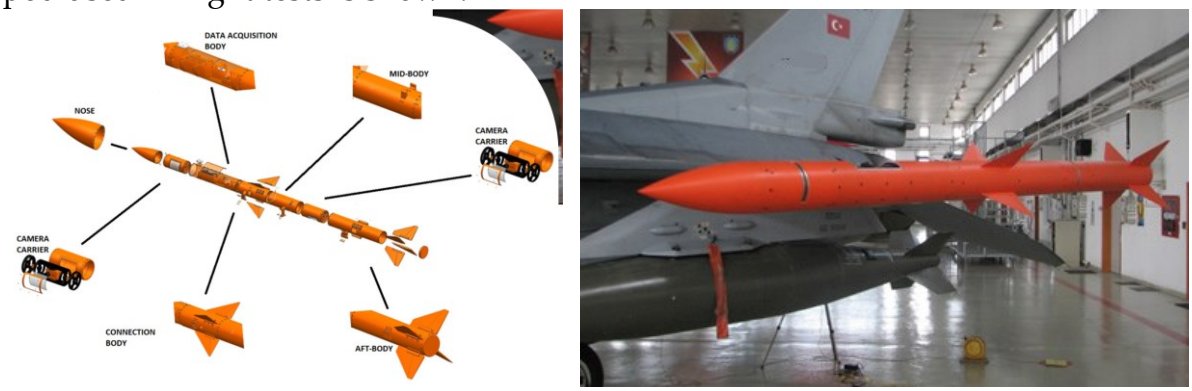

Figure 9: Camera Pod

Expandable store and the background (drop-tanks, wing, fuselage, etc.) should be marked remarkably so that the movement of the marked points on the store can be observed with respect to the background by the software that is used for post-process analysis of the images recorded. The remarks on the cruise missile and the background are shown in Figure 10.

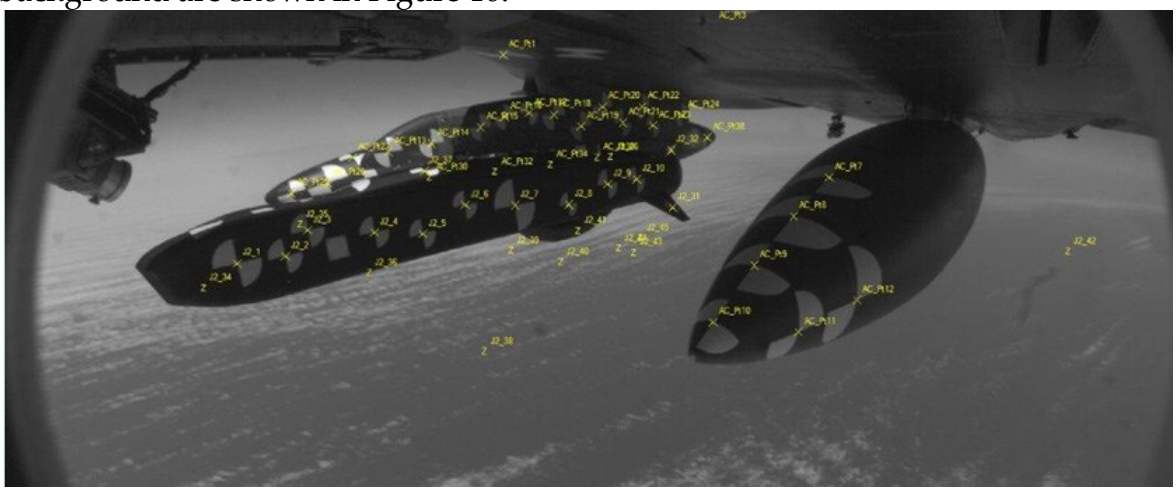

Figure 10: High-Speed Camera Picture

Light condition is a big challenge in high-speed camera recording. Under the wing tip the store may be in shadows and after the release it may be in bright sunlight, after the release there may also be a variety of backgrounds as cloud

white, sea blue, forest green, snow white, etc. The camera system chosen should overcome this lighting and contrast diversity.

The safe separation trajectory is identified by post-flight processing of the images recorded by high-speed cameras using photogrammetric methods. After the methodology for photogrammetric safe separation analysis is determined and the analyses are performed, then the analysis results are compared to the results of computational fluid dynamic analysis to observe consistency.

Photogrammetry is the technique used to extract reliable measurements from video and/or film of the objects and the environment. A photogrammetric solution consists of a 6-DOF time history, from which velocities and rates can be computed. An important quantity that is derived from the 6-DOF time history is the miss distance, which is a time history of the closest point of approach between the surface of the moving store and the surface of another object, such as the aircraft's fuselage or a fuel tank.

2.3 CFD analysis applied to aircraft/store integration and separation

Any time a new aircraft is introduced into service, or an old aircraft undergoes substantial modifications or needs to be certified to carry and employ new stores, the store separation engineer is faced with a decision about how much effort will be required to provide an airworthiness certification for the aircraft and stores. Generally, there are three approaches that have been used: wind tunnel testing, CFD analyses and Flight Testing.

During the last thirty years there have been considerable advances in all three areas. In particular, [6] describe a method for combining the three approaches in a process called the "Integrated Test and Evaluation Approach to M&S for Store Separation".

In the early days, store separation was conducted in a hit or miss fashion: the stores would be dropped from the aircraft at gradually increasing speeds until the store came closer to or sometimes actually hit the aircraft. In some cases, this led to loss of aircraft, and has made test pilots reluctant to participate in store separation flight test programs.

During the 1960's, the Captive Trajectory System (CTS) method for store separation wind tunnel testing was developed. The CTS provided a considerable

improvement over the hit or miss method, and became widely used in aircraft/store integration programs prior to flight testing. However, it was not utilized in an integrated approach.

During the late 1970's and early 1980's, Computational Aerodynamics had finally matured to the point of providing a solution for a store in an aircraft flowfield. However, instead of leading to a renaissance in store separation methodology, it mostly led to an ongoing argument among the three groups. The CFD community claimed they could replace the wind tunnel, the wind tunnel engineers said the CFD was unaware of the complexity of the problem, and the flight test engineers said neither group could provide them with the necessary data to conduct a successful flight test program.

Since the time that CFD was first capable of representing the geometric complexity of an attack aircraft with external stores, there has been the desire to replace/reduce the need for wind tunnel testing. The three detriments for full utilization of CFD in this fashion were computational speed, computer resources and accuracy of the solution.

The most critical feature that determines a store's separation trajectory are the carriage moments, which are principally caused by the aircraft flowfield. For this reason, the first step in separation analysis is to estimate the region of the flight envelope that might have the worst carriage moments. This is done by deriving an estimate of the aircraft flowfield. The primary analytical tool for this purpose to evaluate the aircraft aerodynamics in the early 1980's was the linear potential flow technique.

From 1990's the US Air Force and Navy have made an incredible effort to validate and accelerate the insertion of CFD methods into the store certification process.

Nowadays it seems that CFD for external stores has reached a mature phase. The US Air Force, Army and Navy have long-term, proven CFD modeling and simulation experience and software development expertise that has supported advanced weapon development and integration. Each uses unique CFD codes to augment traditional sources of engineering data such as flight and wind tunnel testing.

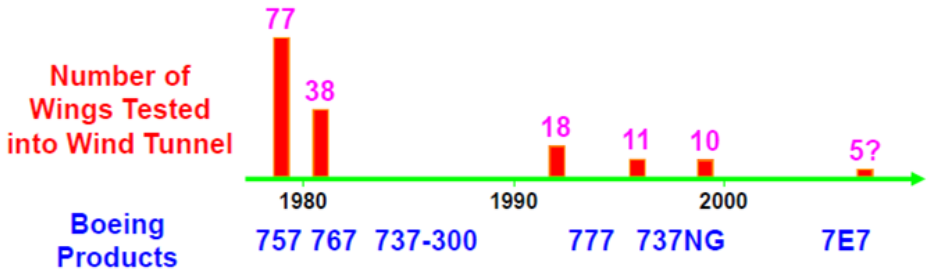

Figure 11: Effect of CFD calculations on wind tunnel tests

Although CFD applications to external store separation problems are well documented, such is not the case for stores separating from bomb bays. There have been recent attempts to determine how CFD can be best used to address this problem.

The flight test process is the most expensive part of store separation testing, and thus can lead to the most overall savings.

As may be seen in Figure 12, an Integrated Test and Evaluation approach to store separation that uses CFD to design the wind tunnel test, which in turn is used to design the flight test matrix is presented. The process has been continuously improved, since the wind tunnel test results are used to validate the CFD predictions, and the flight test results are used to both check the wind tunnel test data, as well as the original CFD predictions. This approach is in accord with ref. [1] that describe how to use M/S in support of flight test.

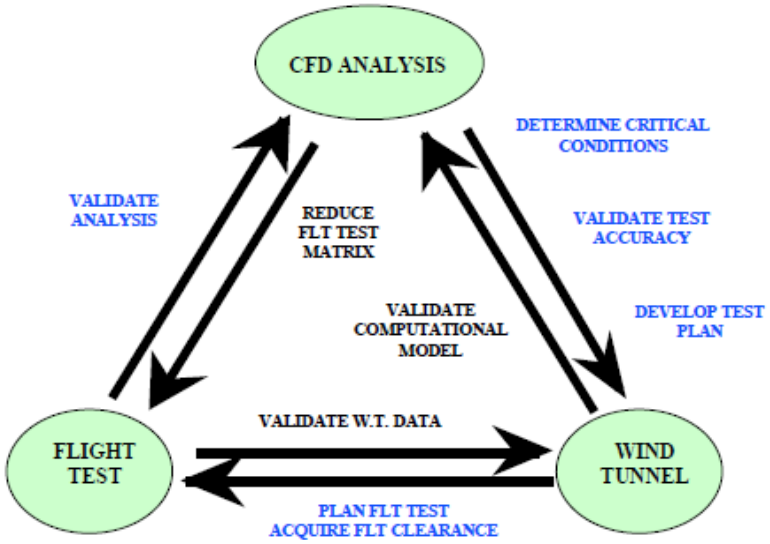

Figure 12: Integrated T&E approach to Store Separation

2.3.1 *Difficult areas for application of CFD*

When the flow conditions are considered "benign or moderate", CFD analysis can predict the aerodynamic flowfield with good accuracy. These conditions are typically the low to medium AOA or angle of sideslip (AOS), and the low transonic or lower supersonic Mach numbers.

Once significant flow separation is present, or at high transonic Mach numbers (approximately 0.90 to 1.10) where very strong shocks are present, discrepancies with test data are likely to be prominent. In typical CFD codes used for full aircraft configuration analysis, turbulence is generally modelled to some approximation in order to provide a reasonably sized problem. The various turbulence models do a fairly good job for small area of separated flow. Once the separation becomes significant, with large areas of stagnated and recirculating flow, these models generally break down. The result is the under or overprediction of the separated regions, with the attendant inaccuracies in the surface pressure distribution and integrated forces and moments. When very strong shocks are present, first the shock strength and location are usually poorly predicted, and then the resulting flow separation and recirculation regions are accordingly mispredicted. When applying CFD under these conditions, great caution should be taken unless there are test data to either validate the results, or to calibrate the errors of the computations.

Even under benign flow conditions, CFD can still be misleading when applied to certain regions of the aircraft shapes flow field. For example, applying CFD in a boattail region, perhaps in an aft-facing step area or in area of the exhaust nozzle, significant flow separation can exist even for benign flow conditions. Drag calculations for a configuration with aft-facing steps will likely be inaccurate. Configurations with landing gear in the flow stream are similarly troublesome. Landing gear are often complex shapes, both difficult to model in the computational grid, and difficult to compute for the CFD flow solver. It is often desired to evaluate the increment of drag with landing gear down versus landing gear retracted, and thus the temptation to use CFD methods to evaluate this early in the design stage. Again, caution should be exercised in these areas of interest unless wind tunnel data is available to calibrate and correct the results.

For the reasons explained before, determining the flow about an aircraft/store combination can be extremely difficult. First of all the geometry of interest is very

complicated due to the presence of pylons, launchers, and internal weapons bays that can create severe acoustic and aerothermodynamic environments, which are challenging to numerically simulate. Moreover, the additional challenge of rapidly and accurately simulating the trajectory of a store separation in a high-volume simulation environment is beyond the capabilities of most CFD programs.

CHAPTER 3

3 MODELING AND SIMULATION PROCESS AND TECHNIQUES

This chapter introduces the techniques that are used in this work to model and simulate the aircraft/store integration problem. In particular, scanning technique for reproduction of physical parts and numerical methods used to simulate the aerodynamic flowfield around an aerodynamic body will be briefly described.

This process, was developed in conjunction with the Italian Air Force Reparto Sperimentale Volo (RSV) that is also responsible for testing and evaluating aircraft/store compatibility.

3.1 M/S process

For our case of interest, the M/S process is strictly connected to a process that is well known as Reverse Engineering (RE) ([8]). In fact, during flight test at RSV, the real geometry was already projected and developed by the designer, and RSV is only responsible to test and evaluate the system of interest. In this case, prediction, if needed, are provided by the designer. For this reason, the RSV decided to invest time and money to develop a own capacity to make numerical prediction to support flight testing.

The generic M/S process used at RSV is showed in Figure 13.

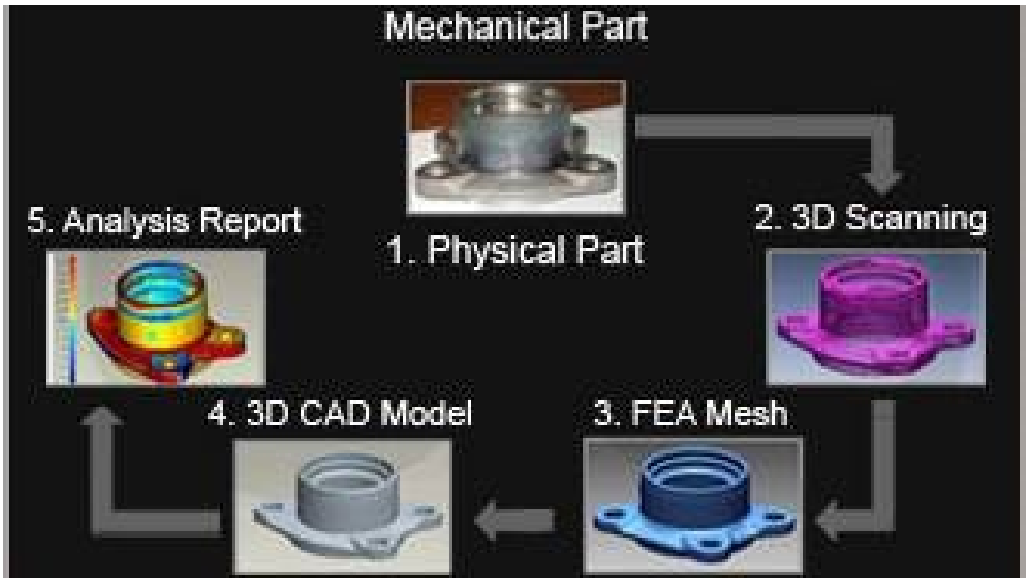

Figure 13: M/S process in support of aircraft/store separation flight test

3.2 Reverse Engineering

In today's intensely competitive global market, product enterprises are constantly seeking new ways to shorten lead times for new product developments that meet all customer expectations. In general, product enterprise has invested in CADCAM, rapid prototyping, and a range of new technologies that provide business benefits.

Engineering is the process of designing, manufacturing, assembling, and maintaining products and systems. There are two types of engineering, forward engineering and reverse engineering.

Forward engineering is the traditional process of moving from high-level abstractions and logical designs to the physical implementation of a system. In some situations, there may be a physical part/product without any technical details, such as drawings, bills-of-material, or without engineering data.

The process of duplicating an existing part, subassembly, or product, without drawings, documentation, or a computer model is known as reverse engineering (Figure 14). RE is also defined as the process of obtaining a geometric CAD model from 3-D points acquired by scanning/digitizing existing parts/products. The

process of digitally capturing the physical entities of a component, referred to as RE, is often defined by researchers with respect to their specific task.

RE is now widely used in numerous applications, such as manufacturing, industrial design, and jewelry design and reproduction. For example, when a new car is launched on the market, competing manufacturers may buy one and disassemble it to learn how it was built and how it works. In software engineering, good source code is often a variation of other good source code. In some situations, such as automotive styling, designers give shape to their ideas by using clay, plaster, wood, or foam rubber, but a CAD model is needed to manufacture the part. As products become more organic in shape, designing in CAD becomes more challenging and there is no guarantee that the CAD representation will replicate the sculpted model exactly.

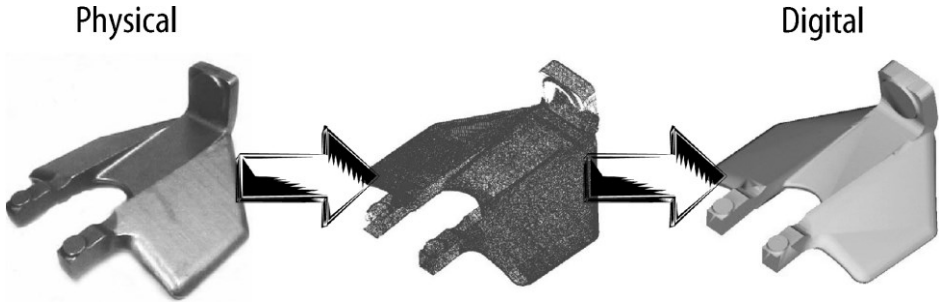

Figure 14: Reverse Engineering process

RE provides a solution to this problem because the physical model is the source of information for the CAD model. This is also referred to as the physical-to-digital process.

The generation of CAD models from point data is probably the most complex activity within RE because potent surface fitting algorithms are required to generate surfaces that accurately represent the three-dimensional information described within the point cloud data sets. Most CAD systems are not designed to display and process large amounts of point data; as a result new RE modules or discrete software packages are generally needed for point processing. Generating surface data from point cloud data sets is still a very subjective process, although feature-based algorithms are beginning to emerge that will enable engineers to interact with the point cloud data to produce complete solid models for current CAD environments.

The applications of RE for generating CAD data are equally as important as the technology which supports it. A manager's decision to employ RE technologies should be based on specific business needs.

The generic process of RE is a three-phase process as depicted in Figure 15.

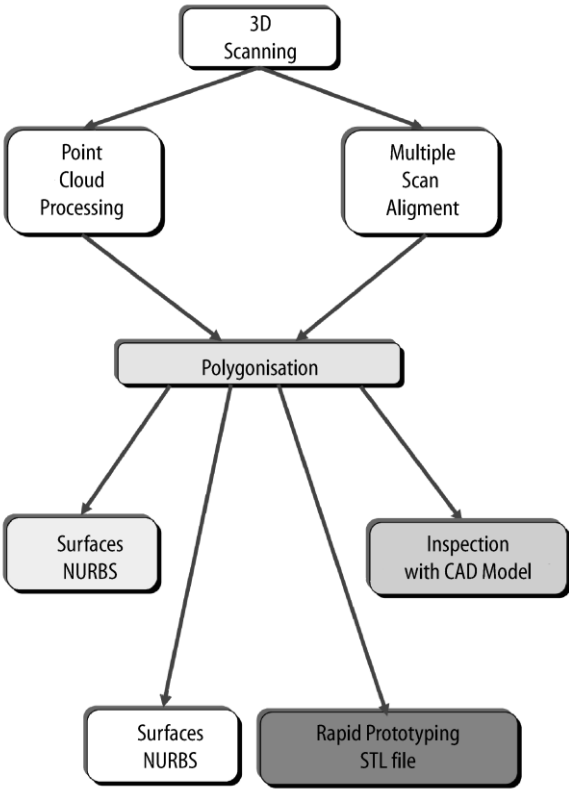

Figure 15: Reverse engineering: generic process

Now, the different phases of the RE process will be described in the following sections.

3.2.1 3D Scanning

This phase is involved with the scanning strategy, selecting the correct scanning technique, preparing the part to be scanned, and performing the actual scanning to capture information that describes all geometric features of the part such as steps, slots, pockets, and holes. Three-dimensional scanners are employed to scan the part geometry, producing clouds of points, which define the surface

geometry. These scanning devices are available as dedicated tools or as add-ons to the existing computer numerically controlled machine tools. There are two distinct types of scanners, contact and noncontact.

- ***Contact Scanners***

  These devices employ contact probes that automatically follow the contours of a physical surface (Figure 16). Depending on the size of the part scanned, contact methods can be slow because each point is generated sequentially at the tip of the probe. Tactile device probes must deflect to register a point; hence, a degree of contact pressure is maintained during the scanning process. This contact pressure limits the use of contact devices because soft, tactile materials such as rubber cannot be easily or accurately scanned.

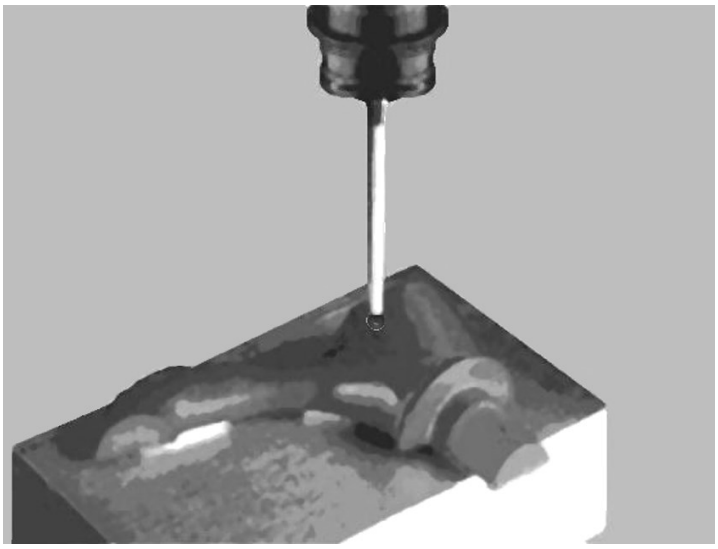

Figure 16: Contact scanning touch probe

- ***Noncontact Scanners***

  A variety of noncontact scanning technologies are available on the market. Noncontact devices use lasers, optics, and charge-coupled device sensors to capture point data, as shown in Figure 17. Although these devices capture large amounts of data in a relatively short space of time, there are a number of issues related to this scanning technology.

The typical tolerance of noncontact scanning is within ±0.025 to 0.2 mm. Some noncontact systems have problems generating data describing surfaces, which are parallel to the axis of the laser.

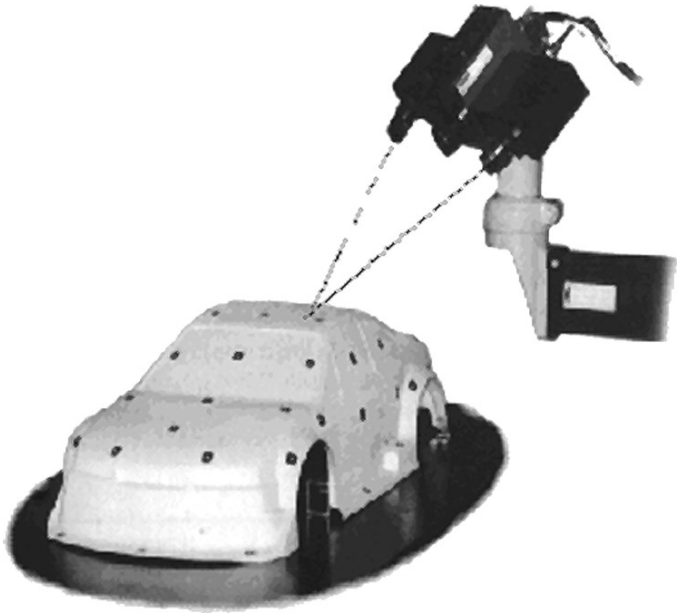

Figure 17: Optical scanning device

Noncontact devices employ light within the data capture process. This creates problems when the light impinges on shiny surfaces, and hence some surfaces must be prepared with a temporary coating of fine powder before scanning. These issues restrict the use of remote sensing devices to areas in engineering, where the accuracy of the information generated is secondary to the speed of data capture. However, as research and laser development in optical technology continue, the accuracy of the commercially available noncontact scanning device is beginning to improve.

After the scanning, the first topic we consider is calibration. Figure 18 demonstrates how calibration allows transforming a range image into a 3-D point cloud. A range image is similar to a conventional digital image that one might find with a digital camera. Consider a pixel (i, j), the distance to the object in the scene is the range value r where the units for rare relative to the configuration of the system, which may not be directly known. Thus, the raw data from a range

scanner is an image with pixel data [r,(i,j)], but we do not necessarily know the units for r nor the relation of pixels to those units. Calibration determines the relationship between [r,(i,j)] and some world coordinate system (x, y, z) in units such as meters or inches. With calibration, we can define a transform T that converts a range image into a 3-D point cloud.

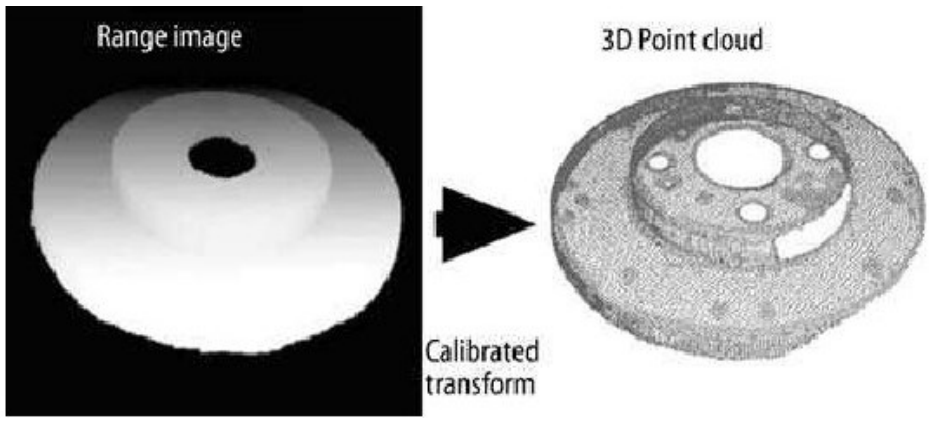

Figure 18: Example of image calibration

The image on the left of Figure 18 is a range image; the one on the right is a screen shot of a 3-D point cloud. The point cloud is difficult to visualize on a 2-D sheet of paper, but using a 3-D viewer, we would be able to navigate in and around the points that the screen shot shows statically.

3.2.2 Data processing

For an overall view of RE software operation, the different RE data processing phases will first be described. The required RE operations are then considered.

The complete RE data processing chain, from scan data to the final Non Uniform Rational Basis-Splines (NURBS) model, can be divided into four main phases: points and images, polygon, curves, and NURBS surfaces.

Figure 19 presents the four phases of the RE data processing chain with the fundamental RE operations. These RE operations are necessary and are available with the most commonly used commercial RE software.

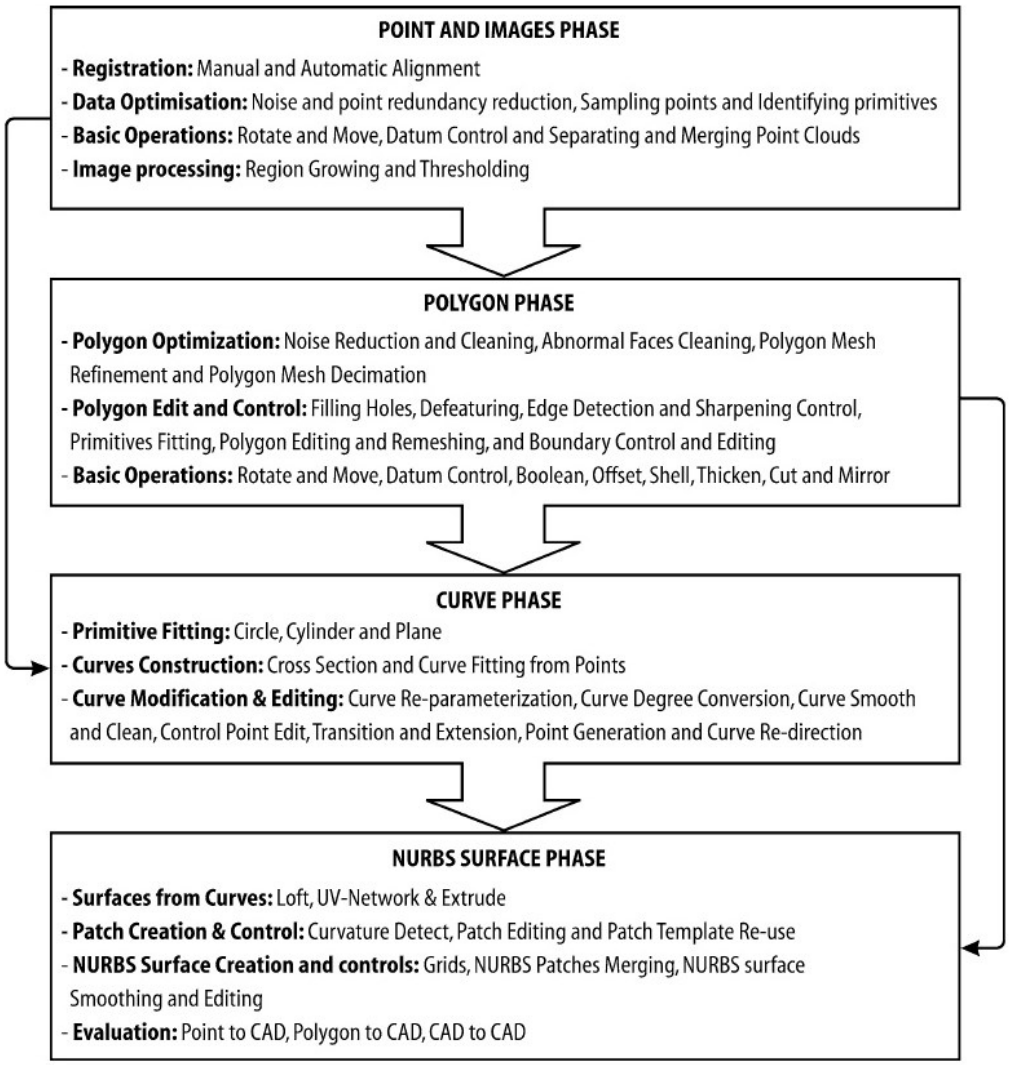

Figure 19: RE data processing chain

3.2.2.1 Points and Images Phase

This phase involves importing the point cloud data, reducing the noise in the data collected, and reducing the number of points. These tasks are performed using a range of predefined filters. It is extremely important that the users have very good understanding of the filter algorithms so that they know which filter is the most appropriate for each task. This phase also allows us to merge multiple

scan data sets. Sometimes, it is necessary to take multiple scans of the part to ensure that all required features have been scanned. This involves rotating the part; hence each scan datum becomes very crucial. Multiple scan planning has direct impact on the point processing phase. Good datum planning for multiple scanning will reduce the effort required in the point processing phase and also avoid introduction of errors from merging multiple scan data. A wide range of commercial software is available for point processing.

The output of the point processing phase is a clean, merged, point cloud data set in the most convenient format.

The most important operations of this phase are:

- ***Registration***

  Although most scanners allow scanning an object from different angles with certain provided degrees of freedom, multiple scans of the object are required to capture the entire geometry of an object or to avoid any occlusions. When using different scan setups, the point cloud from one series of scans is not accurately oriented with respect to the point cloud from another series. Data registration is needed to combine, align, or merge these point clouds so that all point clouds in the series are arranged in their proper orientation relative to one another in a common coordinate system. Registration is very important for downstream RE data processing steps.
  Consider that a point p from one view has coordinates (x, y, z) relative to one world coordinate system, but that same point in the other view has coordinates p' = (x', y', z') relative to a second coordinate system. Although p and p' represent physically the same point on a surface, the different view measurements lead to different coordinate systems.
  Registration is the process of recovering the rigid transformation that relates these two coordinate systems. The equation for this transformation is:

  (1) $$p = Rp' + t$$

  where the matrix R is a rotation and the vector t is a translation. The problem is that R and t are unknown. Registration algorithms recover these variables using the raw data from different views of the object. One criterion is the amount of overlap among the views. If no overlap exists,

registration is practically impossible unless we impose higher order constraints. Some partial overlap is necessary to resolve the registration.

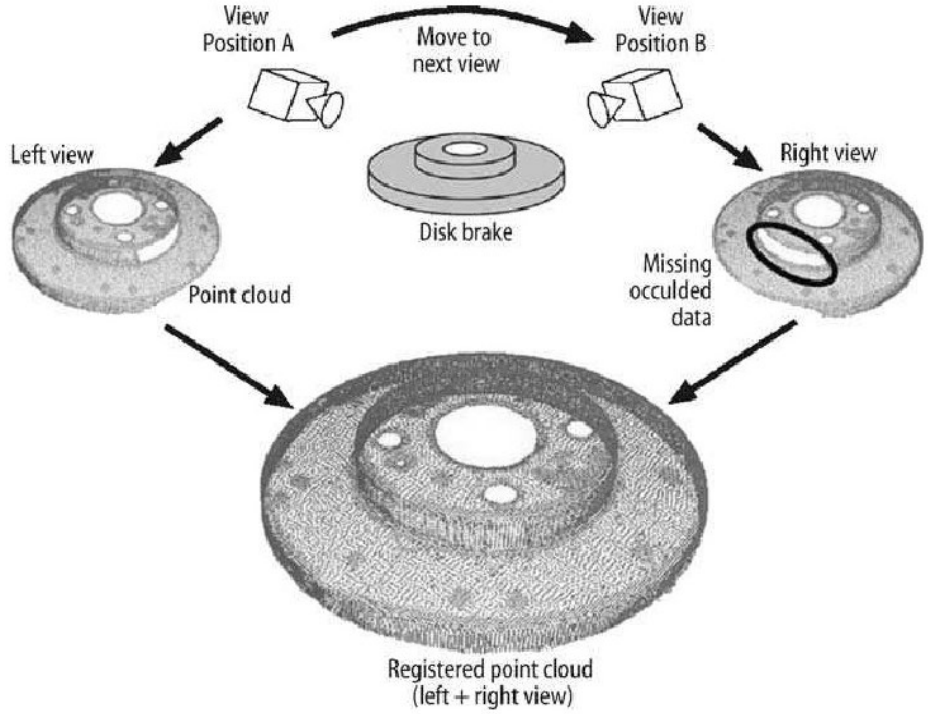

Figure 20: Multiple view scanning and registration process

Therefore, it is necessary to verify the output data carefully. If the number of point is not enough to cover the entire geometry of an object or the expected tolerances are not achieved, more data acquisition as well as scanning schemes are required.

There are two data registration approaches: manual and automatic alignment. In manual alignment, landmark points are manually assigned for fixed and floating point clouds, and they are used as references for alignment. Floating point clouds are translated and rotated to align with the fixed cloud based on these references. The manual registration results in multiple point clouds that need to be fine-tuned to obtain an optimal cloud. This is done in the automatic alignment operation, in which the tolerance between the fixed and floating point clouds is used as the constraint for the alignment process.

- *Data optimization*

  Data optimization may be applied to prepare good point clouds or triangulation meshes for registration. The following data optimization operations are available:

  – Noise and Point Redundancy Reduction

    A certain amount of error is always introduced into scan data, and points may be placed in undesirable regions or overlap because of points that have been scanned more than once when scanning complex shapes. Moreover, when point cloud registration is applied, the aligned scan data normally contains overlapping points.

    Noise reduction tools are used for both manually and automatically removing the noise in scanned data. With automatic approaches, the noise removal operation determines where the points should lie, then moves them to these locations based on statistical information about the point data.

    The redundancy reduction tool is used to reduce the number of points in the point cloud when points are too close to one another or overlap.

  – Sampling Points

    The sampling function is used to minimize the number of points in the point cloud data and to make the data well-structured so that it is easier to handle.

    There are three sampling methods: curvature, random, and uniform; they are based on a curvature, random, and proportional basis.

  – Identifying Primitives

    Identifying primitives such as planes, cylinders, and spheres is very important in the RE process, especially when working with mechanical shapes. This helps to correct imperfections in the scan data, such as noise captured during the scanning process. The primitive creation operation inserts mathematically perfect primitives within a model.

3.2.2.2 Polygon Phase

In this phase, polygon models are constructed. They are then manipulated and controlled to meet the requirements of the applications. The resulting 3-D polygon models are directly employed for applications such as rapid prototyping, 3D

graphics and animations, or are used as reference data for creating CAD entities (points, curves, and primitives) and constructing NURBS surfaces for CAD-CAM-CAE applications.

The most important operations of this phase are:

- ***Polygon optimization***

  The most common and important operations for optimizing polygon models are noise reduction and cleaning, polygon mesh refinement, and polygon mesh decimation.

  – Noise Reduction and Cleaning
    Noise reduction in the polygon phase is the same concept as that in the point phase; noise introduced into polygon models is filtered and removed.
    Cleaning makes the polygonal surface conform to the shape designated by the point set. Depending on the situation, the operation can remove dents, smooth cylindrical sections, or sharpen edges, as well as produce a very good mesh and perform a degree of relaxation or smoothing.
  – Polygon Mesh Refinement and Decimation
    Polygon mesh refinement improves the surface of a polygon model by adding new vertices and adjusting the coordinates of existing vertices, resulting in a greater number of triangles in the selected region and a smoother surface. The operation subdivides selected triangles, producing either three or four triangles for every original triangle. On the other hand, polygon mesh decimation reduces the number of triangles without compromising surface integrity or detail (Figure 21).

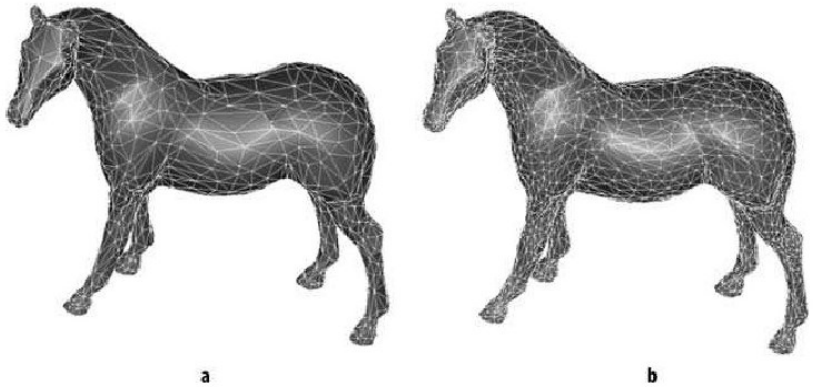

Figure 21: Example of polygon decimation

- *Polygon editing and control*

  The following operations are necessary for editing and controlling polygon models: filling holes, defeaturing, edge detection and control, primitives fitting, polygon editing and remeshing, boundary control, and basic operations (Boolean, cut, mirror, offset, rotate, and move).

  – Filling Holes

    This operation fills gaps in a model that may have been introduced during scanning or because of errors in converting point clouds into polygon models (Figure 22). A polygonal structure is used to fill the hole, and both the hole and the surrounding region are remeshed so that the polygonal layout is organized and continuous. A curvature-based filling option ensures that the polygonal structure used to fill holes in high-curvature regions is curved to match the surrounding area.

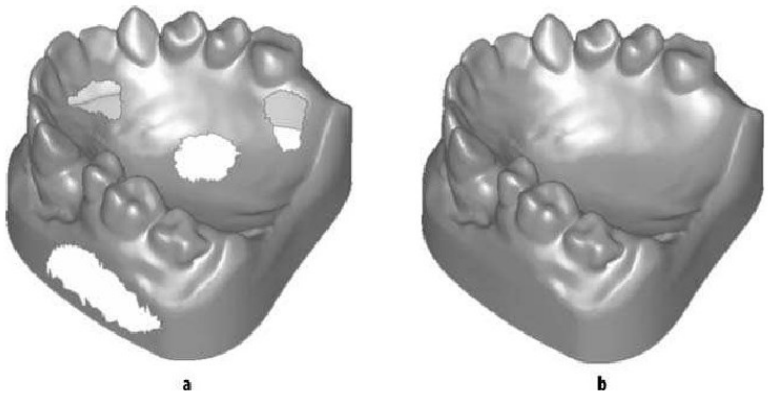

Figure 22: Images before and after the hole filling operation.

  – Defeaturing

    This operation allows refitting selected regions with a new triangulated polygon surface using a curvature-based method. Features in the selected region are deleted. The operation is useful for refining and smoothing the selected region.

  – Edge Detection and Sharpening Control

    Scanning devices are often unable adequately to capture sharp features, such as creases or mechanical edges. When transforming to a polygon mesh, these features are usually filleted or rounded. Tills operation reproduces an edge by redefining it mathematically and then extending the polygon model to that newly defined sharp edge.

- Primitives Fitting
  The primitives fitting operation fits selected regions to primitives such as planes, cylinders, and spheres. It is especially useful for mechanical parts.
- Boundary Control
  This operation is used to repair the boundary edges of a model. It provides the ability to mark edges of triangles to create boundaries, which are a series of triangle edges

3.2.2.3 *Curve Phase*

In many RE projects, especially RE of mechanical parts, CAD entities are mainly used as the reference data for geometric modeling in CAD packages. The CAD entities are constructed directly from point clouds or indirectly from polygon models by manual editing, fitting, and sectioning operations. They are finally imported into CAD packages to complete the geometric modeling.

For simple geometries, a limited number of reference points may be sufficient to model the part using a CAD package, and contact methods with mechanical touch probes are normally employed to collect the data.

Curves are necessary for creating complex parts with free-form surfaces; in this case, more point data are needed, and therefore, noncontact methods are likely to be used for data acquisition. The NURBS surface is defined by a network of curves. Therefore, when applying the "Manual Creation of NURBS from Basic CAD Entities" approach (Figure 23), point clouds and polygon models are normally used for creating curves, especially for parts with free-form surfaces.

Basic CAD entities such as circles, rectangles, and lines can be easily created by manual fitting methods based on reference points. The following operations are the most important in the curve phase: cross section, 3-D curve fitting from points, and curve modification.

Cross-sectioning creates cross-sectional points or curves based on a plane that intersects the model (Figure 23). The 3-D curve fitting from points operation allows creating a curve from a set of points. Curve modification allows controlling a curve to meet modeling requirements.

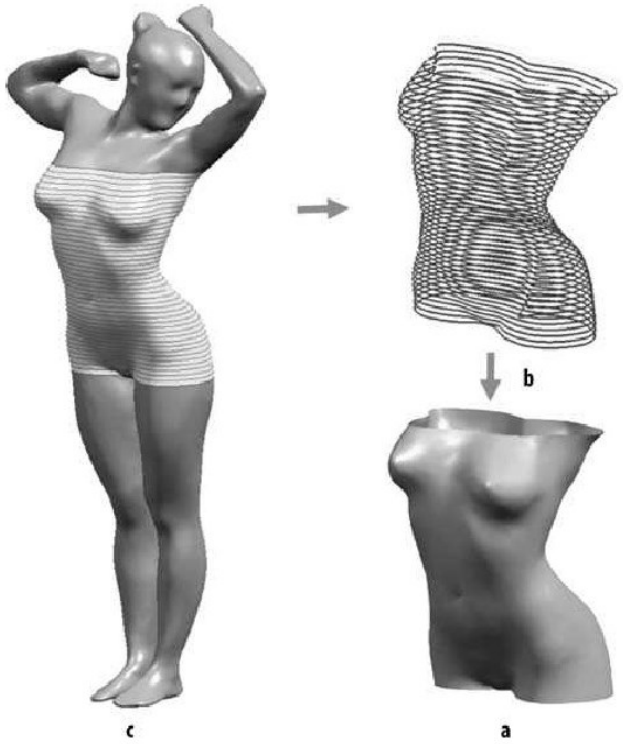

Figure 23: A NURBS surface model (a) constructed by lofting curves (b) that were created by cross-sectioning a polygon model (c).

The most useful curve modification options are as follows:

- curve re-parameterization: changing the number of control points or redistributing control points along the curve;
- curve degree conversion: changing the degree of a curve with a specified tolerance;
- curve smoothing and cleaning: smoothing a curve, cleaning, and removing unnecessary control points;
- control point editing: modifying the control points manually. The control points are moved to the specified positions to change the shape of a curve as desired;
- point generation: creating a specified number of points from a curve with random or uniform distribution;
- curve redirection, transition, and extension: changing the direction of the curves, stitching two curves together to make a new one, and extending a curve to a point or distance with tangent or curvature continuity;

3.2.2.4 NURBS Surface Phase

NURBS surfaces are sometimes the ultimate RE output for CAD-CAM-CAE applications. NURBS surfaces can be constructed based on the CAD entities extracted from the curve phase or by using polygon meshes for surface fitting.

NURBS are an accurate way to define free-form curves and surfaces. NURBS are useful for the following reasons:

- one common mathematical form for both standard analytical shapes and free-form shapes;
- flexibility to design a large variety of shapes;
- reduce the memory consumption when storing shapes (compared to simpler methods);
- can be evaluated reasonably fast by numerically stable and accurate algorithms;
- invariant under affine as well as perspective transformations;
- generalizations of nonrational B-splines and nonrational and rational Bezier curves and surfaces.

Therefore, NURBS are commonly used in CAD-CAM-CAE systems.

A flowchart summarizing the steps in NURBS construction in a RE data processing chain is presented in Figure 24.

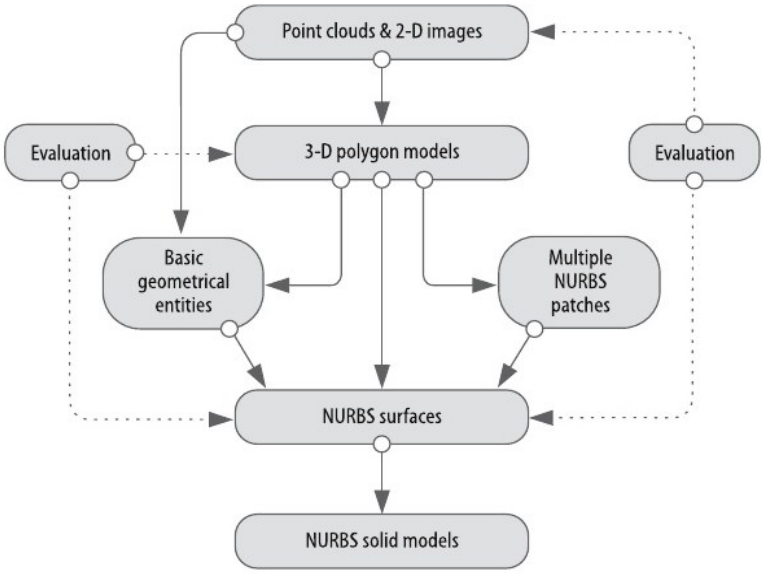

Figure 24: Different RE approaches for NURBS constructions

There are three approaches for creating NURBS surfaces:

- manual creation of NURBS from basic CAD entities
  this approach is the same as CAD modeling, in which CAD models are built from basic CAD entities: points, primitives, and curves. The fundamental difference is that CAD entities are constructed based on RE scan data in the points and images phase as well as in the curve phase; they are then imported in to CAD packages as references for modeling the object;
- manual creation of NURBS from patches
  in this approach, the model is fitted with a patch structure of quadrangular shapes, from which NURBS patches are constructed. A patch is defined by four polylines traced on the polygonal surface.
  The quality of the NURBS surfaces depends on the layout of the patches and the number of control points in the directions for defining a NURBS patch surface.
  This is the most efficient NURBS surface fitting approach, especially when working with very complex shapes. The optimal patch layout helps generating good grids of control points for constructing NURBS patches. A smaller number of control points will produce an inaccurate NURBS surface for the patch; on the other hand, one with many control points will create a CAD model with a large file size. Depending on the required accuracy of the final NURBS model, the number of control points for the NURBS patch is flexibly adjusted;
- automatic creation of NURBS from Polygon Models:
  most of the common RE software packages provide a one-step process for creating NURBS surfaces from a polygon model. The process combines the most frequently used operations in the NURBS patch approach. This automated method gives quick results. However, it is suitable only for simple geometries or when a draft NURBS surface model is needed for a specific application.

3.3 CFD Simulation

CFD is the branch of fluid dynamics providing a cost-effective means of simulating real flows by the numerical solution of the governing equations. The

governing equations for Newtonian fluid dynamics, namely the Navier-Stokes equations, have been known for over 150 years. Computational techniques replace the governing partial differential equations with systems of algebraic equations that are much easier to solve using computers.

The basic concept of CFD methods is the to find the values of the flow quantities at a large number of points in the system. These point are usually connected together in what is called numerical grid or mesh. The system of differential equations representing the flow is converted, using some procedure, to a system of algebraic equations representing the interdependency of the flow at those points and their neighbouring points.

The resulting system of algebraic equations, which can be linear or non-linear, is usually large and requires a digital computer to solve. In essence, we end-up with a system with the unknowns being the flow quantities at the grid points. Solution of this system results in the knowledge off these quantities at the grid points.

With the development of fast and validated numerical procures, and the continuous increase in computer speed and availability of cheap memory, larger and larger problems are being solved using CFD methods at cheaper cost and quicker turnaround times. In many design and analysis applications, CFD methods are quickly replacing experimental and analytical methods.

CFD simulations also enable flow solutions at the true scale of the engineering systems with the actual operating conditions, while experimental measurements mostly require either scaling up or down. In most cases, realistic conditions cannot be economically represented and thus results need to be extrapolated. This problem does not exist in CFD simulations.

CFD methods are now widely used in most aerospace applications for the purpose of predicting component performance and as an integral part of the design cycle. The applications are numerous and we will only list few examples here.

The first example is flow around an aircraft. Wind tunnel tests require substantial scaling which leads to some difficulties of matching the important flow parameters. If we attempt to model the correct Mach number, the Reynolds number will be substantially lower than the full scale Reynolds number leading to errors in the modelled shear stress and other flow features. It is also very expensive to replicate altitude conditions within a wind tunnel.

On the other hand, full scale flight tests are extremely expensive and are not without risk. For these reasons, CFD provides a useful tool in predicting the performance of the airframe components under various conditions and this leads to substantial cuts in the time and cost of the design process.

In particular, meshing strategy and Fluid Structure Interaction (FSI) method will be explained in the following sections.

3.3.1 Meshing strategy

In order to solve the aerodynamic flowfield around a geometry of interest, first of all it is necessary to discretize the domain in which solve the system of algebraic equations.

A mesh is a discretization of a geometric domain into small simple shapes, such as triangles or quadrilaterals in two dimensions and tetrahedral or hexahedra in three. Meshes are essential in the numerical solution of partial differential equation arising in physical simulation. In fact, CFD uses a series of cells (referred to as control volumes), elements and nodes that combined form the so called mesh. It is at each of these node locations, that CFD calculates the fundamental equations of fluid dynamics. The shape of the cells greatly impacts the accuracy of the solution due to discretization errors, therefore the meshing stage is one of the most crucial stages in the problem simulation.

There are 3 types of meshing predominately used in CFD today, namely:

1. structured meshing: all interior vertices are topologically alike (typically quadrilaterals and hexahedra);
2. unstructured meshing: vertices may have arbitrarily varying local neighbourhood (typically triangles and tetrahedra);
3. block-structured or hybrid meshing: formed by a number of small structured meshes combined in an overall unstructured pattern.

In general, structured meshes offer simplicity and easy data access, while unstructured meshes offer more convenient mesh adaptivity and a better fit to complicated domains. High-quality hybrid meshes enjoy the advantages of both approaches.

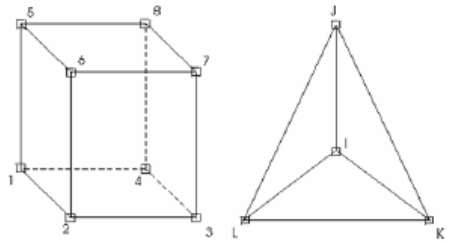

Figure 25: hexahedral (structured) and tetrahedral (unstructured) elements

Each method has advantages and disadvantages and it is imperative that the CFD user understands which meshing type is applicable for the given problem. Table 1 and Table 2 summarize advantages and disadvantages of structured and unstructured mesh.

STRUCTURED MESH	
Strengths	**Weakness**
• High degree of user control. Mesh can be accurately designed to user's requirements. • Hexahedral cells are very efficient at filling space, support a high amount of skewness and stretching before affecting solution. • Grid is flow aligned which helps the solver converge. • Post-processing is easier due to the logical grid spacing act as excellent reference points for examining the flow field.	• Excessive time spent producing the mesh compared to unstructured mesh • Some geometries don't allow structured topology due to the high skewness angles and stretch of cells that are required.

Table 1: Structured mesh: strengths and weaknesses.

UNSTRUCTURED MESH	
Strengths	**Weakness**
• Automated grid generation allows much less effort by user to define mesh. • Well suited to inexperienced users • Will generate a valid mesh for most geometries	• Lack of user control – mesh may not be defined as well as the user may like in certain areas. • Tetrahedral elements do not twist or stretch well, which will severely impact accuracy of results. • Require excellent CAD surfaces. Small mistakes in the geometry can lead to large meshing problems.

Table 2: Unstructured mesh: strengths and weaknesses.

Mesh generation, in most cases is the timeliest task in the CFD simulation and can be quit challenging to generate a mesh that accurately defines the problem, especially for complicated geometries.

For the objective of this thesis, structured and hybrid meshes will be used to perform CFD calculations and comparisons between the obtained results will be presented.

3.3.1.1 Unstructured Grid Generation

Unstructured grids have become very popular in recent years, due both to the influence of the finite-element method and to the increase in the power of computers.

Unstructured grids and unstructured solvers have successfully demonstrated their capabilities to handle complex geometries in the demanding field of aerospace applications (an area dominated for many years by structured grids). The most flexible and automatic grid generation codes create unstructured grids. They are well suited to point-wise adaptive refinement and to moving mesh methods.

It is difficult to achieve good performance on unstructured grids, more memory is required and it is quite hard to apply certain fast algorithms such as implicit methods and multigrid. Attaining performance on vector, parallel and cache based computer architectures is not easy for solvers using unstructured grids because these machines prefer that operations be performed on data that is stored locally in memory. On an unstructured grid the data belonging to the neighbour of a point may be stored a long distance away. Moreover, triangular and tetrahedral meshes inherently require more elements and more computations per grid point; in three dimensions, there are some five to six times more tetrahedra per grid point than on a corresponding mesh of hexahedra. The creation of better-quality grids for hyperbolic problems and forming highly stretched elements in boundary layers continue to be active areas of research.

Figure 26 shows a three-dimensional unstructured grid for use in a viscous flow calculations.

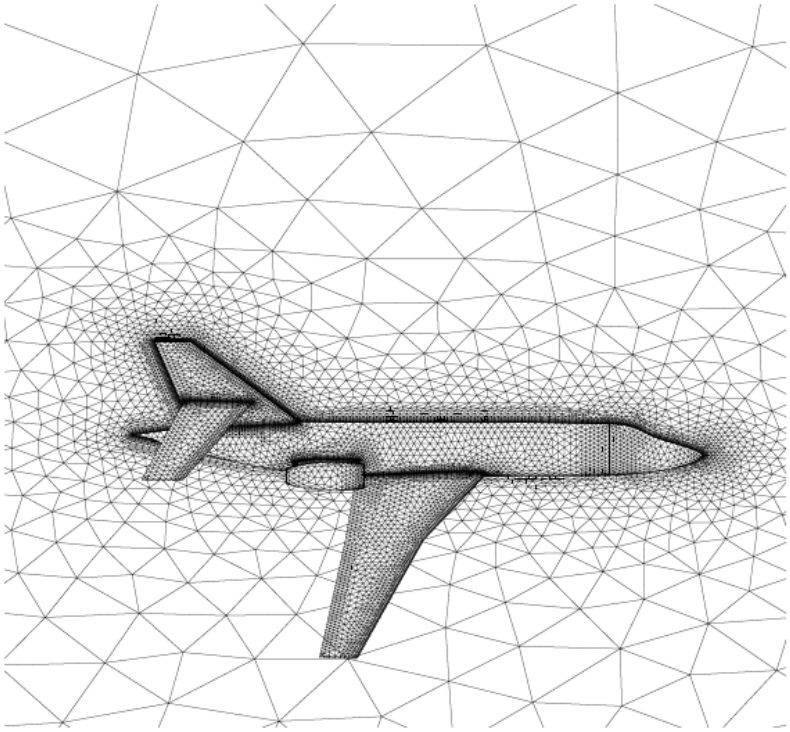

Figure 26: Three-dimensional unstructured grid for viscous flow computation

3.3.1.2 Structured Meshing

Structured meshes offer simplicity and efficiency. A structured mesh requires significantly less memory than an unstructured mesh with the same number of elements (a factor of three less). Moreover a structured mesh can also save time.

On the other hand, it can be difficult or impossible to compute a structured mesh for a complicated geometric domain. Furthermore, a structured mesh may require many more elements than an unstructured mesh for the same problem, because elements in a structured mesh cannot grade in size as rapidly. These two difficulties can be solved by hybrid structured/unstructured approach, which decomposes a complicated domain into blocks supporting structured grids.

As mentioned previously a structured mesh uses hexahedron shaped elements to create the mesh used to simulate the problem.

However, difficulty with a structured mesh comes from trying to adapt a hexagon shaped element to a curved or complex shape and can result in a poor quality cells.

Figure 27 shows an example of two-dimensional unstructured grid around an airfoil with flap and slat.

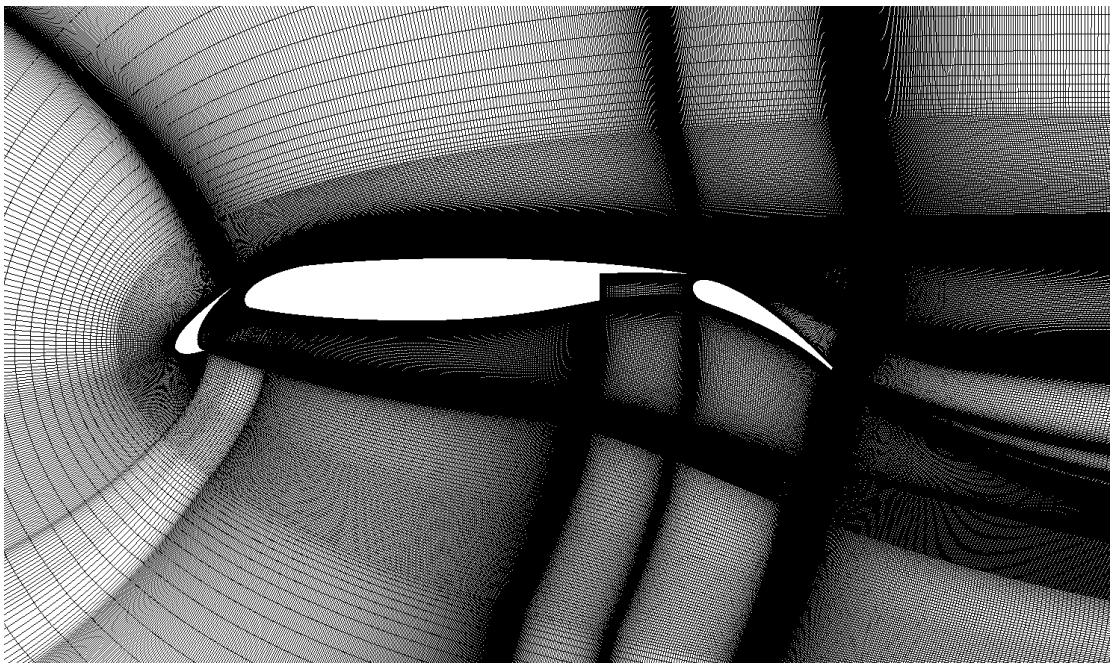

Figure 27: Example of structured grid

3.3.1.3 Hybrid Meshing

As previously anticipated, a hybrid mesh consist of a union between structured and unstructured mesh.

In particular, when you want to resolve a viscous boundary layer, it is possible to use viscous hybrid meshes that use a layer of prism elements along the wall, with tetrahedral elements in the bulk flow region. The prismatic cells allow you to resolve the normal gradients associated with boundary layers with fewer cells. The resulting mesh is referred to as a "viscous" hybrid mesh. You can create a viscous hybrid mesh by growing prisms from the faces on the surface mesh. High quality prism elements are created near the boundary and tetrahedral elements in

the rest of the domain. Automatic proximity detection and height adjustment while growing prisms in a narrow gap are also supported.

Compared to all-tetrahedral meshes, viscous hybrid meshes result in dramatic savings, with far fewer elements required to accurately resolve boundary layers and give good near-wall prediction of shear stress, heat transfer, and flow separation.

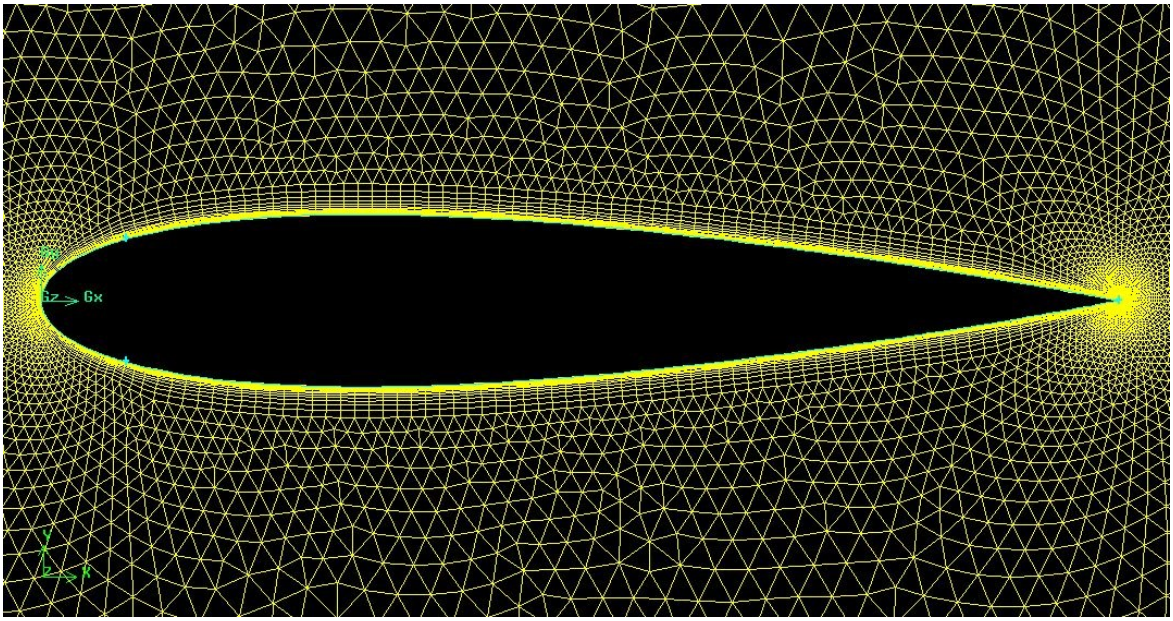

Figure 28: Example of hybrid viscous grid

3.3.1.4 Mesh quality

The quality of the mesh is determined by the shape of the individual cells. The shape of the elements in a mesh have a pronounced effect on numerical methods. If the quality of one cell is poor it can cause inaccurate results or convergence failure. Key factors that affect the quality of the cells are skewness and aspect ratio.

- Skewness
  For quad elements, the skew is obtained by first connecting the midpoints of each side with the midpoint of the opposite side. The angle α is the smaller of the two angles (Figure 29). The result is usually normalized by dividing α by 180 degrees.

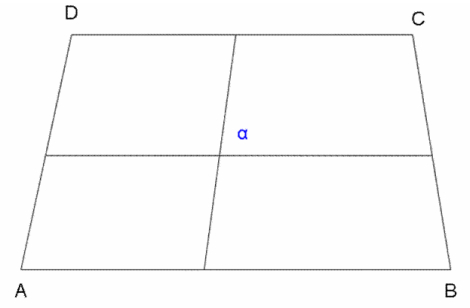

Figure 29: Skewness definition (quadrilateral element)

For triangular elements, the skewness is the ratio of the difference between the optimal cell size and the actual cell size to the optimal cell size (Figure 30) .

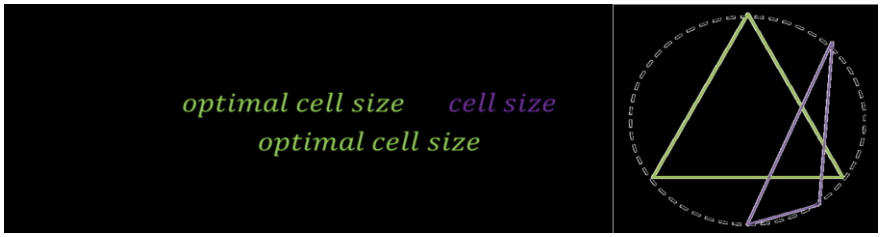

Figure 30: Skewness definition (triangular element)

- Aspect Ratio
  The aspect ratio is determined by the size of the maximum element edge divided by the size of the minimum element edge. In general, elements of large aspect ratio are bad. Large aspect ratio lead to poorly conditioned matrices, worsening the speed and accuracy of linear solver. Speed degrades before accuracy. In Figure 31 the aspect ratio is determined by B divided by A.

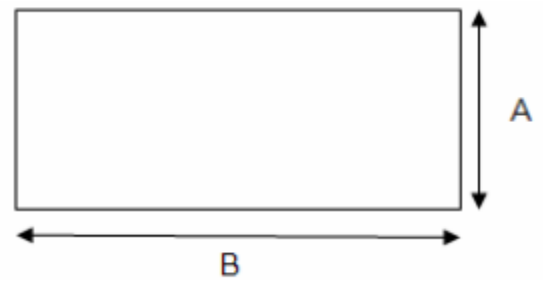

Figure 31: Element aspect ratio determination

Sometimes, however, elements of large aspect ratio are good. If the solution to the differential equation is anisotropic, meaning that its second derivative varies greatly with direction, then properly aligned high-aspect-ratio elements give a very efficient mesh. Fluid flow problems, especially full Navier-Stokes simulation are strongly anisotropic. For example, in aerodynamic simulations ideal aspect ratio may reach 10,000 along the surface of the aircraft. Quadrilateral and hexahedral meshes have an advantage in accuracy over triangular and tetrahedral meshes for control-volume formulations of the problems, as they allow faces of elements in the boundary layer to be either almost parallel or almost orthogonal to the surface.

Simulations with shock fronts – for example supersonic air flow over a wing – are also strongly anisotropic. In this case, however, the locations and directions for high-aspect-ratio elements cannot be predicted in advance. The need for adaptivity now tilts the balance in favour of triangles and tetrahedra.

3.3.2 Fluid Structure Interaction

The structure of a wing, as stated in 2.2.2, is not rigid, but all loads acting on it (wing weight, external stores weight, aerodynamic loads) cause its deformation. A representative example is given by military aircrafts at the moment in which one of the carried bodies is released and a sudden change of the total load occurs with a subsequent variation of its shape over the time.

Assuming an airplane in flight at a certain subsonic Mach number, the wings will be in a condition of elastic equilibrium, due to the different loads applied (wing weight, external stores weight, aerodynamic loads). If at a certain moment there is the release of one of the external stores, the wing will lose its equilibrium beginning to oscillate. This is an unsteady event and the prediction of the transient behaviour is capital because the pilot can be provided in advance with all information necessary to get the right reaction. Our aim is to precisely predict this wing aeroelastic response following an event of store separation.

One strategy commonly adopted by the majority of multi-physics software allows to face the Fluid Structure Interaction (FSI) problem through an exchange of data between the structural solver and the fluid dynamic one. However, this involves a substantial overhead in the analysis times, since it is necessary to modify the geometry and the mesh consistently with the deformations calculated by the Finite Element Method (FEM) module external to the CFD solver at each time step (Figure 32).

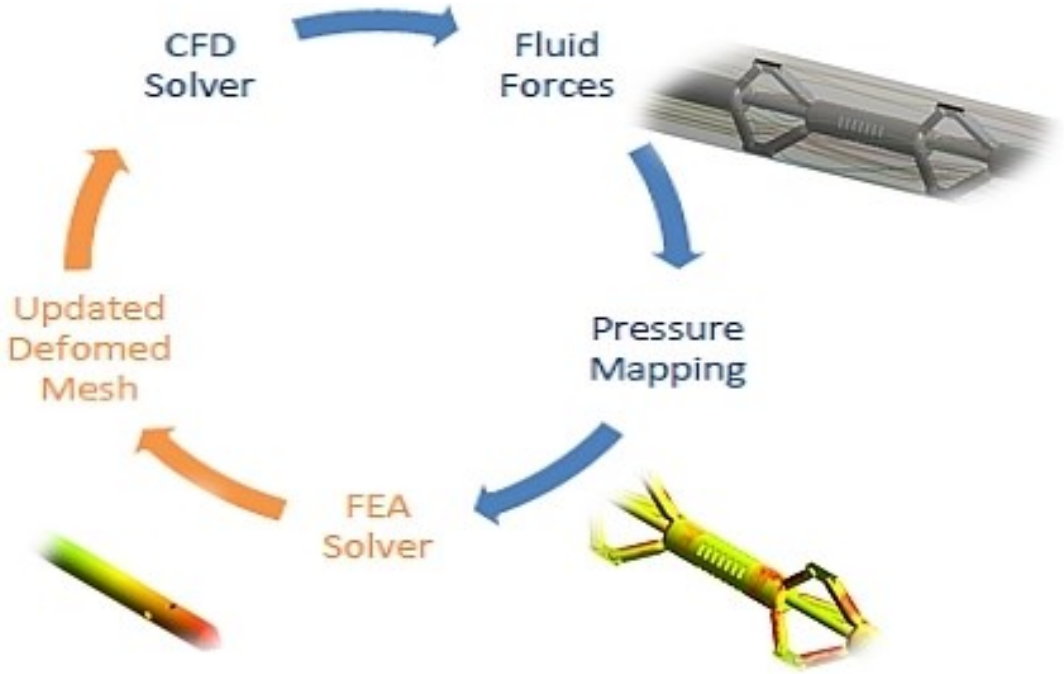

Figure 32: FSI workflow

The methodology used in this thesis is based on the FSI module of RBF Morph, a morpher based on Radial Basis Functions and fully integrated in ANSYS Fluent. Thanks to structural modes embedding, the calculation time overhead due to

structural deformations is very small, if compared with the rigid case, and is mainly due to the enabling of Fluent Moving and Deforming Mesh algorithm.

RBF Morph uses a series of radial basis functions (RBFs) to produce a solution for the mesh movement using source point defined by the user and their displacements. The solution of the RBF problem, calculated for the source points, can be stored if needed and later applied to the volume mesh by using a smoother. This morphing operation can be executed in a matter of seconds, even on very large meshes, by using the parallel processing capabilities of high performance computing (HPC) clusters.

In this case, first of all was necessary to obtain the vibration modes of the wing structure and perform structural analysis to determine the effect of the loads on the wing. Then, using the obtained modal displacement and nodal forces were performed two different FSI analyses: an aeroelastic steady analysis to determine the condition of elastic equilibrium of the wing in the presence of the store and, starting from this, an unsteady analysis to get the transient aeroelastic response of the wing due to the release of the underwing body. This event was simulated by imposing the disappearance of the store.

In this way it is possible to set an unsteady FSI analysis updating the CFD mesh at each time step according to the aerodynamic and inertial loads, allowing to carry all the calculations (fluid and structure) within the CFD solver without having to periodically exchange data such as geometry and mesh. The modal superposition method exploited is valid under the assumption of linear deformations that for the aeroelastic response of the wing considered was assumed acceptable

CHAPTER 4

4 CFD PREDICTIONS FOR A REAL FLIGHT TEST ACTIVITY

In this chapter will be illustrated the application of the M/S process presented in chapter 3 to a practical case of store/aircraft integration. In particular, the integration of a rocket launcher on the AMX aircraft will be considered ([7],[10]).

4.1 Geometry of interest

For the problem of interest, the geometry was simplified considering the basic wing of the aircraft AMX with two pylons (an inboard and an outboard one), one tank and one Aircraft Rocket Launcher (ARL) (Figure 33).

Figure 33: Geometry of interest

4.2 CAD for CFD calculations

All the geometries were generated using the reverse engineering technique explained in 3.2. The geometries were acquired using a high-resolution time of flight laser scanner (FARO CAM 2 Photon 80 represented in Figure 34).

Figure 34: laser scanner FARO CAM 2 Photon 80

The principle behind all time-of-flight implementations is to measure the amount of time (t) that a light pulse (i.e., laser electromagnetic radiation) takes to travel to the object and return. Because the speed of light (C) is known, it is possible to determine the distance travelled. The distance (D) of the object from the laser would then be equal to approximately one half of the distance the laser pulse travelled $D = C \times \frac{t}{2}$.

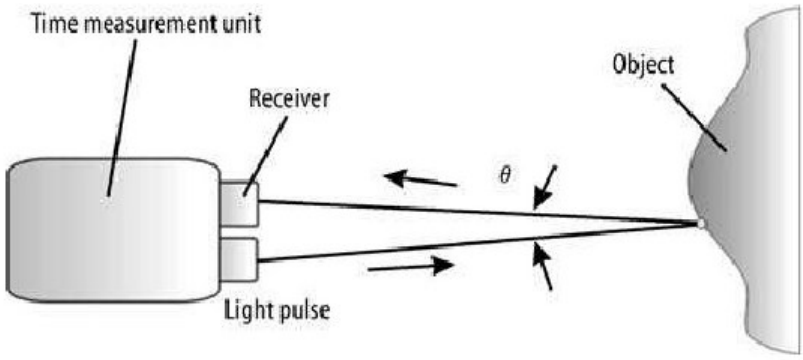

Figure 35: principle of time of flight scanner

Figure 35 illustrates how a time-of-flight laser scanner works. For all practical purposes, the angle ϑ is very small and thus has no effect on the accuracy of the distance measurement. The high velocity of light allows time of flight scanners to make hundreds, or even thousands of measurements per second. The accuracy of reverse engineering hardware based on time of flight is reasonable and approximately between a few millimetres. The accuracy depends on the pulse width of the laser, the speed of the detector, and the timing resolution; the shorter the pulse and the faster the detector, the higher the accuracy of the measurement.

The main disadvantage is that this scanners are large and do not capture an object's texture, only its geometry. They are not practical for fast digitization of small and medium-sized objects. Moreover, it takes time to complete the digitization process because the object (or environment) has to be swept during scanning.

4.2.1 AMX aircraft wing

The CAD of the AMX aircraft wing was obtained using the already presented RE technique.

In particular, the real wing was transformed in a point cloud data (Figure 36) using a laser scanner scanning and transforming it in a CAD for CFD calculations through the process already explained in paragraph 3.2.2. All the data processing operations were done using the software Geomagic®.

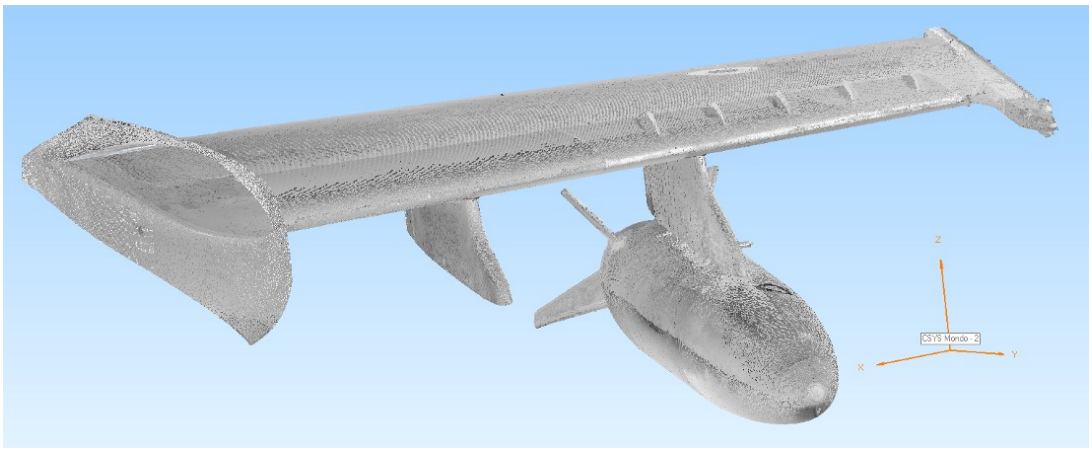

Figure 36: point cloud of AMX wing

Two different approaches were used to obtain the CAD but only one permitted to obtain a good final surface for CFD calculations.

The first approach consisted in transforming the original point cloud data in 3D polygon models used to generate NURBS surfaces (process showed in Figure 24) from which the final solid body was created.

In this case the final body presented gaps, holes, cut edges as well as unnecessary geometries. In particular the wing's leading edge was not completely designed and the surface had some discontinuities. The obtained geometry and some defects are showed in Figure 37. For these reasons it was necessary to use a different strategy to obtain the CAD.

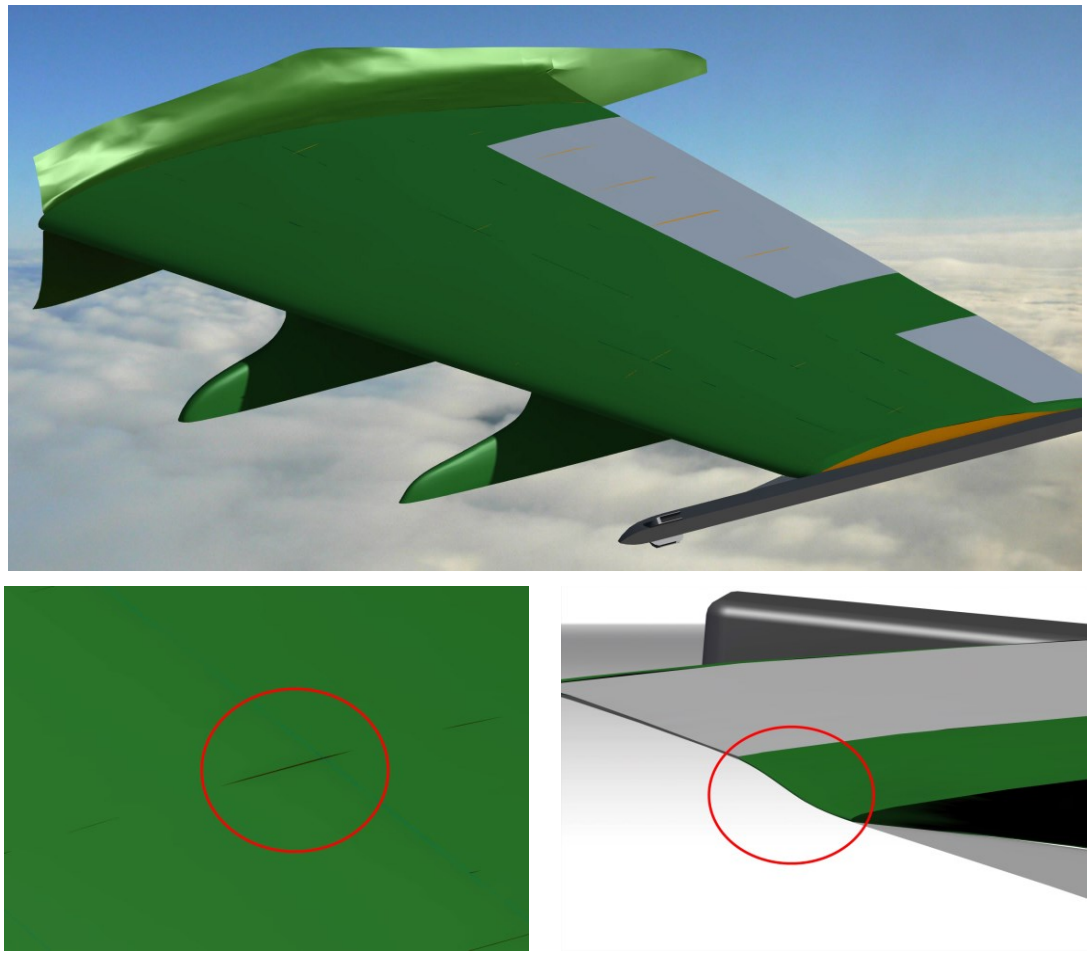

Figure 37: Unsatisfactory CAD and defects of AMX wing

As showed in Figure 24, the second approach consisted in creating basic geometrical entities from point cloud data. Using these entities, the obtained NURBS surfaces permitted to realize a satisfactory solid model of the wing.

Figure 38 represents the basic geometric entities obtained cross-sectioning the point cloud with different planes (process explained in 3.2.2.3).

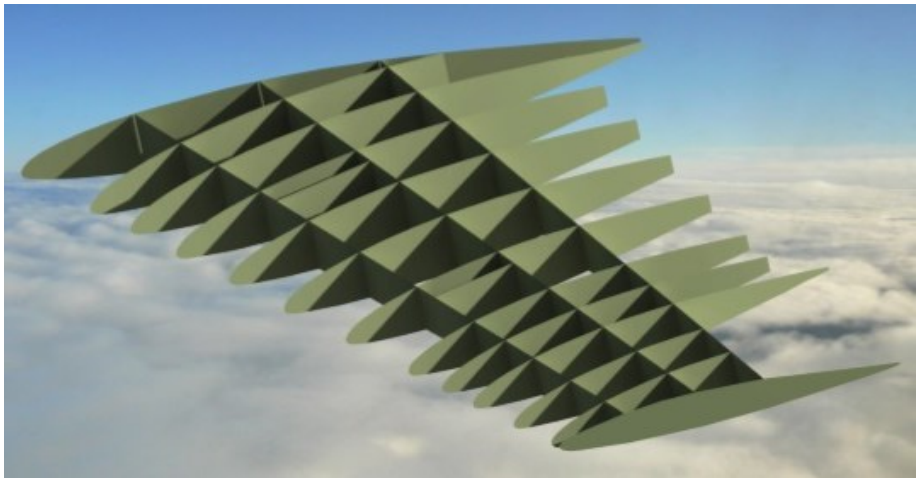

Figure 38: Basic geometric entities of the AMX Wing

Following step consisted in recreating wing surface using the basic geometric entities. During this process the wing surface was created step by steps. At the initial stage, many surfaces were generated using the basic geometric entities (Figure 39).

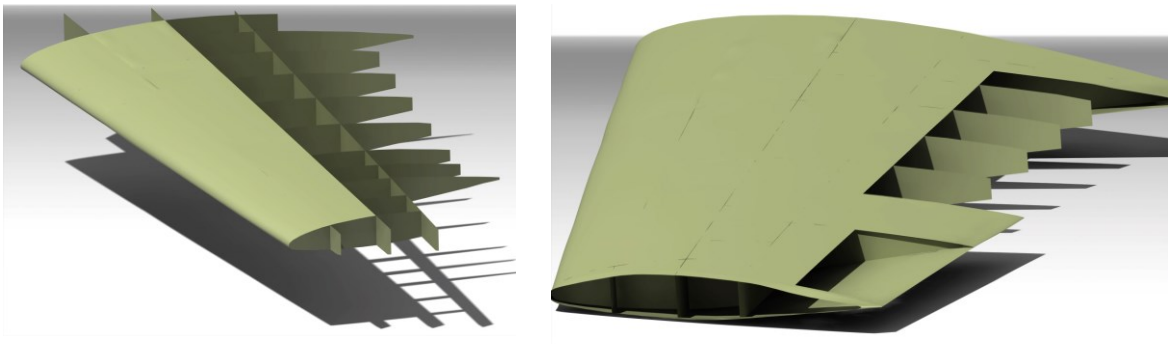

Figure 39: Surfaces generation

At this point, the final surface was not completely satisfactory because the different surfaces had different curvature at the joining point. To solve this

problem, the adjacent surfaces were joined in order to create only one continuous surface. The final result is presented in Figure 40.

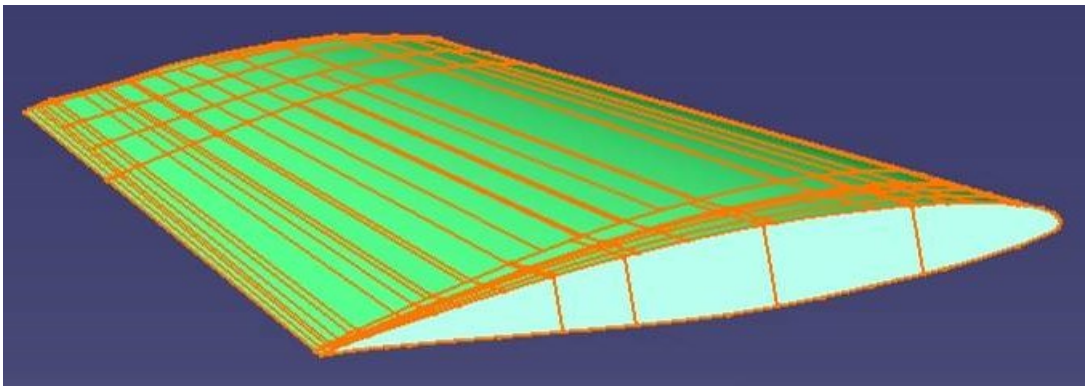

Figure 40: Final wing body

4.2.2 Pylons

Pylons were obtained starting from the point cloud data and using the same successful strategy used for obtaining the wing. The final geometry is represented in Figure 41.

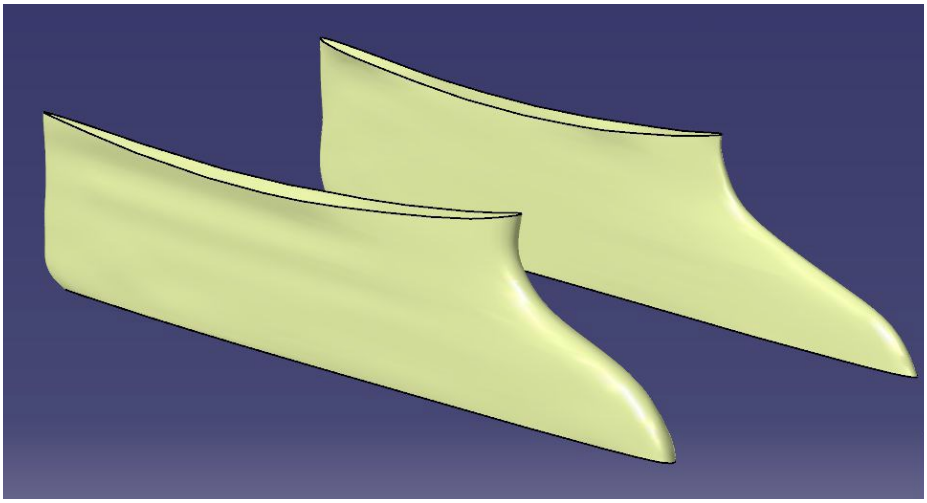

Figure 41: pylons CAD

4.2.3 *Fuel Tank*

As made for pylons, also fuel tank was obtained in the same manner. The final fuel tank body is showed in Figure 42.

Figure 42: Fuel tank CAD

4.2.4 *Aircraft Rocket Launcher*

The ARL geometry is shown in Figure 43.

Figure 43: Aircraft Rocket Launcher

The load on the ARL consists of six rockets that can be launched together or in a certain sequence. The rockets are seated in their launch tubes and blocked by clamping systems.

In this case, having technical data of the ARL, the CAD was obtained using a forwards engineering approach.

The assembly design was started with the principal structural element. Individual parts were designed in relative isolation from the overall assembly.

With this approach, as the design of a key component is completed, its geometry may or may not be used to aid the design of related mating components.

For creating the ARL 3D model the entire body has been divided in several single components, each one of them has been draw as separated part (Figure 44).

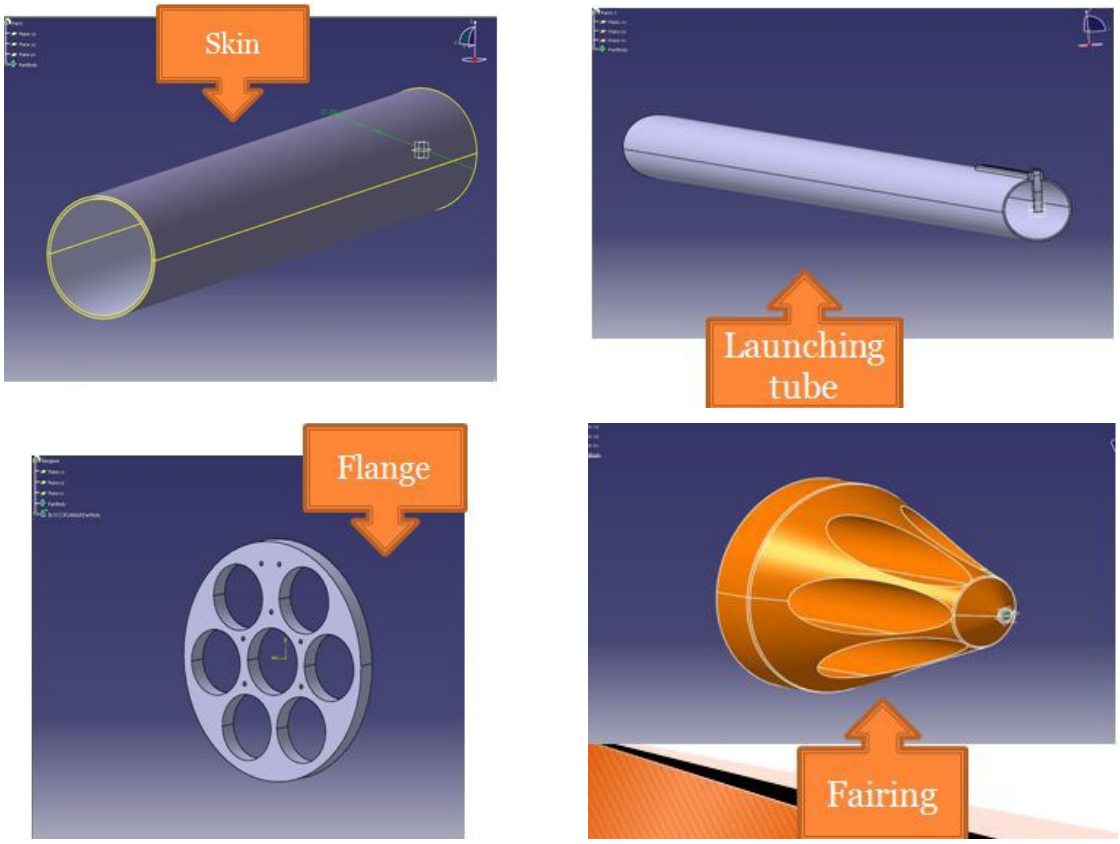

Figure 44: ARL main components

After creating every-single components it was necessary to put together all the components. In this phase all the parts were assembled together obtaining the final result that is showed in Figure 45.

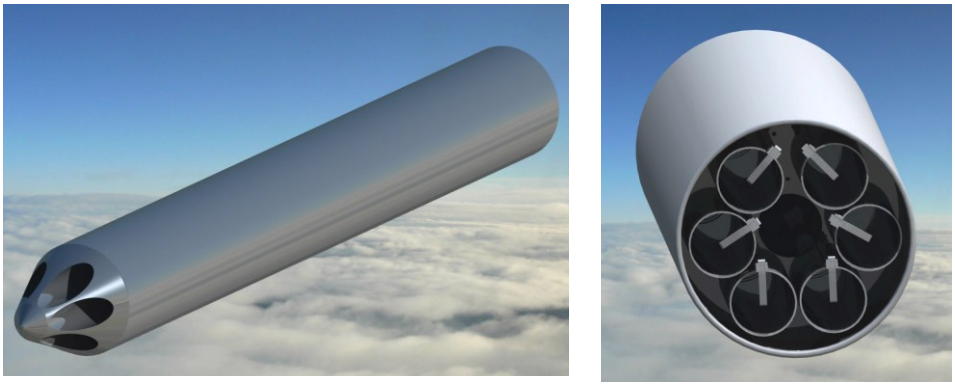

Figure 45: ARL CAD

For CFD calculations, it was decided to simplify the geometry of the ARL closing the holes in the front-side and in the rear-side obtaining the CAD showed in Figure 46.

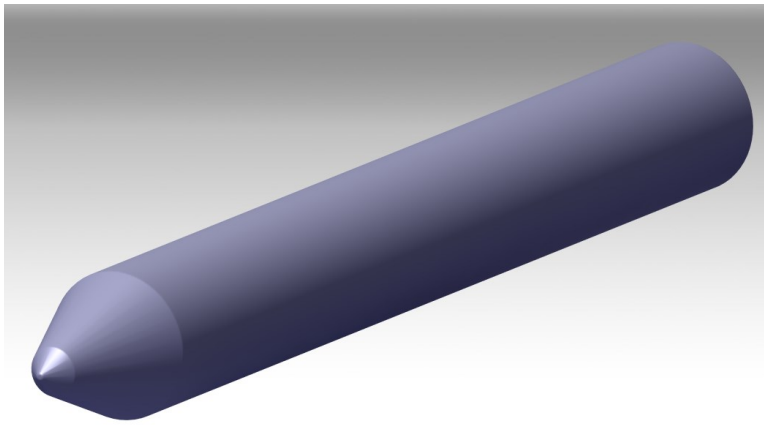

Figure 46: ARL CAD for CFD calculations

4.2.5 Wing with stores

Finally, using all the CAD showed in 4.2.1, 4.2.2, 4.2.3 and 4.2.4, it was possible to obtain the CAD of the geometry of interest for CFD calculation presented initially in Figure 33.

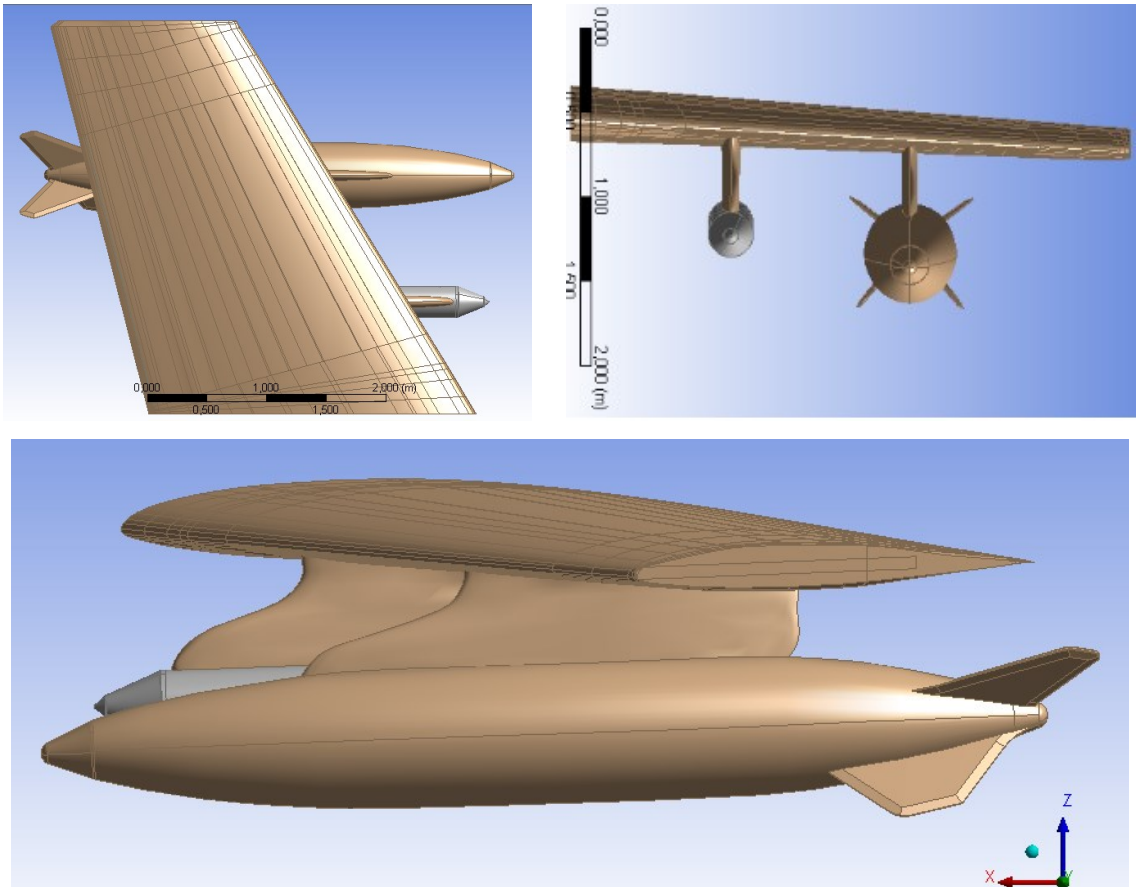

Figure 47: Wing with stores CAD for CFD calculations

4.3 Preliminary CFD results

In this section will be presented all the preliminary CFD calculations performed in order to validate the methodology used to predict the aerodynamic performances of the final test case.

4.3.1 Juncture flows

The flow which characterizes the store integration problem is the so-called juncture flow ([9]). In fact, juncture flows are of importance in external aerodynamics (e.g. wing-body junctures, wing-pylon junctures).

Studying the generic juncture flow problem may help to understand the characteristics of this flow and thereby to learn how to optimize the grid distribution. Figure 48 represents the classic geometry of a juncture flow.

In order to validate the methodology to use for the store integration problem, numerical calculations on the juncture flows were performed and results were compared to those presented in [9].

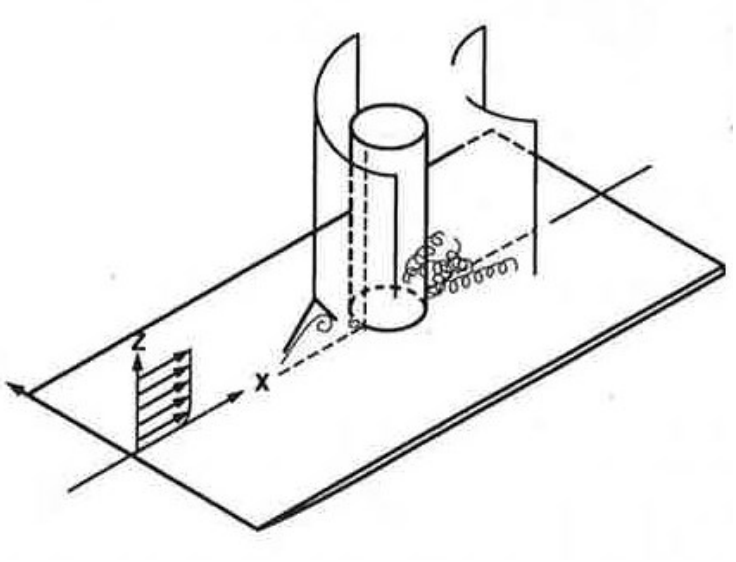

Figure 48: Generic geometry of a typical juncture flow

First of all, the geometry of the juncture flow consisted of a cylinder attached to a plate. The diameter of the cylinder was 1m and the length was 6m. The inflow boundary was located at 20 cylinder diameters away from the cylinder.

For the resolution of the juncture flow, the symmetry of the problem was utilized in order to reduce the dimension of the grid and reducing the computation time. The structured mesh near the wall was created using the operation of inflation. The obtained mesh had about 1'400'000 elements with a maximum skewness value equal to 0.89.

As in [9] the equation solved were unsteady, three-dimensional, compressible, Reynolds-averaged Navier-Stokes with an algebraic turbulence model used for closure. The flow was considered laminar.

For the subsonic flow when $M_\infty = 0.2$ and $Re_D = 500$, a Blasius profile was used as initial condition. When $M_\infty = 0.2$ and $Re_D = 1500$, the initial solution used was the solution of the case with $Re_D = 500$.

For this type of calculations the choice of the time step was of fundamental importance. For this purpose we made use of equation (2):

$$time\_step = \frac{1}{200}\frac{total\_length}{input\_speed} \quad (2)$$

Equation (2) is a good starting point in order to obtain a Courant number almost unitary.

Figure 49 is a comparison between the pressure coefficient obtained from CFD calculations and the same coefficient presented in [9]. It is possible to observe a good agreement between the obtained results and [9].

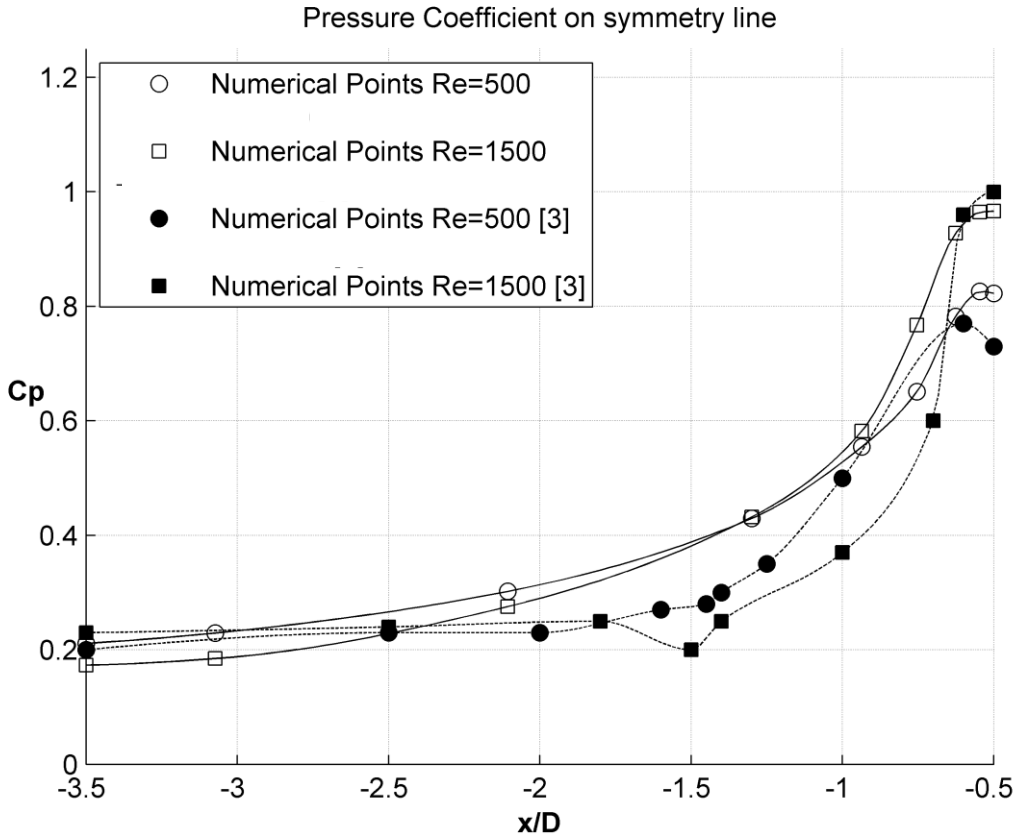

Figure 49: Pressure Coefficient for Juncture Flow on symmetry line

Figure 50 and Figure 51 represents the typical topology of the flow for a juncture flow problem.

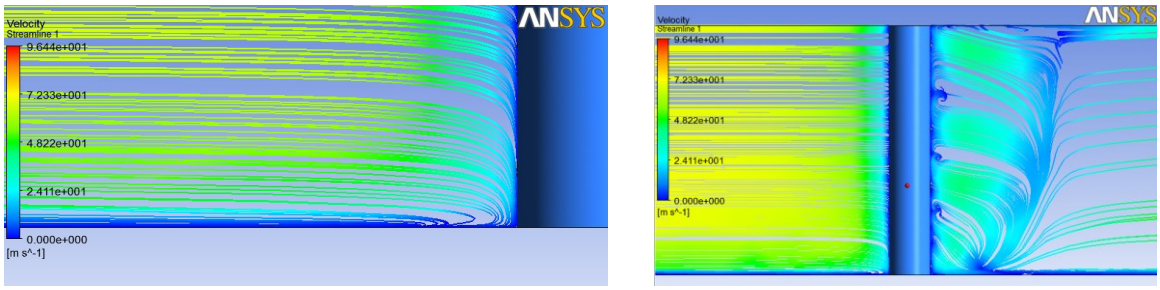

Figure 50: Streamline-Re$_D$=500

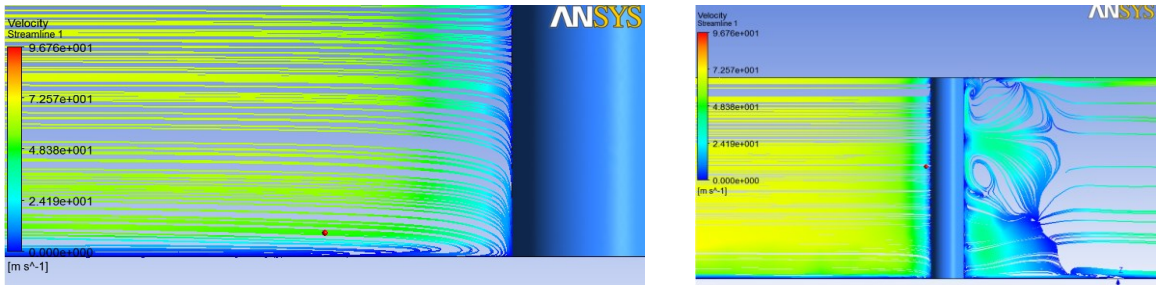

Figure 51: Streamline-Re$_D$=1500

4.3.2 Root airfoil

First of all, it was necessary to generate the necessary mesh in order to perform after the numerical calculations.

In order to perform comparisons, two different meshes were generated: structured mesh was created using ANSYS ICEM CFD, hybrid viscous mesh was produced using ANSYS MESHING.

Figure 52 shows the structured meshes obtained for the root airfoil.

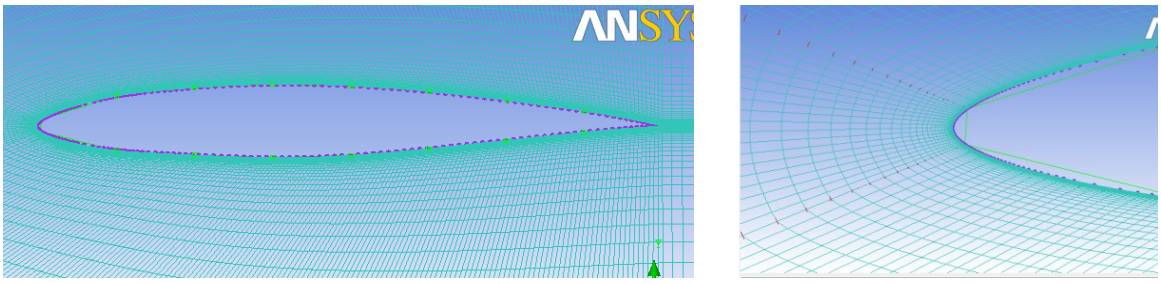

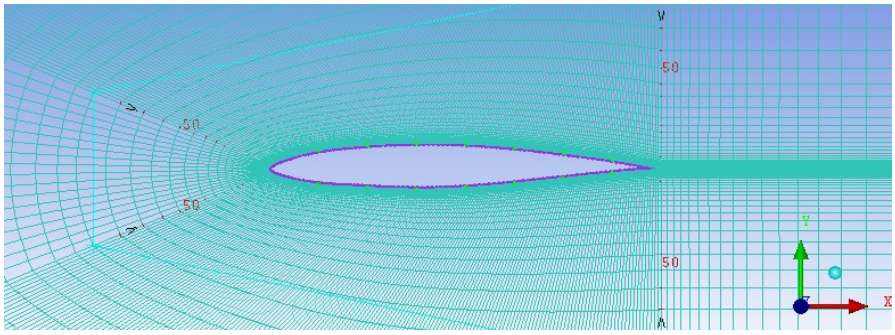

Figure 52: Root airfoil structured grid

Figure 53 represents the hybrid viscous mesh obtained for the root airfoil of the aircraft. In this case, the creation of the structured layer (hexahedral elements) close to the wall was possible using the inflation command of ANSYS MESHING. This structured layer was made of 15 layers and the first layer thickness was choose in order to obtain a good y_+. In detail, the order of magnitude of the so-called first layer thickness is given by equation (3):

$$\frac{\Delta y}{y_+} = 8.6L\left(\mathrm{Re}_L\right)^{-\frac{13}{14}} \quad (3)$$

Equation (3) permitted to calculate the value of the first layer thickness in order to obtain a desired value of y_+. However the right distance that along with the number of layers provides a correct y_+ and an acceptable value for the skewness is generally left to the experience of the engineer.

For the airfoil grid, the number of elements of the obtained hybrid mesh was 8500 with a maximum skewness value of 0.84.

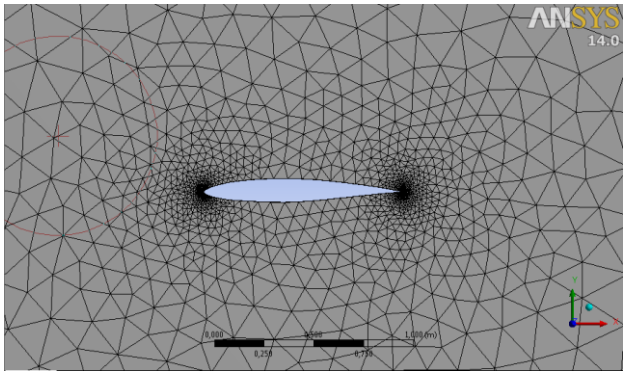

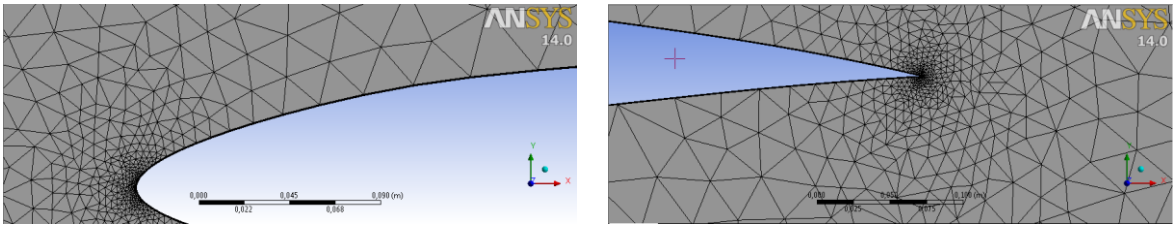

Figure 53: Hybrid viscous Mesh for root airfoil

We now present the results obtained in Eulerian flow using structured and hybrid mesh.

First of all, a comparison between the results obtained with MSES code and FLUENT will be presented. Figure 54 presents the comparison between the pressure coefficients obtained with MSES and FLUENT for a Mach number equal to 0.1 and α = 0° and α= 2°. Both calculations were performed with structured grids. Results obtained with the two different codes show a good agreement.

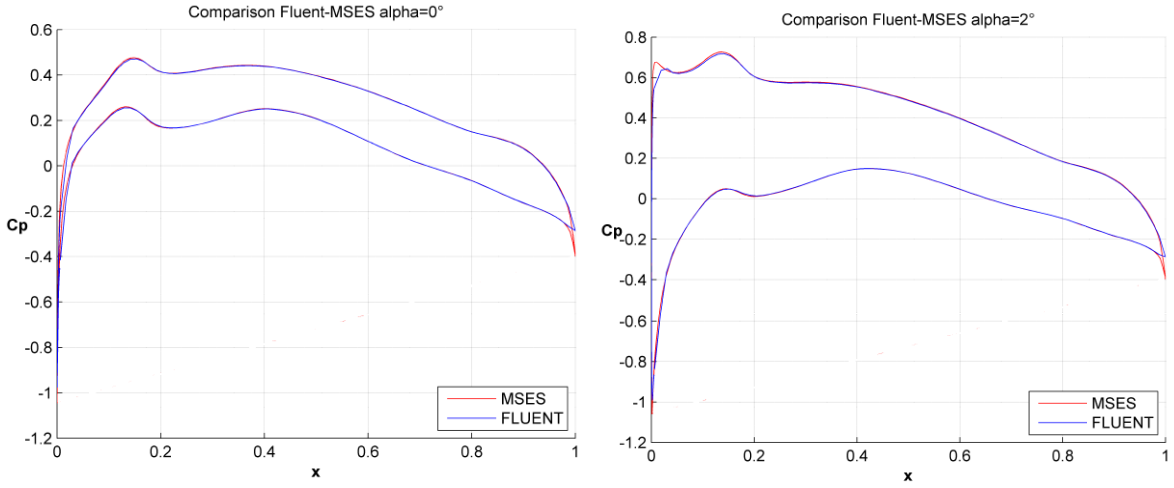

Figure 54: Root airfoil pressure coefficient–Eulerian Incompressible flow-structured grid [(α=0°,M∞=0.1);(α=2°,M∞=0.1)]

Figure 55 shows the results obtained for the hybrid viscous grid with FLUENT in the same conditions showed in Figure 54. It is possible to observe that the obtained results are practically the same of the structured grid.

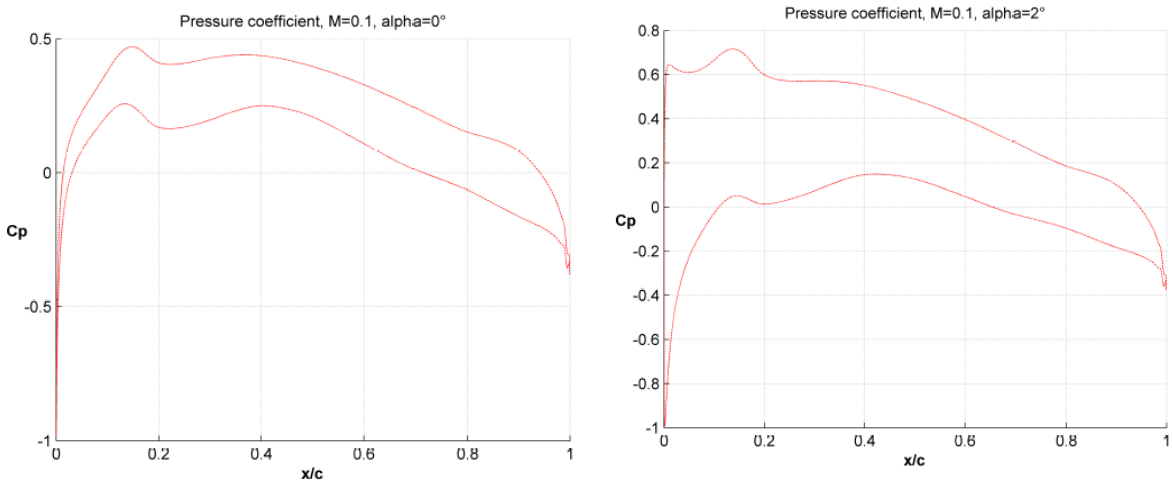

Figure 55: Root airfoil pressure coefficient–Eulerian Incompressible flow–hybrid viscous grid [(α=0°,M_∞=0.1);(α=2°,M_∞=0.1)]

Figure 56 shows the effect of the AOA on the pressure coefficient. It is possible to observe that increasing the AOA the expansion on the leading edge is stronger and there is an increasing in the lift coefficient that is related to the area inside the pressure coefficient curve.

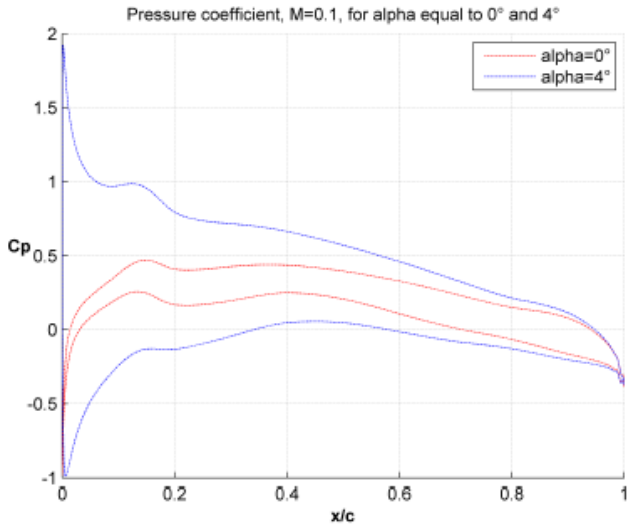

Figure 56: Effect of AoA on pressure coefficient-Eulerian Incompressible flow–hybrid viscous grid [(α=0°,M_∞=0.1);(α=4°,M_∞=0.1)]

We present now the results obtained for Eulerian transonic flow. Also in this case we performed a comparison with MSES code.

Figure 57 shows the comparison of the pressure coefficients obtained with MSES and FLUENT using a structured grid. Also in this case it is possible observe that there is a good agreement between the obtained results.

Figure 58 shows the comparison between the results obtained using a structured mesh and an hybrid mesh. Also in this case is possible to observe a good agreement.

Observing Figure 57 and Figure 58, it is possible to note that varying the Mach number, the effects of expansion and compression are exalted.

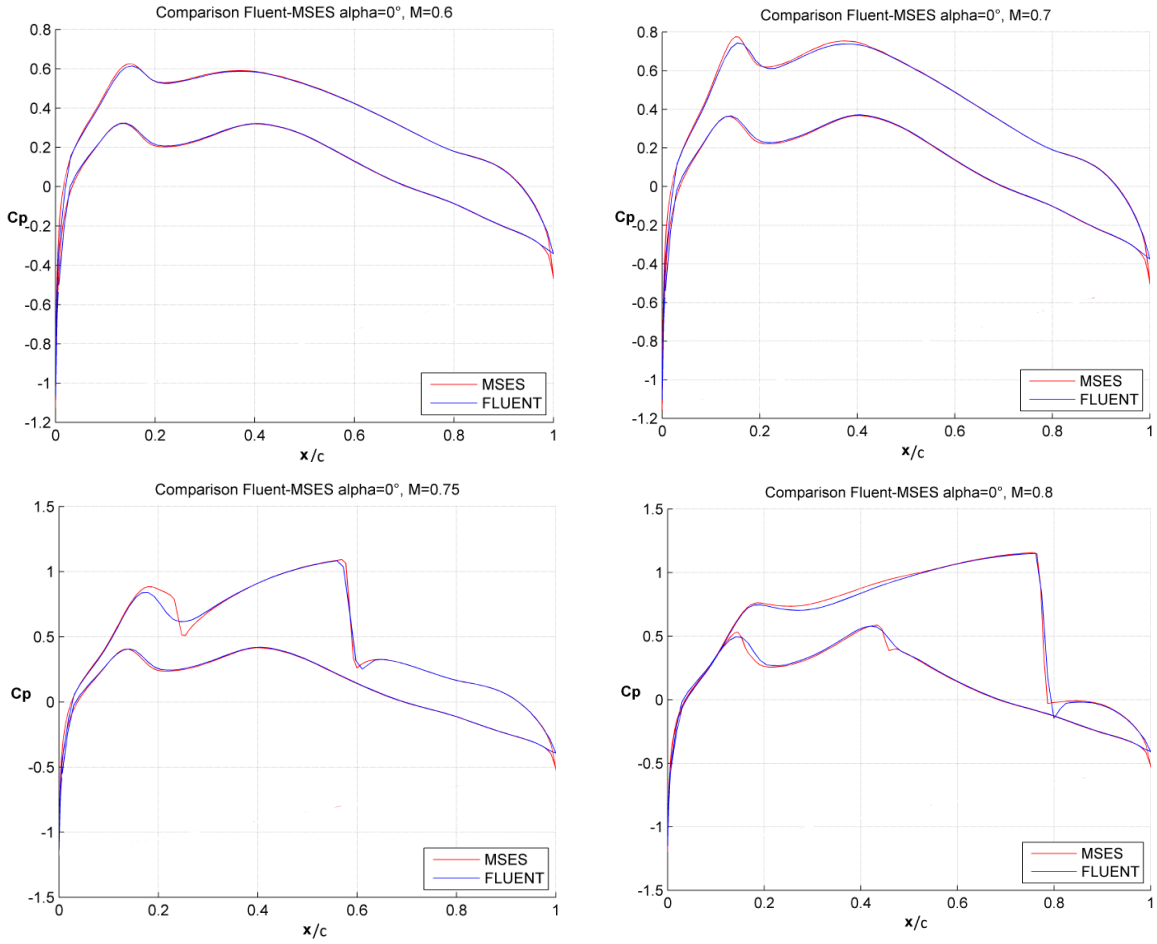

Figure 57: Root airfoil pressure coefficient–Eulerian transonic flow-Structured grid [α=0°,M_∞=(0.60, 0.70, 0.75, 0.80)]

For Mach numbers away from the critical Mach number, the expansion of the pressure coefficient is similar to the expansion of the pressure coefficient in incompressible regime. When the Mach number reaches and exceeds the critical

Mach number, the shape of the pressure coefficient change completely (Figure 57). In fact, when the Mach number reaches and exceeds the critical Mach number, there is at some point the formation of a shock wave. Increasing the Mach number, it is possible to observe that the wave moves downstream. Increasing the AoA, the shock wave anticipates and becomes stronger.

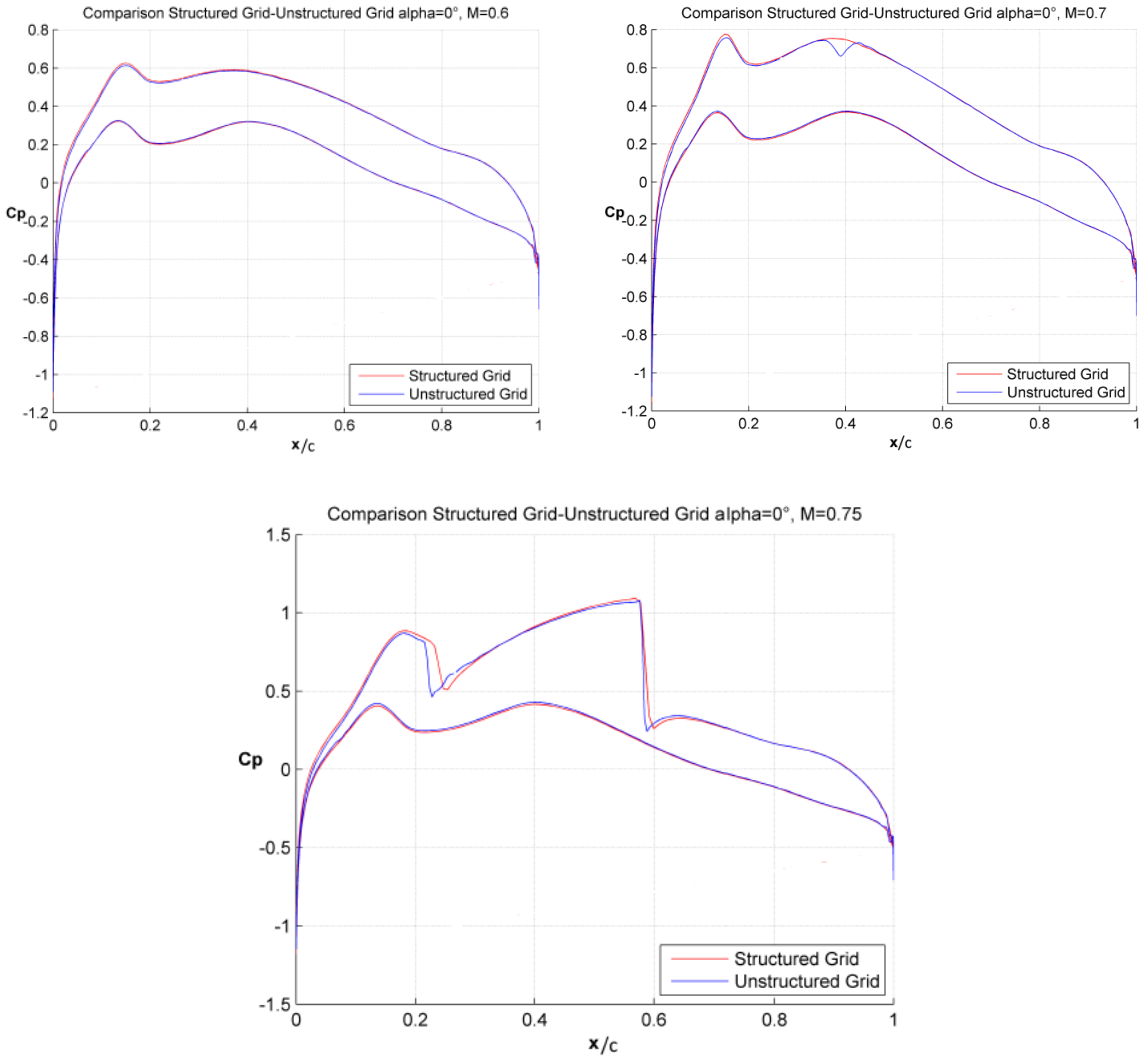

Figure 58: Root airfoil pressure coefficient–Eulerian transonic flow-Structured/hybrid grid comparison [α=0°, M_∞=(0.60, 0.70, 0.75)]

Figure 59 and Figure 60 show the effect of the variation of the asymptotic Mach number and of the AOA on the flow-field. For α=0° it is possible to observe that the critical Mach number is between 0.70 and 0.75; increasing the AOA to α=2°, the

expansion becomes stronger and the critical Mach number decreases to the range 0.65 and 0.70.

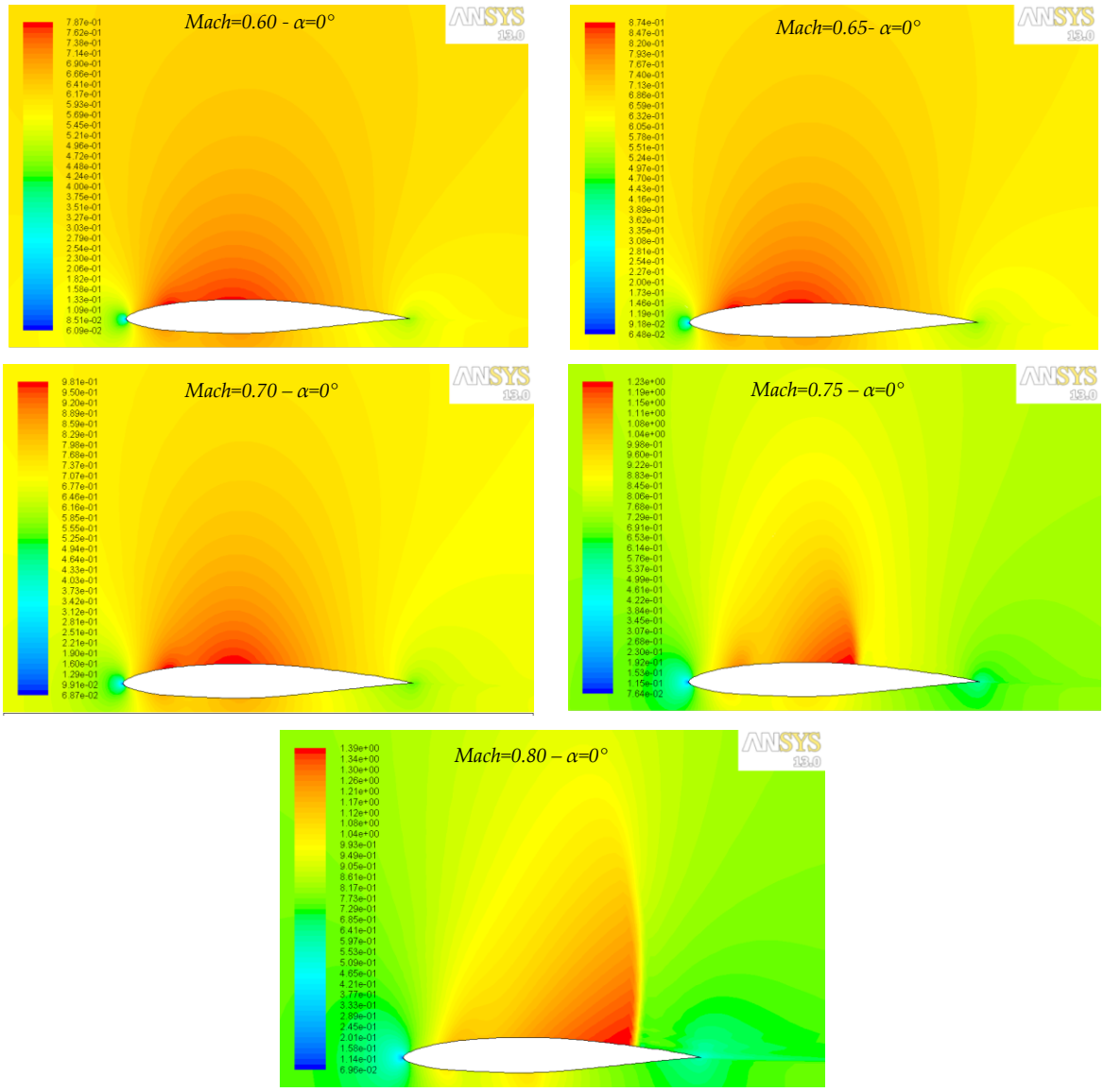

Figure 59: Contour of Mach Number around the root airfoil for α=0° and different Mach number in Eulerian transonic flow

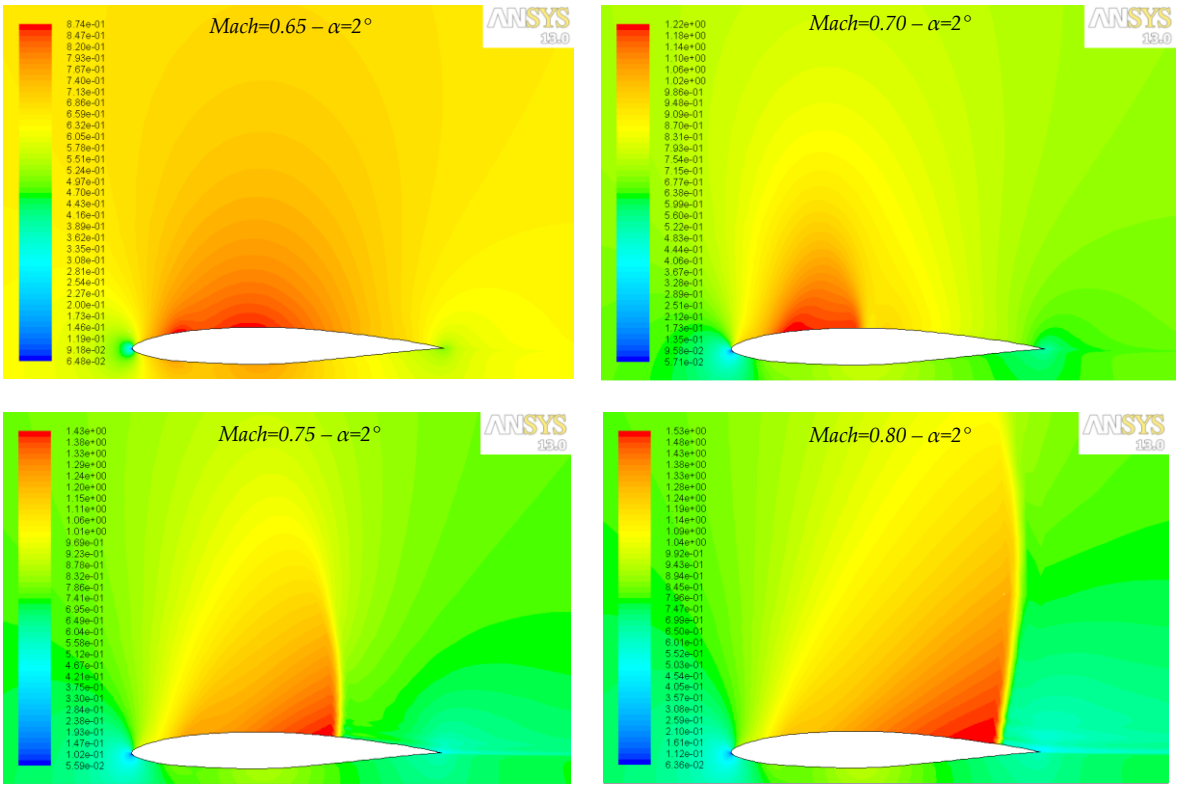

Figure 60: Contour of Mach Number around the root airfoil for α=2° and different Mach number in Eulerian transonic flow

Figure 61 shows the effect of the Mach number on lift and drag coefficients. It is possible to observe that these variation are in accord with literature. In fact there is an increasing of the lift coefficient with the second order of the Mach number while the drag coefficient diverges close to the value of the critical Mach number.

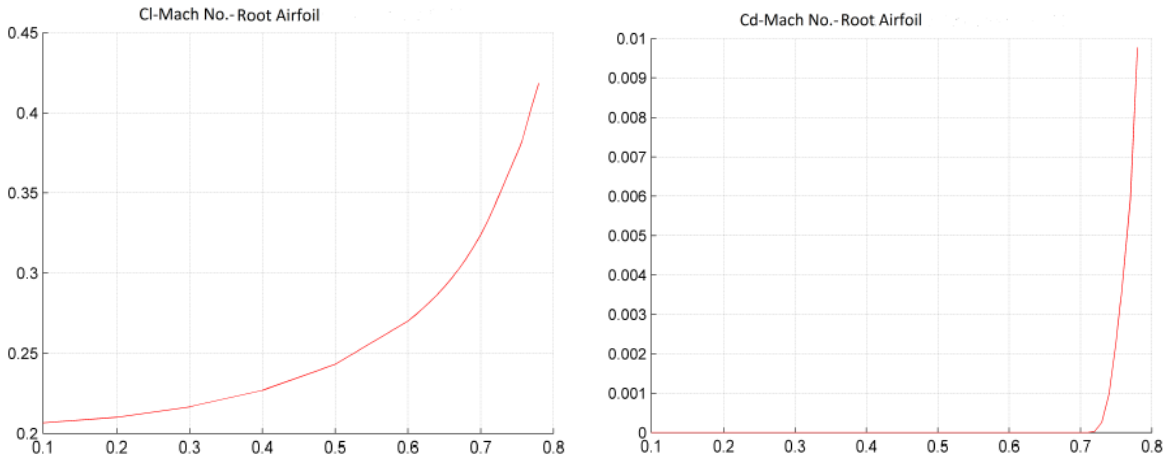

Figure 61: Effect of Mach number on lift and drag coefficient in Eulerian flow

Table 3 reports the value of the aerodynamic coefficient (lift and drag coefficient) obtained for different conditions of Mach number and AOA and different meshes (structured and unstructured).

It is possible to observe a good correlation between the computation performed with the structured grid and the calculation done with the unstructured grid. In particular, it is possible to observe an optimal agreement between the value of the lift coefficients while there is a difference in the estimation of the drag coefficient especially when this coefficient assumes little values.

Mach number	α	Structured grid		Unstructured grid	
		C_l	C_d	C_l	C_d
0.60	0°	0.265	0.0012	0.264	0.0003
0.70	0°	0.315	0.0013	0.314	0.0004
0.75	0°	0.365	0.0037	0.356	0.0028
0.60	2°	0.574	0.0020	0.572	0.0010
0.70	2°	0.698	0.0034	0.694	0.0028
0.75	2°	0.759	0.0246	0.746	0.0238
0.80	2°	0.867	0.0695	0.841	0.0671
0.60	4°	0.883	0.0043	0.885	0.0028
0.70	4°	1.010	0.0261	0.998	0.0250

Table 3: Aerodynamic coefficients in transonic flow

Also the comparison between the pressure coefficients, showed in Figure 58, confirm a good agreement between the results obtained with the two different meshes.

We present now the results of the viscous calculations for the root airfoil. The used turbulence model was k –ω SST.

Figure 62 shows the effect of the AOA on the aerodynamic coefficients (C_d-C_l-C_m) in viscous incompressible flow.

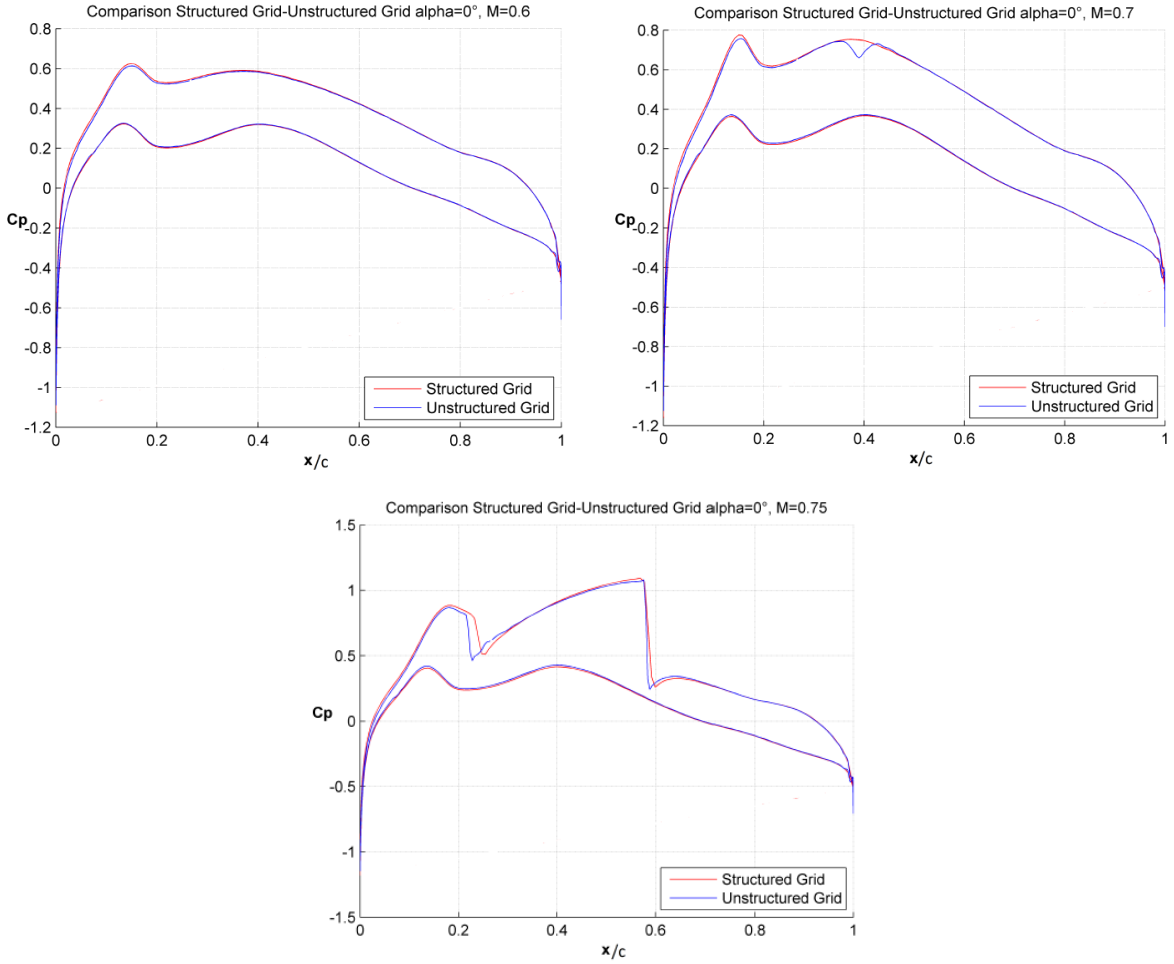

Figure 62: Effect of AOA on the aerodynamic coefficient in viscous-incompressible flow for the root airfoil.

Table 4 reports the aerodynamic coefficient obtained for viscous-transonic flow using structured and unstructured flow. Also in transonic-viscous flow, it is

possible to observe a good agreement between the results obtained with the two types of grids.

Mach number	α	Structured Mesh		Unstructured Mesh	
		C_L	C_D	C_L	C_D
0.70	0°	0.216	0.0086	0.212	0.0088
0.70	2°	0.533	0.0106	0.525	0.0108
0.70	4°	0.810	0.0229	0.816	0.0233

Table 4: Aerodynamic coefficients–transonic flow

Figure 63 shows the effect of the AOA on the aerodynamic coefficients in transonic flow. It is possible to observe that the linearity of the lift coefficient terminate at a lower AOA in transonic flow respect to incompressible flow but the value of the lift coefficient at the same AOA is higher.

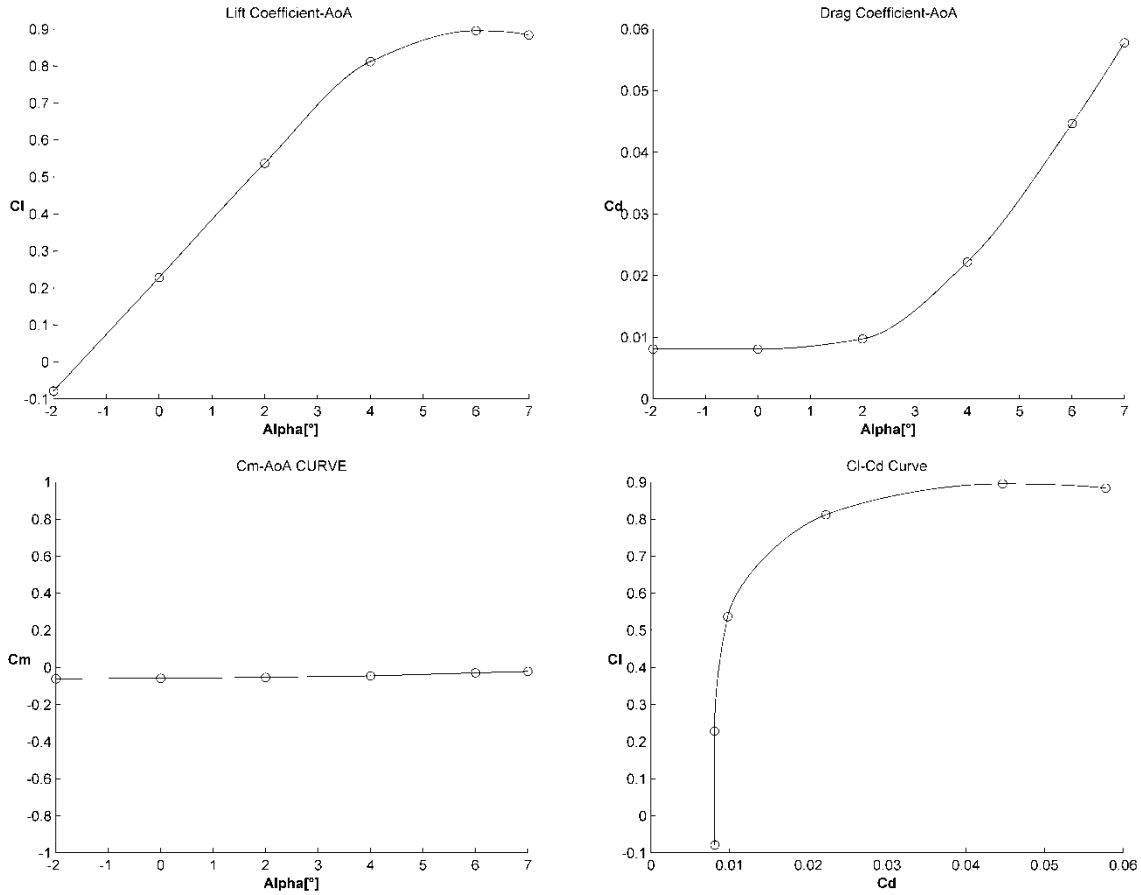

Figure 63: Effect of AOA on aerodynamic coefficient in transonic-viscous flow (M_∞=0.70)

Figure 64 shows the effect of the Mach number on the aerodynamic coefficients in viscous flow. Figure 65 shows the effect of the Mach number on the pressure coefficient.

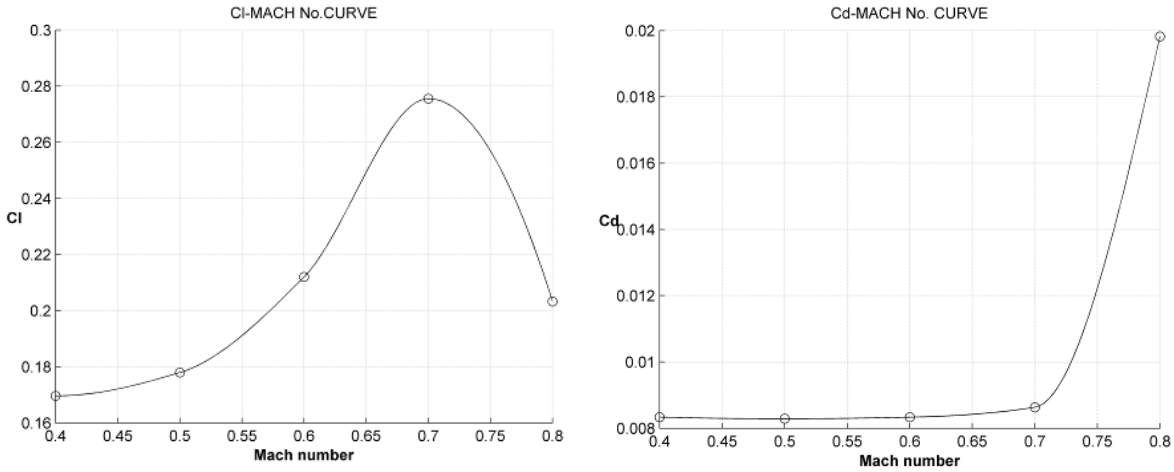

Figure 64: Effect of Mach number on aerodynamic coefficients in viscous flow

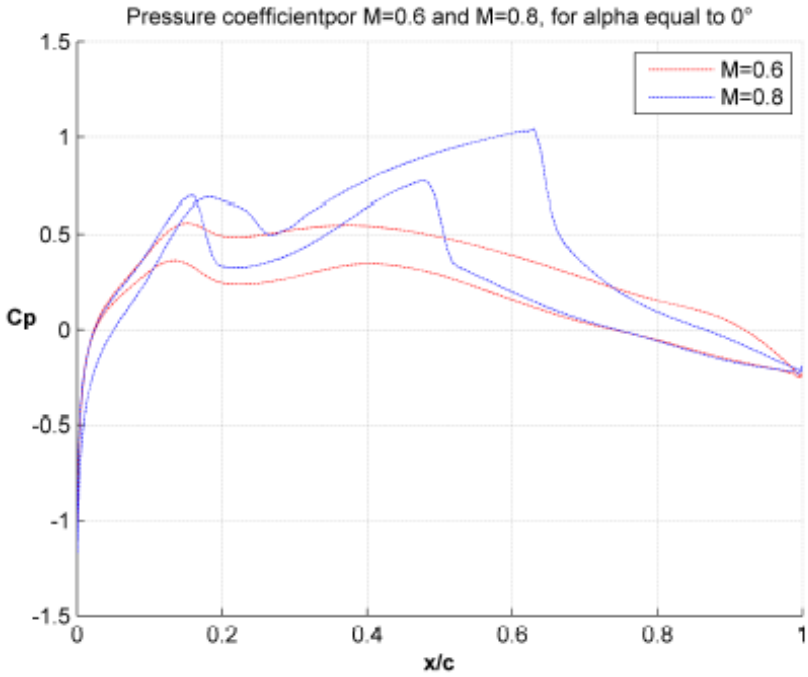

Figure 65: Effect of Mach number on pressure coefficient in transonic-viscous flow

4.3.3 *Clean wing*

The structured mesh for the clean wing was created as already described for the root airfoil in 4.3.2. Figure 66 shows the structured grid obtained for the clean wing.

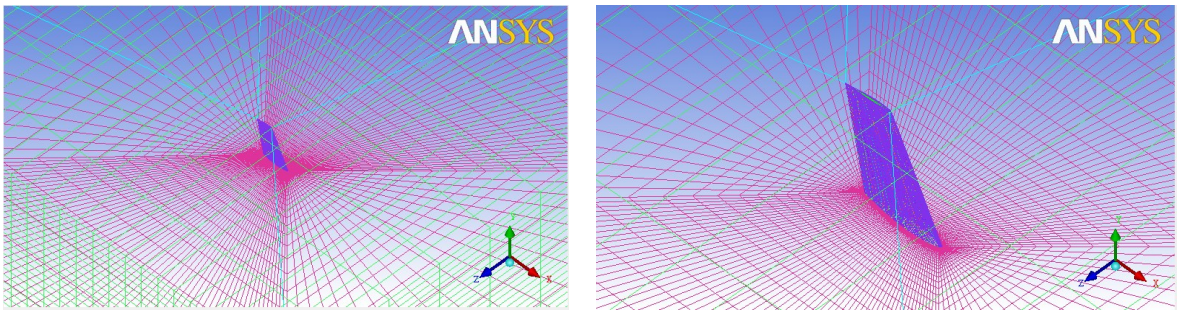

Figure 66: clean wing structured grid

However, also in this case we decided to generate a hybrid mesh to make comparison between the two kind of grids.

The obtained hybrid grid for the clean wing had a maximum skewness value of 0.91. In this case the mesh parameters was also selected in order to minimize the maximum value of skewness. The elements with the highest skewness were located on the trailing edge of the wing that is a critical zone for meshing. In order to reduce the skewness, we decided to slightly increase the value of the first layer thickness and the grid growth rate, permitting to obtain a significant reduction of the skewness. Figure 67 shows some details of the obtained mesh.

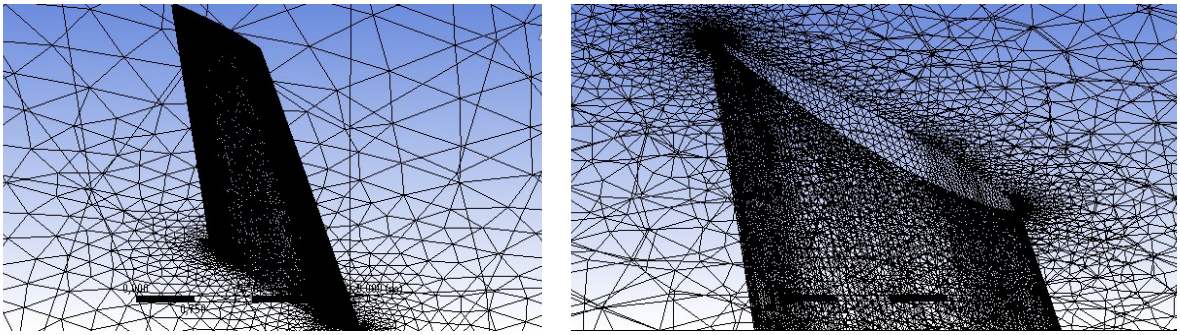

Figure 67: hybrid viscous mesh for clean wing

Also for the clean wing calculations the results of the unstructured mesh were compared with those of the structured mesh. In particular, the aerodynamic coefficients obtained with the two different meshes were in good agreement and

for this reason we performed the major part of the calculations using the hybrid viscous grid.

Now we will present the results obtained in Eulerian flow for the clean wing. Calculations were performed at M_∞=0.7 and H=1000 ft. Figure 68 shows the effect of the AOA on the aerodynamic coefficient in Eulerian transonic flow.

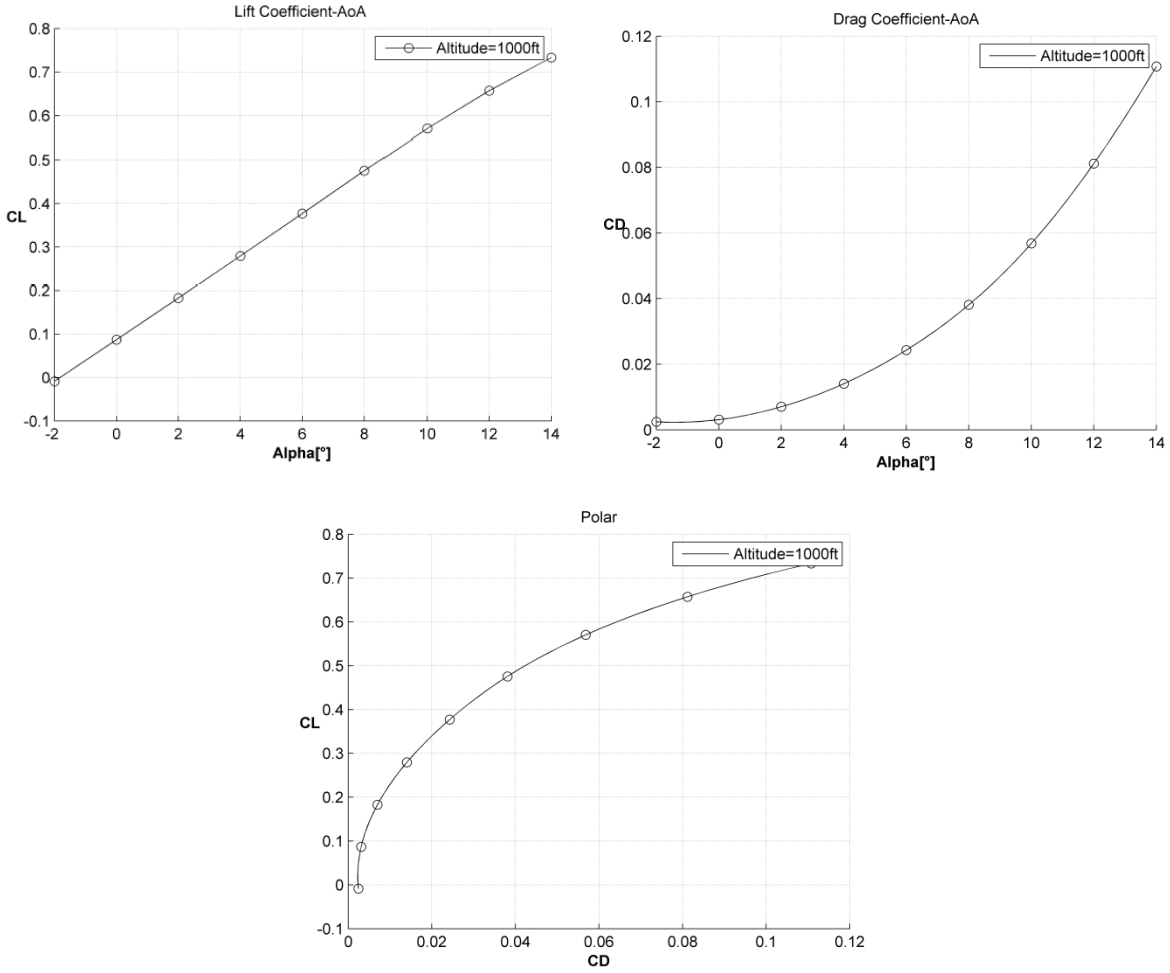

Figure 68: Effect of the AOA on the aerodynamic coefficient in Eulerian flow for the clean wing.

Moreover, also the effect of the Mach number on the aerodynamic coefficient was taken into account (Figure 69).

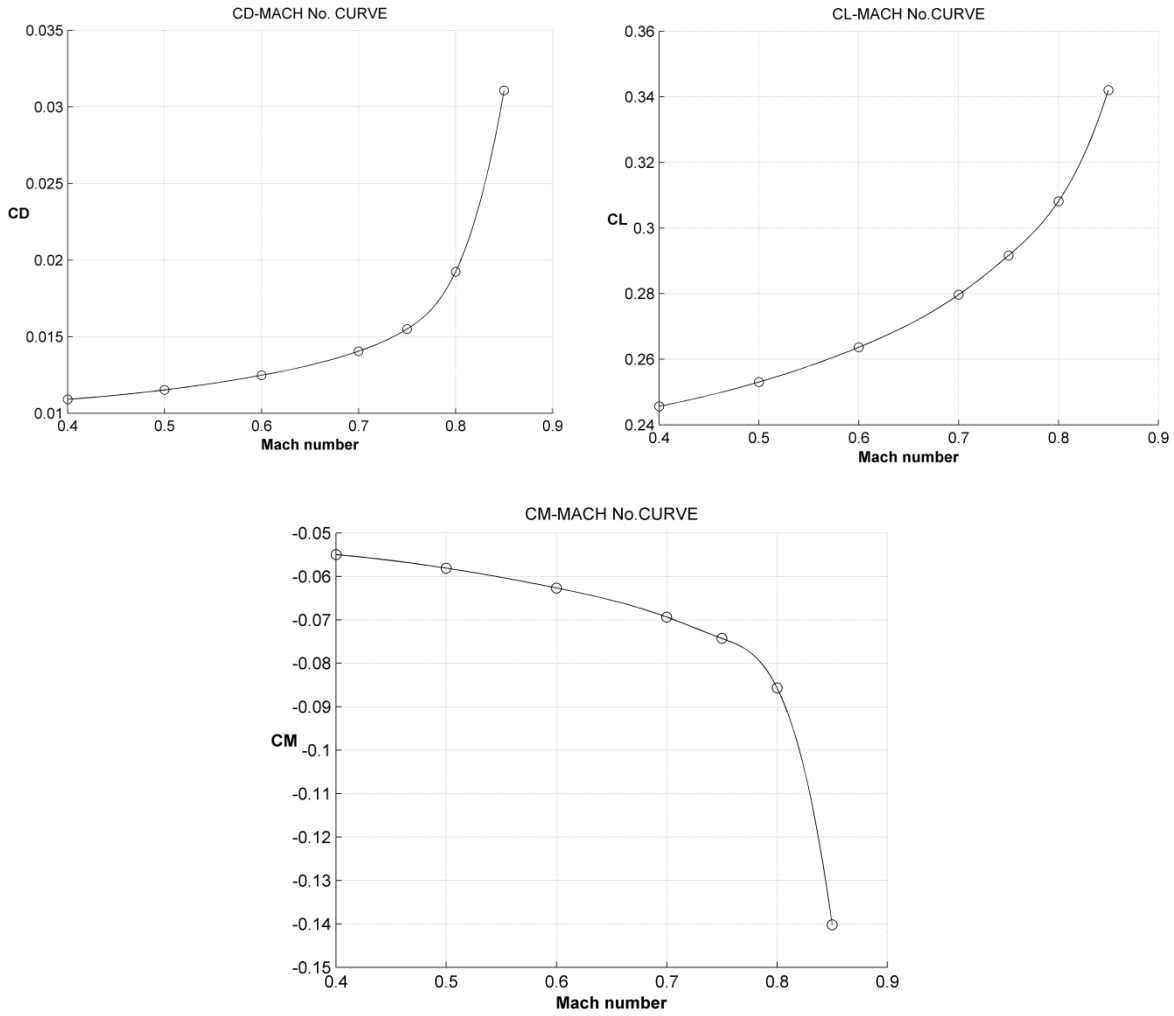

Figure 69: Effect of the Mach number on the aerodynamic coefficient in Eulerian flow for the clean wing.

Figure 70 represents an example of streamlines around the clean wing. The 3D-effect on the streamlines at the tip of the wing is visible. The 3D effect of the wing is also visible in Figure 71 where the pressure coefficients at different stations of the wing are displayed.

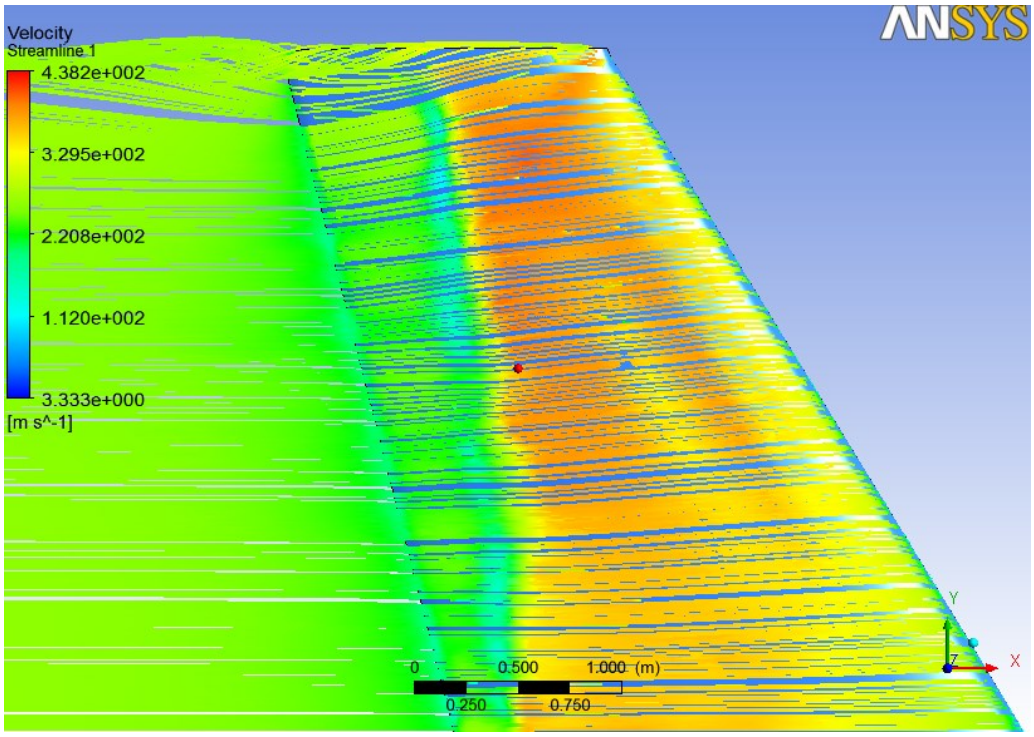

Figure 70: Streamlines in Eulerian flow for the clean wing (M_∞=0.85,H=1Kft,α=4°)

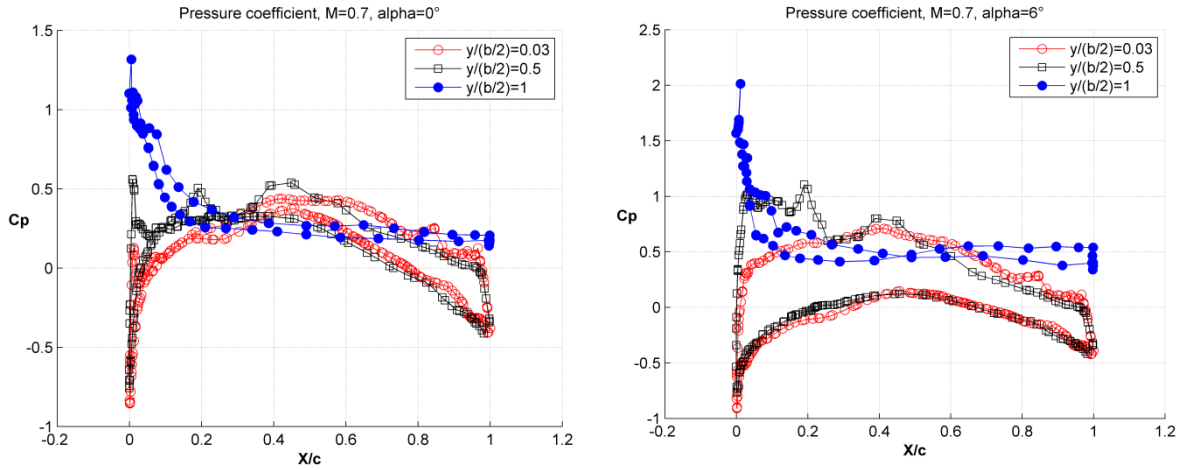

Figure 71: Effect of AOA on pressure coefficient at different wing station in Eulerian flow (M_∞=0.70)

Viscous calculations were performed at (M_∞=0.70; H=1Kft) and (M_∞=0.75; H=25Kft). The Reynolds number based on root chord (2.7m) was 34 millions and 18 millions respectively.

Figure 72 shows the effect of the AOA on the aerodynamic coefficient. At the same time, also the effect of the Reynolds number and the Mach number is showed. It is possible to see that increasing the Reynolds number, the stall is postponed. On the other hand, when the Mach number increases there is also a raise in $C_{L\alpha}$. The effect of the Reynolds number on the aerodynamic polar is visible also in Figure 73.

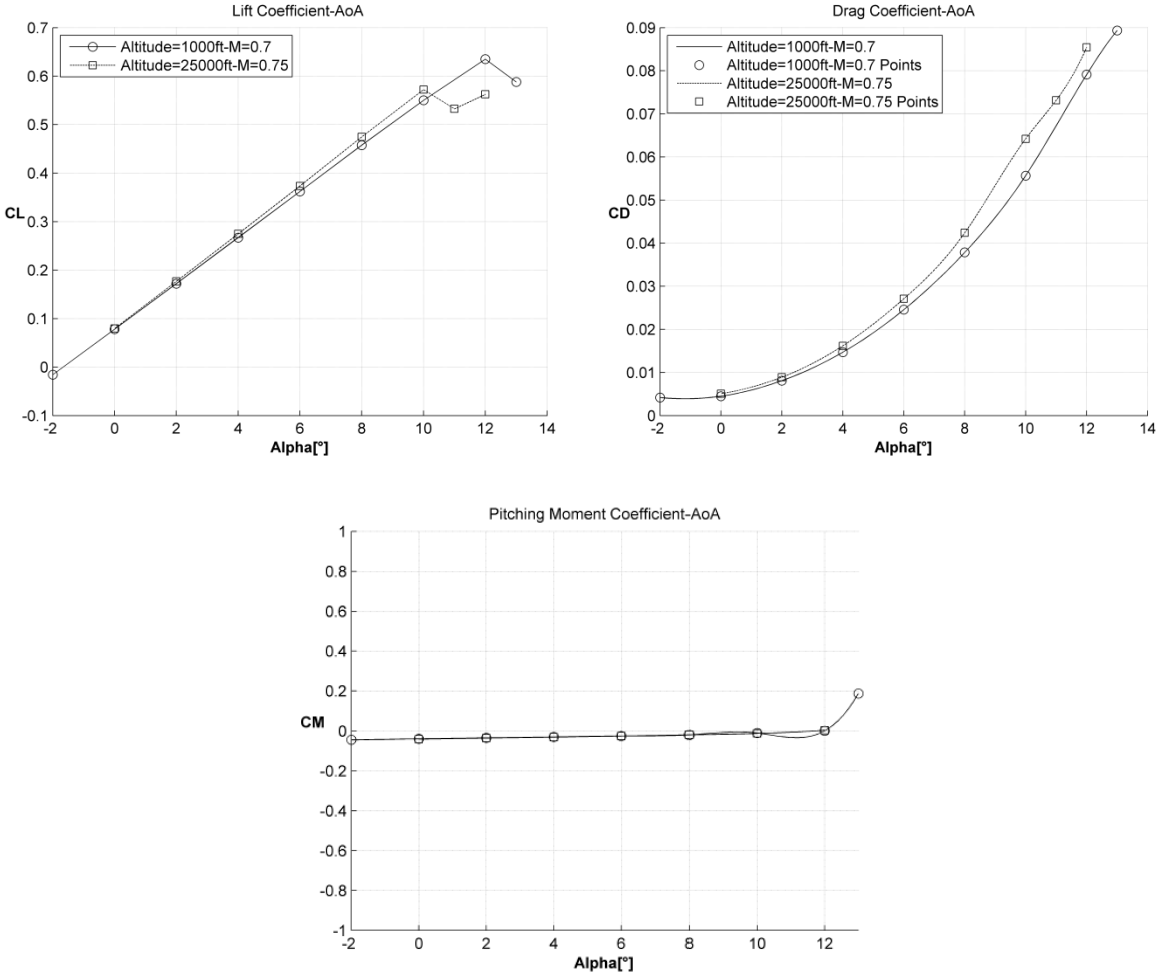

Figure 72: Effect of AOA, Mach number and Reynolds number on aerodynamic coefficient in transonic-viscous flow for the clean wing

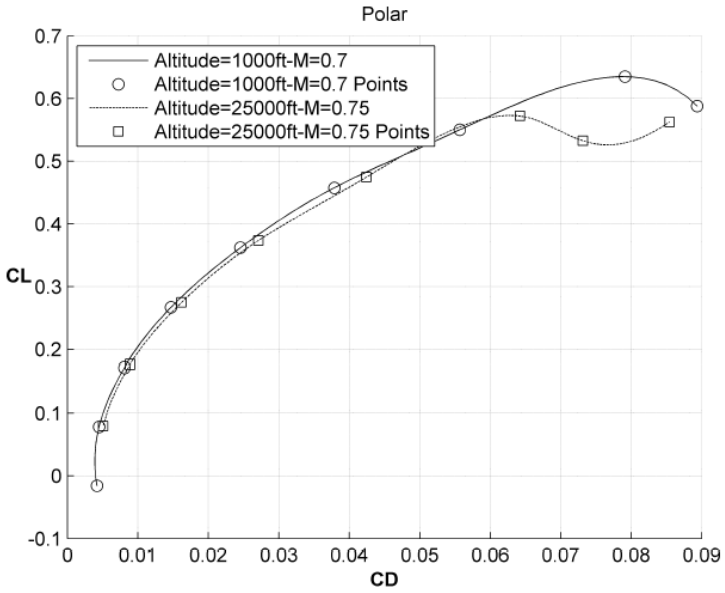

Figure 73: Effect of Mach number and Reynolds number on the aerodynamic polar in transonic-viscous flow

4.4 Final CFD results

4.4.1 Wing with pylons

The process followed for the creation of the hybrid viscous mesh was the same already described in the previous paragraph so we will not dwell in all the details.

In this case the critical element for the creation of the mesh were pylons and stores. In any case, thanks to the experience gained by the mesh of the clean wing, it was easily found a good set of parameters that provided a mesh with a good skewness. In this case the number of layers has been reduced to ten in order to obtain an acceptable value of the skewness.

Figure 74 shows the obtained hybrid mesh and a detail of the inflation near the wall.

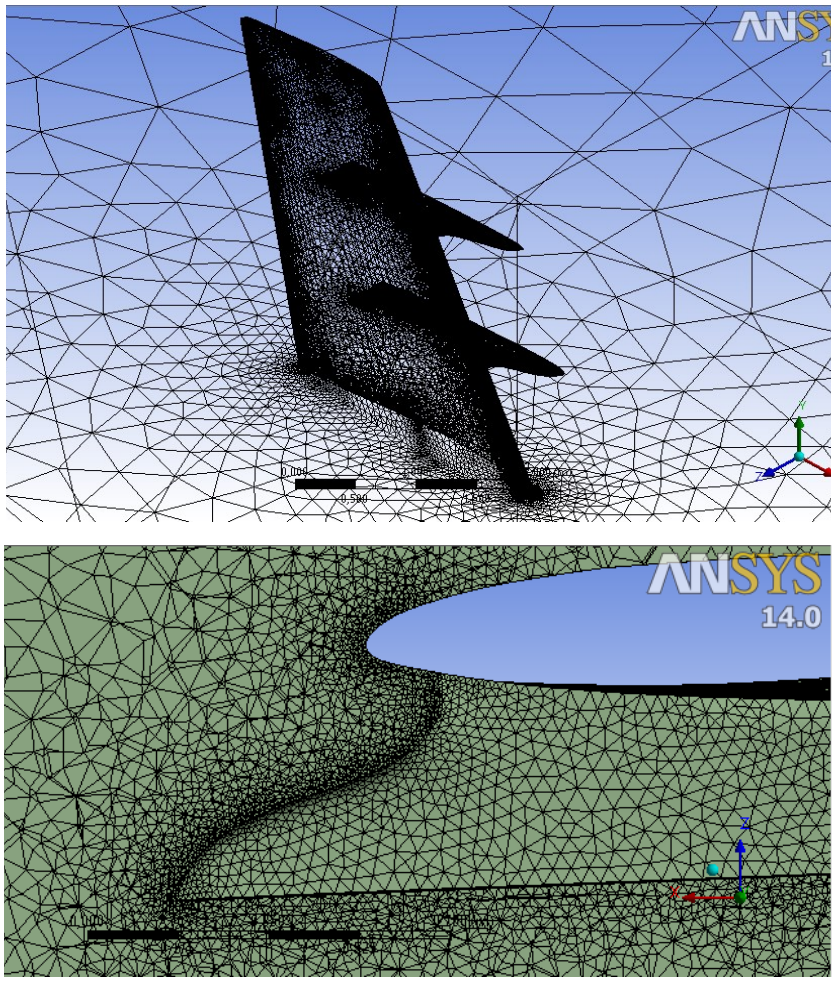

Figure 74: Hybrid grid for wing with pylon

In this case only viscous calculations were performed because Eulerian calculations were limited to preliminary cases. Calculations were performed at H=25Kft and M_∞=0.75 in order to compare aerodynamic performances of clean wing and wing with pylons.

Figure 75 shows the comparison of aerodynamic coefficients between the clean wing and the wing with pylons. It is possible to observe a minor decrease of the lift coefficient due to the presence of pylons and a slight increase in drag coefficient at low AOA that become negligible at high AOA because the drag component of the wing become predominant.

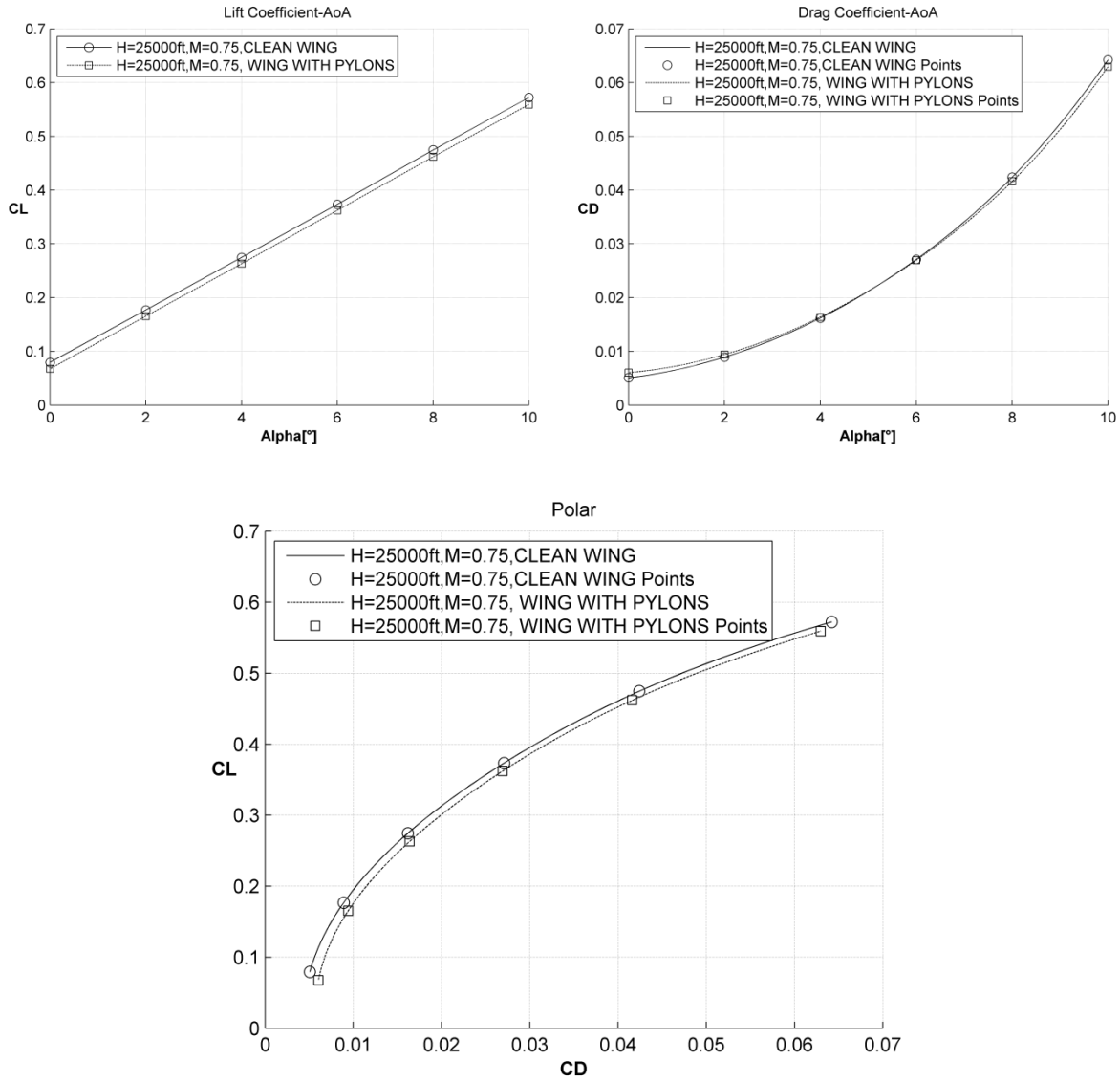

Figure 75: Aerodynamic performance of wing with pylons in transonic viscous flow (M_∞=0.75, H=25Kft)

4.4.2 Wing with stores

The creation of the hybrid viscous mesh was identical to grid created for the wing with pylons. In this case the problem was that the CAD geometry was really

complex. In fact, the presence of the stores, not permitted to reduce the maximum value of the skewness under 0.938 that was considered an acceptable value.

The inflation for this mesh was set to 10 layers and the number of elements was 2'800'000. The first layer thickness chosen is slightly lower compared to the previous cases, but a good y^+ is still assured. The final grid is showed in Figure 76.

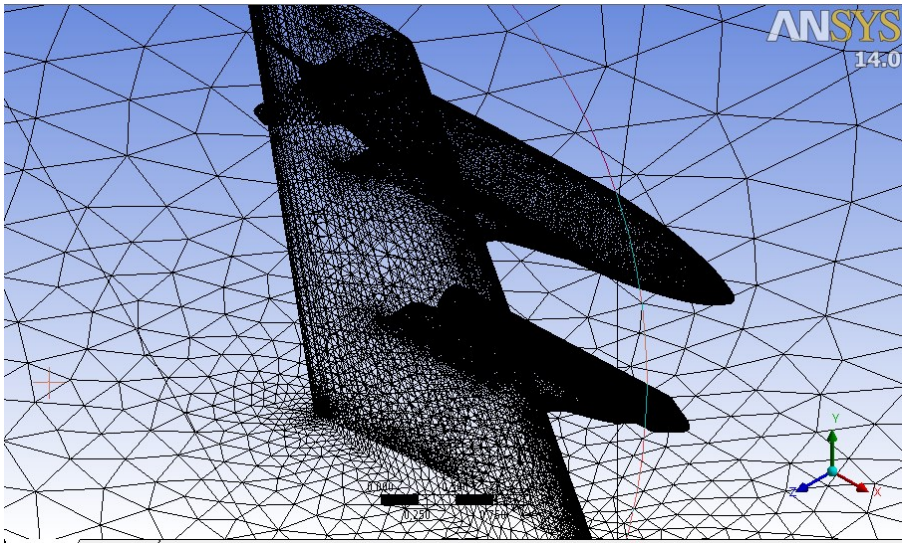

Figure 76: Hybrid grid for wing with stores

Also in this case only viscous calculations at H=25Kft and M=0.75 were performed. In this case we were interested in understanding the change in performance introduced by the stores in the aerodynamic flowfield.

Figure 77 shows the comparison of aerodynamic coefficients between the clean wing and the wing with pylons. It is possible to observe a decrease of the lift coefficient due to the presence of the stores; this reduction is practically constant with the AOA. There is also an increase of the drag coefficient, that is significant at low AOA and become negligible at high AOA because the contribution of the wing become predominant.

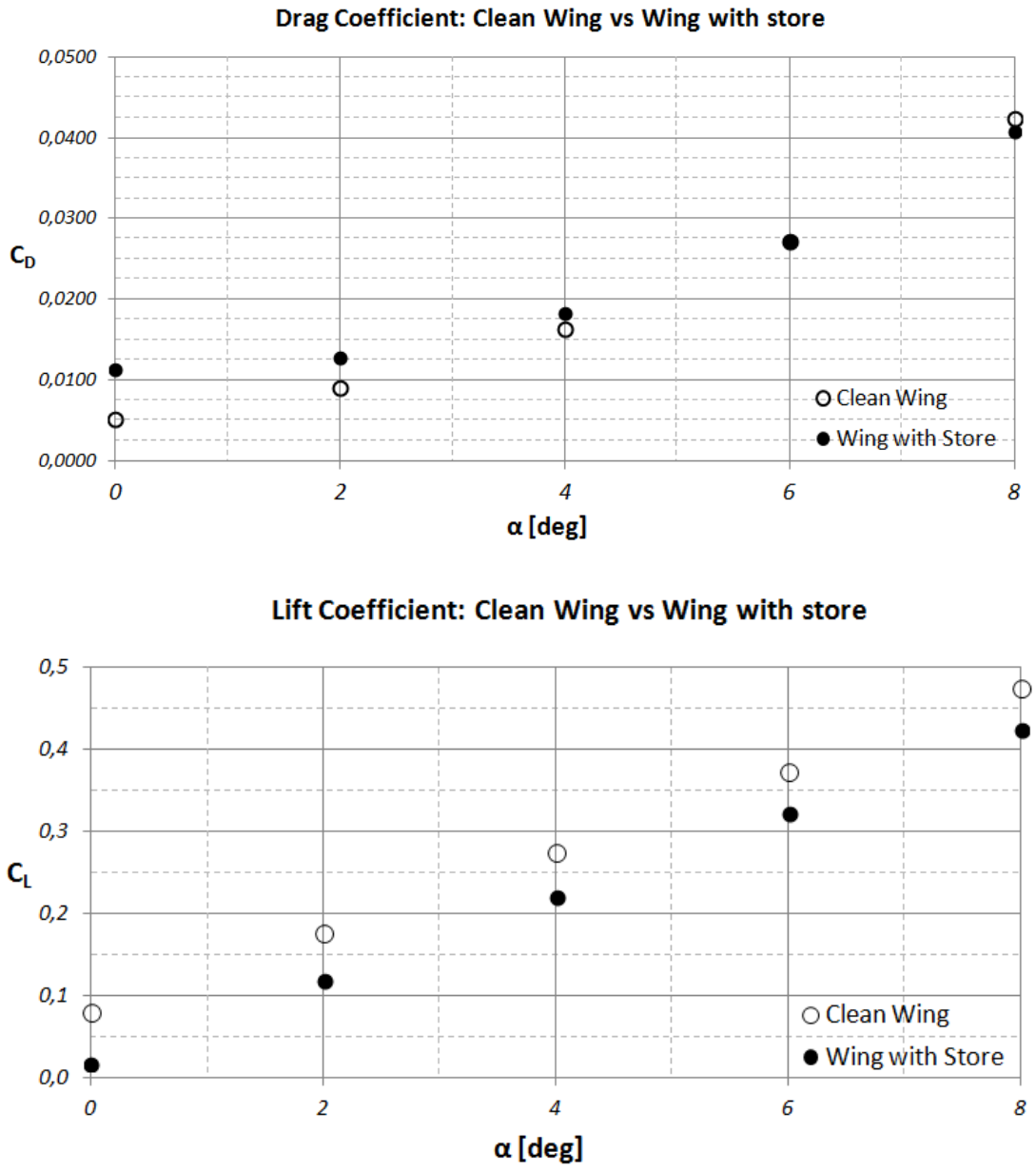

Figure 77: Comparison of aerodynamic coefficients for wing with stores and clean wing

The combination of the two effects is showed in the aerodynamic polar (Figure 78). It is possible to observe that, as expected, the configuration with the stores exhibits more drag at the same lift coefficient especially at low AOA.

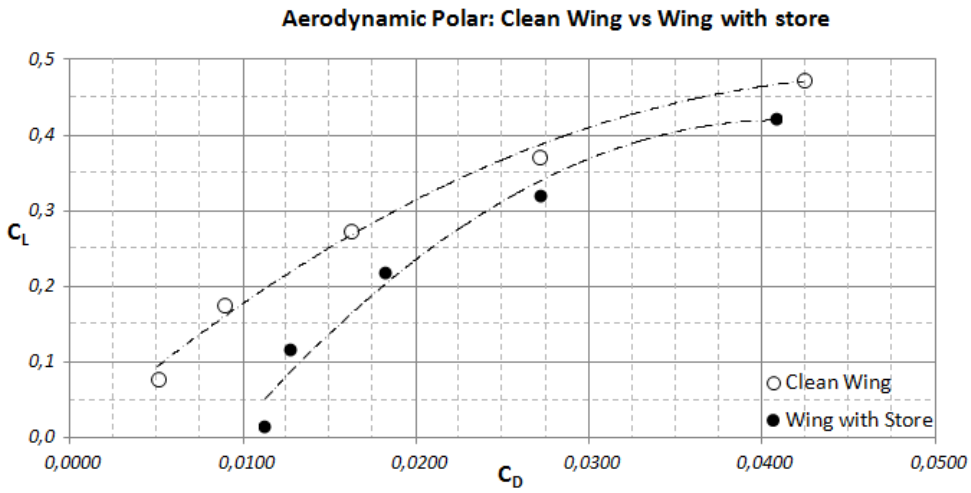

Figure 78: Comparison of aerodynamic polar for wing with stores and clean wing

Figure 79 shows the pressure difference between clean wing and wing with stores on the surface wing. It is possible to observe that the presence of the stores cause a significant decrease of the expansion on the upper surface that is noticeable in the pressure field. This reduction of the expansion cause also the reduction of the lift coefficient.

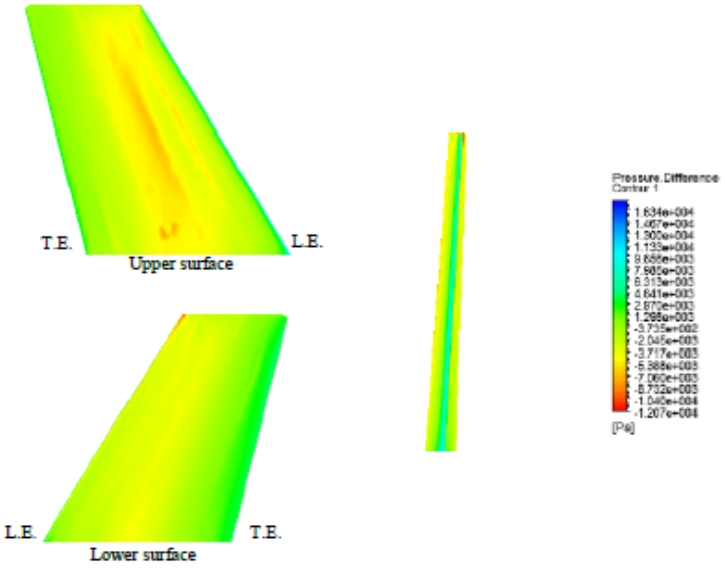

Figure 79: Pressure difference on wing surface between wing with stores and clean wing

Figure 80 shows the streamlines around the wing with stores. It is possible to observe that the stores cause a significant disturb in the flowfield, but there is not a significant flowfield separation after the stores.

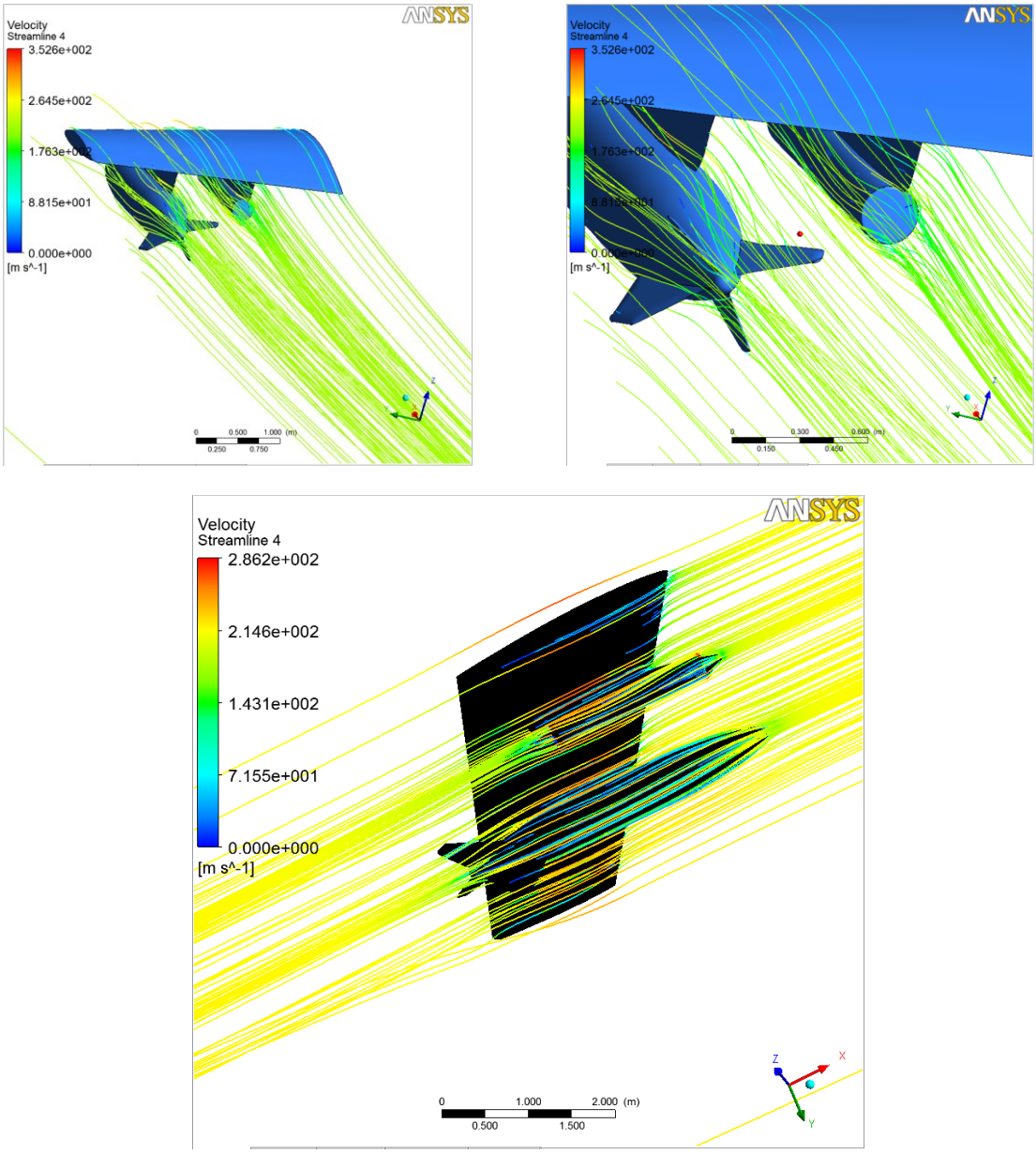

Figure 80: Streamlines for wing with stores.

4.5 Fluid Structure Interaction in a store separation problem

As explained in 3.3.2, when an aircraft release one of the external underwing stores, the wing will lose its equilibrium beginning to oscillate. Using the FSI was possible to determine the wing aeroelastic response following an event of store separation ([21]).

Since the aim of this work is to determine the validity of a methodology, we choose a simplified geometries. For this reason we created a geometry of a wing from the simple extrusion of a NACA 0012 airfoil. The half wingspan was imposed to 2.5 m. Regarding the store, we created a simple model of an air-to-ground missile with a weights of 650 lb. The final geometry is presented in Figure 81.

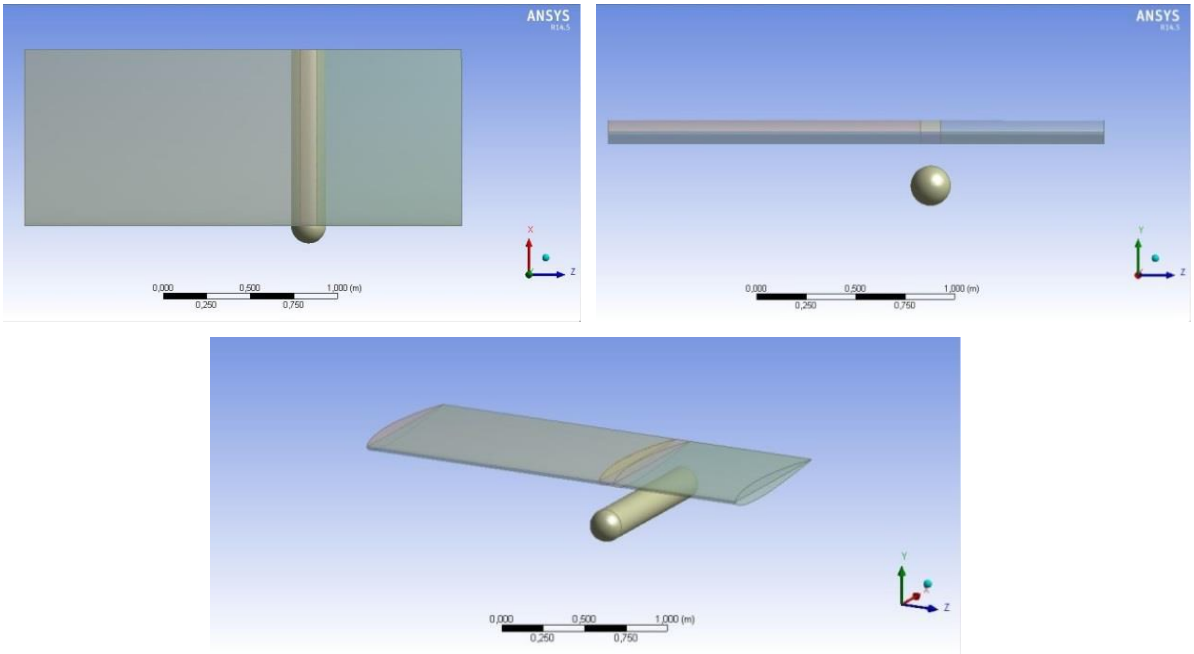

Figure 81: Final geometry for FSI analysis

After the creation of the geometry, the CFD and FEM meshes were generated. Once the grids were obtained, the modal and structural analyses of the wing were calculated. A linear elastic material has been selected for the wing (Al 6061-T6); the model has been constrained fixing all the nodes on the surface at the root of the airfoil. The first six modes of vibration and the relative frequencies were

calculated. The same structural model was used also for the determination of the effect of the loads acting on the wing. In particular, were considered two loads: the weight of the structure itself and the weight of the store, supposed to be applied only to the wing sections which in reality are in contact with the pylon. In order to emphasize elastic effects it was decided to consider a hundredfold heavier store than the reality.

Once derived the condition of elastic equilibrium in the case of loaded wing (Figure 82), it was possible to proceed with the unsteady case to determine the transient from the disappearance of the missile. To do this, a procedure very similar to the static case was followed.

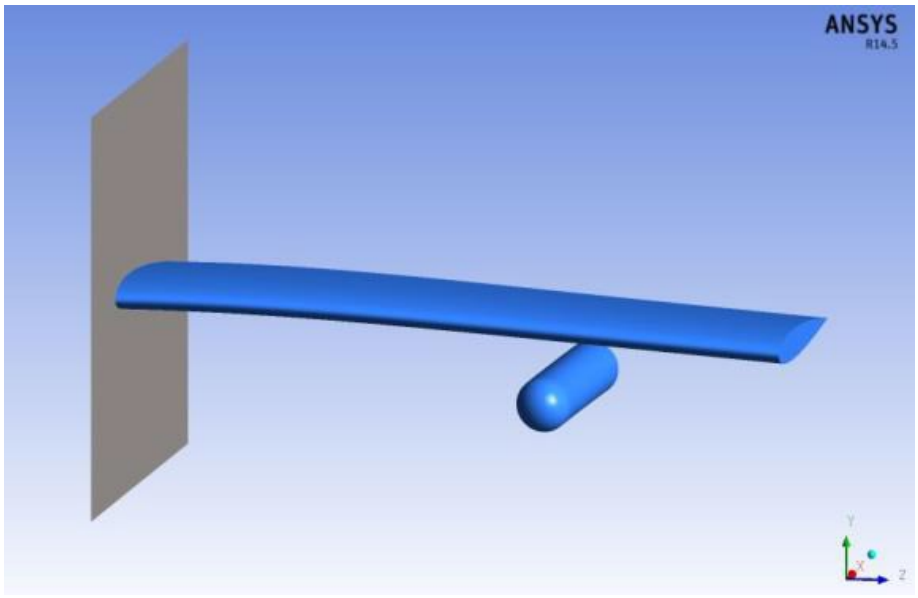

Figure 82: Final wing configuration after steady FSI calculation

For this task the unsteady RBF Morph FSI module was used, removing the load of the store and imposing as an initial condition the deformed shape obtained by the steady analysis

From the point of view of the flow field, then, it was decided to simulate the fall of the store making it disappear at the beginning of the calculation, transforming its surfaces from wall to interior inside the Boundary Conditions panel and changing the internal material from solid to fluid in the Cell Zone Conditions.

One of the main results of this work is that this approach involves a moderate overhead of only 9% with respect to the rigid unsteady calculation without the

mesh morpher, making the FSI approach affordable and attractive especially considering that data exchanging between CFD and FEA mesh at each time step is avoided.

Another important result is definitely provided by the monitors of the aerodynamic coefficient. In particular, we are interested in evaluating the evolution of the lift coefficient. It is easy to imagine, in fact, that the release of such a heavy body influences the wing structure especially in the vertical direction. Figure 83shows the trend of obtained (blue line): it can be seen as the diagram is characterized by large fluctuations, related to oscillation of the wing after the release of the store, that tend to fade after approximately 0.6 s. Furthermore it is evident that in the first instants occurs a significant increase of aerodynamic load, whose prediction is very important to evaluate the behavior of the wing from the structural point of view. This increase in load is even more significant when compared with the trend of in the case of rigid wing, previously calculated (green line).

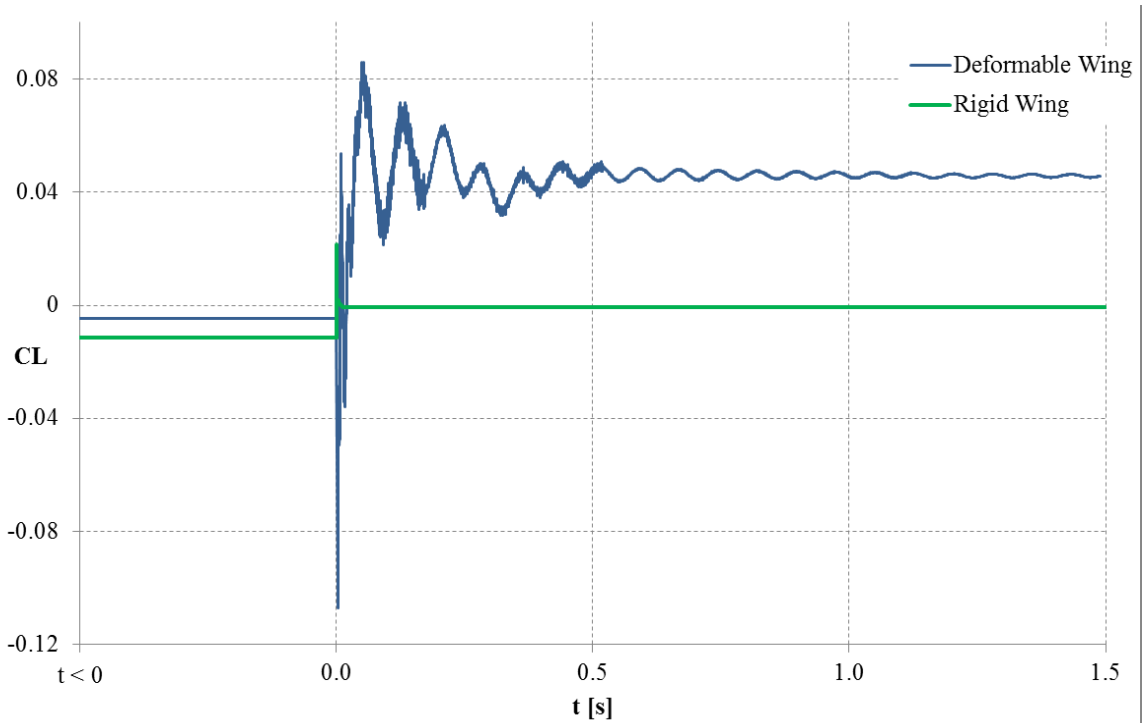

Figure 83: Lift Coefficient vs. time for deformable wing and rigid wing

Figure 84 shows instead a comparison between the trend of and the graph of the dimensionless wing tip deflection , in which is the tip deflection in presence of

the store, as a function of dimensionless time . It is clearly noted that the damped oscillatory is similar for both curves.

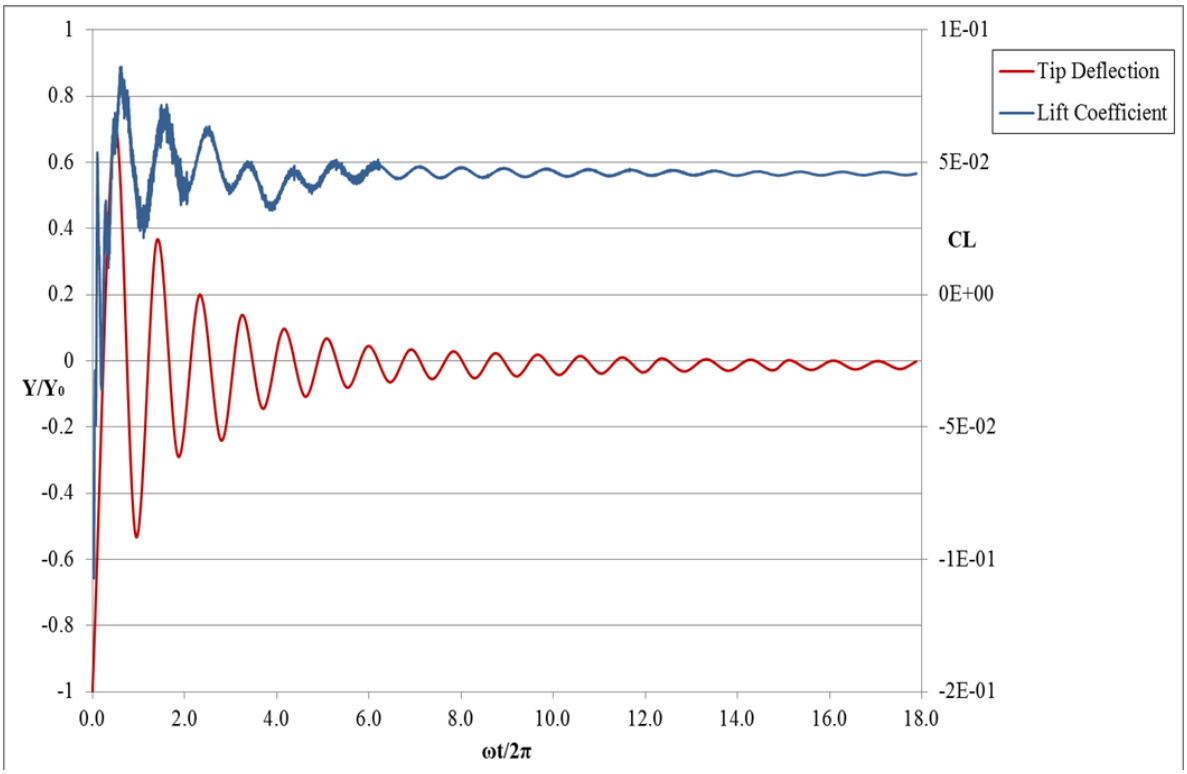

Figure 84: Comparison between Lift Coefficient and Tip Deflection vs. dimensionless time

Finally in Figure 85 are shown the contours of pressure on the surface of the wing at different instants of time.

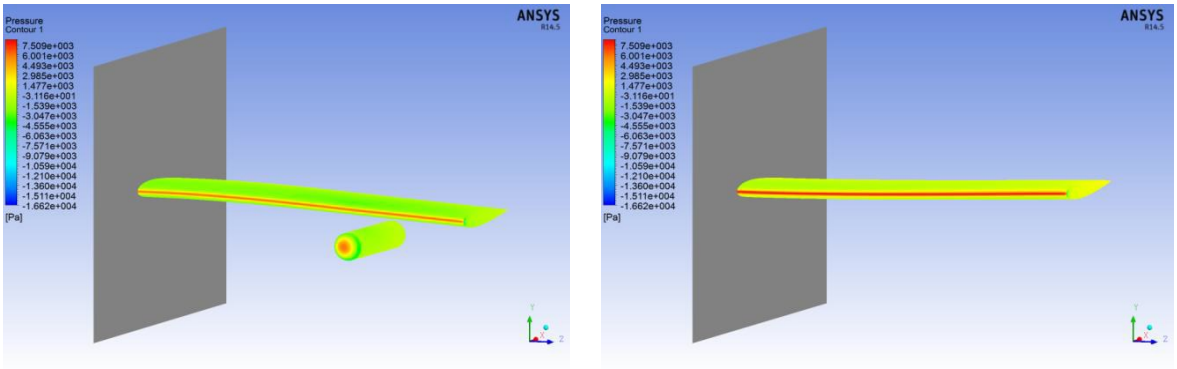

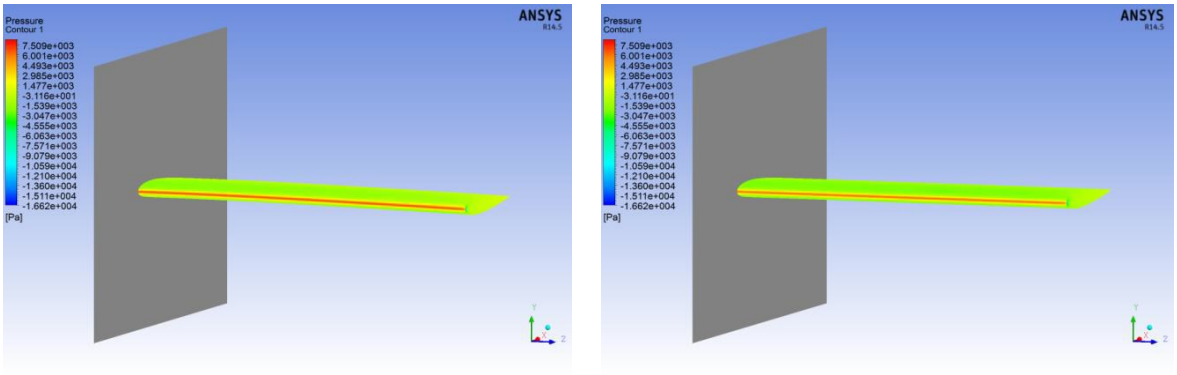

Figure 85: Pressure contours on the wing surface during the oscillation of the structure

CHAPTER 5

5 DoE Optimization Techniques

A typical question is what is design of experiments? To begin, experiments are used to study the performance of processes or systems. It is typically no longer cost effective for experiments to be performed in a trial-and-error manner; changing one factor at a time. A far more effective method is to apply a computer-enhanced, systematic statistical-based approach to experimentation, one that considers all factors simultaneously. That approach is called design of experiments (DoE).

When designing a set of experiments, it is important to find an optimal test point distribution in order to maximize efficiency and minimize costs.

In some cases, i.e. flutter or envelope expansion testing, the test organization deals with unique prototype. For this type of aircraft, limiting the total flight hours of testing is a mandatory requirement not only for the significant cost associated, but also for the consideration of minimizing the risk of failure/loss of the highly valuable asset; in the last decade, a fatal mishap to an F-22 prototype fully instrumented brought to almost one year of delay in the Raptor Development Program and, unfortunately, to the loss of the experimental crew. Cost wise is useful to highlight that the average cost of a 4th/5th generation fighter type aircraft could range between 50 K$ and 100 K$. Therefore, when testing is required in the entire flight envelope, it is essential to find out a way to distribute the test points efficiently in order to gather all the required data, but at the same time saving time and reducing the number of test points. This means that given some test constraints and key parameters to be evaluated, all efforts should be spent in order to optimize test points distribution, covering the entire envelope following the rules imposed by the objective functions, whose aim is populating

the areas where the test execution has a higher priority based on engineering requirements.

While the optimality criteria are dictated by the specific problems at hand, the optimization process itself is applicable to wide classes of problems. Many techniques can be found in the literature, although only few deal with the problem of spatial location. The same problem has been approached as a non-cooperative game in the paper [19]. In this thesis is presented a new approach based on the concept of potential and repulsive fields to optimize the design of a test matrix in an envelope expansion flight test activity. The optimization effort was focused on utilizing this new methodology to optimal distribute the number of test points preserving test coverage ([20]).

5.1 Classical Approach

Experimental design is a critically important tool in the engineering world for improving the product process. For example, some applications of experimental design in process development and engineering design include:

- improved process yields;
- reduced variability;
- reduced development time;
- reduced overall costs;
- evaluation and comparison of basic design configurations;
- selection of design parameters so that the product will work well under a wide variety of field conditions; robustness Formulation of new products.

The way to perform DOE is problem dependent. However, a common approach in flight testing is to use One Factor At Time (OFAT) technique to design test matrixes. In this way it is possible to vary one variable at time, generally Mach number or altitude, maintaining constant the others.

Classical methods used in this kind of test are the so called Economy Method, which consists on a choice of a subset of flight conditions in accordance with the build-up approach principle in dynamic pressure, and the Extensive Method, which basically attempts to cover the most part of the flight envelope, resulting very expensive and time consuming.

In Figure 86, a typical flight flutter test clearance envelope is showed.

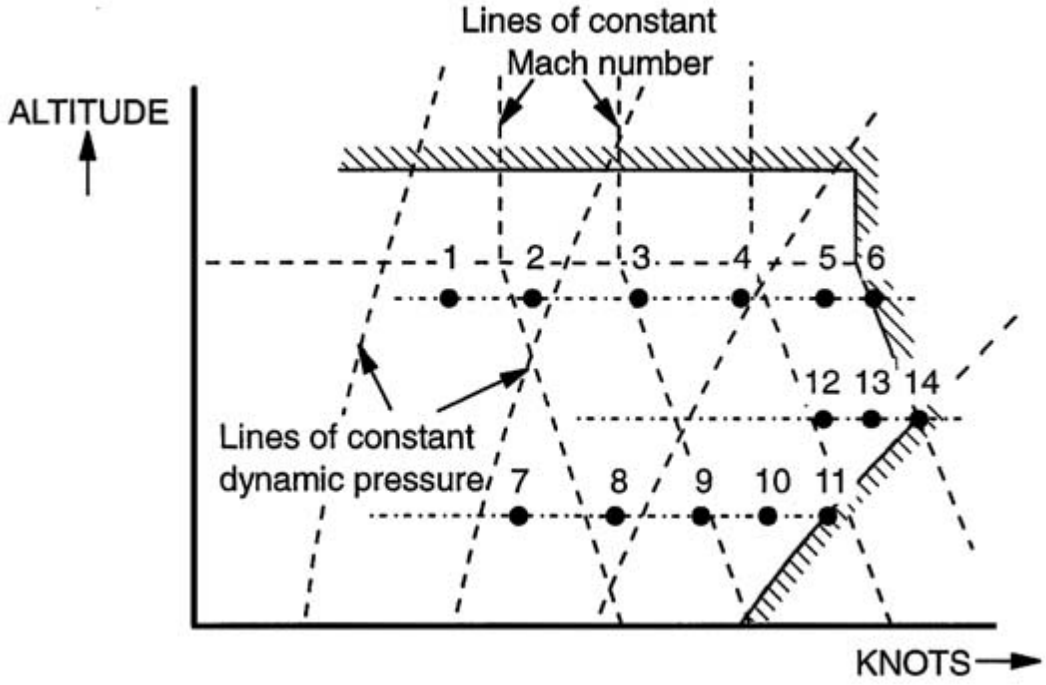

Figure 86: Typical flight flutter test clearance envelope

5.2 Innovative Approach

In this paragraph is presented a computational methodology for designing an experimental test matrix based on the concept of potential and repulsive fields.

When designing a set of experiments, it is important to find an optimal test points distribution in order to maximize efficiency and minimize costs. While the optimality criteria are dictated by the specific problems at hand, the optimization process itself is applicable to wide classes of problems. Many techniques can be found in the literature, although only few deal with the problem of spatial location ([11],[12],[13],[14],[15],[16]).

In general terms the proposed method aims at locating points in a two dimensional space according to soft constraints (minimization of potential) and hard constraints (boundaries of the permitted domain). The method makes use of the concept of potential of a point immersed in the field generated by other points ([17],[18]), producing mutual repulsive forces.

The idea has been tested against a practical case: the definition of a flight test matrix for the evaluation of the aero-elastic and environmental characteristics of an aircraft. The goal is to distribute flight test points in the flight envelope in such a way to satisfy the requirements of structural engineers, interested in an optimal distribution in terms of airspeed and Mach, and systems engineers, more interested in the altitude and airspeed distribution. The method provides means to combine all objectives in a single test campaign, through an optimization of the test points distribution, being the result of a compromise of all needs.

The key idea of the proposed method is to consider each point as the source of a different field for each parameter to be controlled and let the points move as a result of the mutual repulsive forces generated by the fields. Eventually the points will come to a rest when the equilibrium of forces is reached, which corresponds to the condition of minimum potential energy. The solution of such a problem cannot be found analytically, thus an iterative process is adopted, letting the points evolve until numerical convergence is reached (the sum of all forces is below a given threshold). The block diagram of the iterative algorithm is showed in Figure 87.

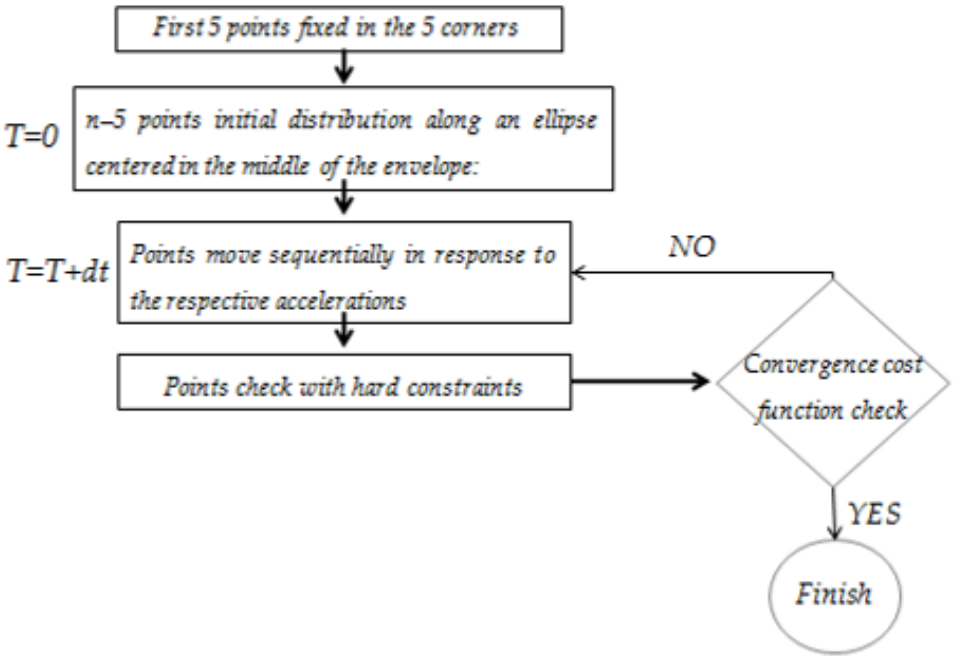

Figure 87: Iterative algorithm

Repulsive forces are similar to those acting between electrical charges having the same sign, except that the intensity decreases with the cubic power of the distance (to reduce the effect of distant points compared to near ones). The acceleration to which a point is subject only depends on its position in the field and the field intensity (same as electric or gravitational fields). To improve convergence, momentum is not preserved from step to step: in other terms the point is allowed to move according to the acceleration imposed by the fields, but at the next step it is assumed initially at rest and it further evolves only by virtue of the new acceleration produced by the new spatial configuration, regardless of the previous velocity. All points move sequentially and the time step for each point is chosen in such a way that the distance travelled (at the given step) exponentially decreases with elapsed time (to improve convergence) and the point is not allowed to exit the permitted domain (violate the hard constraints).

For the specific problem, three fields are introduced, associated with Mach number, pressure altitude and equivalent airspeed. The intensity of each field is a function of the value of the related parameter at the specific position of the point. Moreover Mach and pressure altitude fields act only along the corresponding direction (Mach and altitude respectively), while airspeed field acts radially in both directions.

Thus the airspeed field plays the dual role of distributing points in airspeed and spreading points over the envelope. Engineering considerations suggest that large Mach number and airspeed and low altitude are more critical for aero-elastic and environmental issues, thus test points are expected to be more concentrated in the bottom right region of the envelope. This is achieved by establishing field intensity laws reflecting this objective: Mach field intensity decreases with Mach number, altitude field intensity increases with altitude and airspeed field intensity decreases with airspeed. The relative importance of different parameters is attributed by properly scaling the intensities of the three fields.

5.2.1 The relocation problem

This method has been also extended to the additional task of dynamically relocating the remaining test points, after an initial subset has been performed and a need to change (either increase or reduce) the number of test points has arisen.

Suppose that a test matrix has been designed and a certain amount of test points has been performed according to a predefined execution order. Suppose also that initially unforeseen events (partial test results, budget reviews, changes of the trial objectives) require a modification of the amount of test points. The relocation problem of the remaining test points (which may be either more or less than the original plan) can be approached similarly to the initial task described in paragraph 5.2. The only difference is that the remaining points must be distributed with an additional hard constraint: the presence in the envelope of the test points already performed along with their respective fields. With this minor adjustment, the same algorithm can be used for the relocation problem.

5.2.2 The execution order problem

Once the test matrix is defined, a preliminary chronological order must be established of the test points. To this end several approaches can be followed depending on the particular application. In our example we considered two requirements: safety and efficiency. Given the hazardous nature of flutter (aero-elastic phenomenon) testing, safety is the first and paramount priority. Thus efficiency can be sought only when safety is assured. Assuming that a 20 KEAS (Knots Equivalent Air Speed) margin between test points is a cautious and safe approach to the envelope expansion task, test points are ordered with increasing airspeed; however, if more than a single point meet the 20 KEAS margin criterion, efficiency considerations suggest that points are ordered to best manage energy (either in ascending or descending order).

The two forms of energy attributed to a flight condition represented by a point in the envelope are potential and kinetic energy, leading to the following expression for the specific energy (energy per unit weight):

$$SE = H + \frac{1}{2}\frac{V^2}{g}$$

where H is the pressure altitude, V is the equivalent airspeed and g is the acceleration of gravity. Of course this is just a possible simple criterion to attribute an a priori execution order. Depending on the complexity of the problem, several additional constraints might apply and the actual execution order might need to be dynamically adjusted while in progress based on the results gathered from previous points.

However different choices of the execution order do not invalidate the effectiveness of the proposed method for identifying the location of the test points.

5.3 Algorithm

Let n be a fixed natural number (n > 5) that is the number of the prescribed flight tests. Each test point is defined by a pair (M_i;H_i), where i is an integer number, i ∈ [1;n], M_i and H_i are real numbers chosen in the following sets: M_i ∈ [M_L;M_U] and Hi ∈ [H_L;H_U], where the nonnegative constants $0 \le M_L < M_U$ and $0 \le H_L < H_U$ define the bounds of Mach number and altitude choices.

An additional hard constraint on the test points (M_i;H_i) is the condition that the equivalent airspeed is bounded: V_i ∈ [V_L;V_U] ($0 \le V_L < V_U$): the equivalent airspeed can be computed as a function of M_i and H_i under the assumption of International Standard Atmosphere.

(4) $$V_i(M_i, H_i) = aM_i(1 - bH_i)^C$$

with a, b, c positive real constants.

A graphical depiction of the domain (flight envelope) is shown in Figure 88 where [M_L;M_U] = [0;1] and [H_L;H_U] = [0;35000].

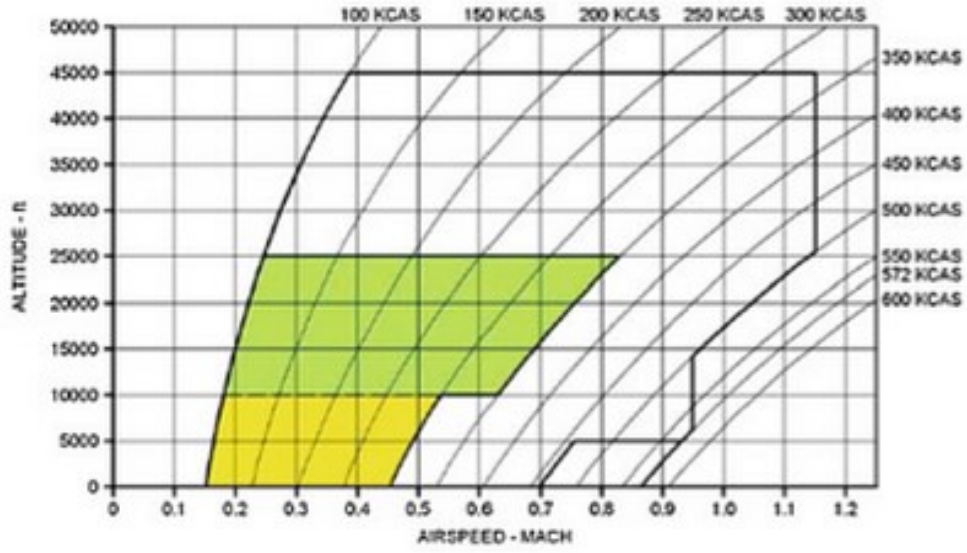

Figure 88: Flight envelope

Let the first five points stay fixed in the 5 corners of the flight envelope (hard constraint). The remaining n-5 points are free to travel within the permitted envelope; let the initial distribution of those points be according the following:

$$M_i = \frac{M_L + M_U}{2} + \frac{M_U - M_L}{4}\cos\left[\frac{2\pi(i-6)}{n-5}\right] \qquad i \in [6;n]$$

$$H_i = \frac{H_L + H_U}{2} + \frac{H_U - H_L}{4}\sin\left[\frac{2\pi(i-6)}{n-5}\right] \qquad i \in [6;n]$$

Let each test point be the source of three distinct fields, whose intensities are respectively:

$$m_{M_i} = W_M\left(1 + K_M\frac{M_i - M_L}{M_U - M_L}\right)$$

$$m_{H_i} = W_H\left(1 + K_H\frac{H_i - H_L}{H_U - H_L}\right)$$

$$m_{V_i} = W_V\left(1 + K_V\frac{V_i - V_L}{V_U - V_L}\right)$$

where $W_M;W_H;W_V$ are positive real numbers (defining relative weight of the three fields), while $K_M;K_H;K_V$ are real numbers (prescribing the desired distribution trend of the corresponding parameters). The first two fields act along a single dimension (the respective parameter), while the third field acts radially. Assuming repulsive forces proportional to the inverse of the cubic distance from the field source, the resulting accelerations (in the two directions: M and H) to which all points are subjected (except the 5 fixed points) are:

$$a_{M_i} = M_U\left\{\sum_{\substack{j=1,3\\ j\in[6,n]\\ j\neq 1}}\frac{m_{M_j}}{\left(\frac{M_i - M_j}{M_U}\right)^3}\right\} + \sum_{\substack{j\in[1,n]\\ j\neq 1}}\frac{m_{V_j}\left(\frac{M_i - M_j}{M_U}\right)}{\left[\left(\frac{M_i - M_j}{M_U}\right)^2 + \left(\frac{H_i - H_j}{H_U}\right)^2\right]^2}$$

$$a_{H_i} = H_U\left\{\sum_{\substack{j=1,3\\ j\in[6,n]\\ j\neq 1}}\frac{m_{H_j}}{\left(\frac{H_i - H_j}{H_U}\right)^3}\right\} + \sum_{\substack{j\in[1,n]\\ j\neq 1}}\frac{m_{V_j}\left(\frac{H_i - H_j}{H_U}\right)}{\left[\left(\frac{M_i - M_j}{M_U}\right)^2 + \left(\frac{H_i - H_j}{H_U}\right)^2\right]^2}$$

where the first fixed point (j=1) is at the bottom left corner of the envelope (M_L;H_L) and the third fixed point (j=3) is at the top right corner of the envelope (M_U;H_U). The points are then allowed to move sequentially in the envelope in response to the respective accelerations. At each iteration the time step is chosen such that displacements are progressively smaller and smaller (as the distribution converges toward the optimal solution) while the Mach and altitude hard constraints are not violated.

The displacements consequent to the accelerations acting during the time step are computed as:

$$dM_i = \frac{1}{2} a_{M_i} dt^2$$

$$dH_i = \frac{1}{2} a_{H_i} dt^2$$

thus ignoring any velocity gathered in the previous time steps, in order to facilitate convergence. Here

$$dt = \min\left\{ dt_{\min}; \sqrt{\frac{2dM_{\max}}{|a_{M_i}|}}; \sqrt{\frac{2dH_{\max}}{|a_{H_i}|}} \right\}$$

where $dt_{min} = 0.01/n$ and

$$dM_{\max} = \begin{cases} \min\left\{ \frac{M_U - M_i}{2}; \frac{M_U - M_L}{2} e^{-\frac{t}{10}} \right\} & if \quad a_{M_i} > 0 \\ \min\left\{ \frac{M_i - M_L}{2}; \frac{M_U - M_L}{2} e^{-\frac{t}{10}} \right\} & if \quad a_{M_i} \le 0 \end{cases}$$

$$dH_{\max} = \begin{cases} \min\left\{ \frac{H_U - H_i}{2}; \frac{H_U - H_L}{2} e^{-\frac{t}{10}} \right\} & if \quad a_{H_i} > 0 \\ \min\left\{ \frac{H_i - H_L}{2}; \frac{H_U - H_L}{2} e^{-\frac{t}{10}} \right\} & if \quad a_{H_i} \le 0 \end{cases}$$

The displacements thus computed do not guarantee adherence to the last hard constraint: airspeed within the two permitted boundaries. An additional check must be performed: if airspeed limits are exceeded with the computed time step and accelerations, then the new position is set at 90% of the airspeed limits (moving the point along the direction of the acceleration). Then acceleration is set

to zero, because points constrained on the border are assumed to be subjected to a reaction force (acceleration) equal and opposite to the force (acceleration) which tends to push them out of the envelope.

Define

$$dM_{V_{\max}} = 0.9\frac{V_U - V_i}{\left(\frac{dV}{dM}\right)_i + \left(\frac{dV}{dH}\right)_i\left(\frac{dH}{dM}\right)_i}$$

$$dM_{V_{\min}} = 0.9\frac{V_L - V_i}{\left(\frac{dV}{dM}\right)_i + \left(\frac{dV}{dH}\right)_i\left(\frac{dH}{dM}\right)_i}$$

where, differentiating equation (4),

$$\left(\frac{dV}{dM}\right)_i = a\left(1 - bH_i\right)^c$$

$$\left(\frac{dV}{dH}\right)_i = -abcM_i\left(1 - bH_i\right)^{c-1}$$

$$\left(\frac{dH}{dM}\right)_i = \frac{dH_i}{dM_i}$$

then

$$if \quad dM_i < dM_{V_{\min}} \; we \quad let \begin{cases} dM_i = dM_{V_{\max}} \\ dH_i = dM_{V_{\max}}\left(\frac{dH}{dM}\right)_i \\ a_{M_i} = a_{H_i} = 0 \end{cases}$$

and

$$if \quad dM_i < dM_{V_{\min}} \; we \quad let \begin{cases} dM_i = dM_{V_{\min}} \\ dH_i = dM_{V_{\min}}\left(\frac{dH}{dM}\right)_i \\ a_{M_i} = a_{H_i} = 0 \end{cases}$$

Finally the position is updated according to the calculated displacements, the field intensities are updated pursuant with the new configuration

$$M_i^{k+1} = M_i^k + dM_i$$
$$H_i^{k+1} = H_i^k + dH_i$$
$$t^{k+1} = t^k + dt$$

Weights m_{Mi} ;m_{Hi} ;m_{Vi} are also updated at each iteration and we assume that the EAS weight decreases with time: initially points must be quickly spread over the envelope and the weight is large, then the weight must decay with time to the desired final value. More precisely we let

$$m_{V_i}^{k+1} = W_V e^{-\frac{t^k}{10}} \left(1 + K_V \frac{V_i^k - V_L}{V_U - V_L} \right)$$

The process is reiterated until a convergence cost function decays below a predetermined threshold. The convergence cost function is a measure of the residual accelerations to which the test points are subject, thus the potential energy of the configuration:

$$J(M,H) = \sum_{i=1}^{n} \left[\left(\frac{a_{M_i}}{M_U} \right)^2 + \left(\frac{a_{H_i}}{H_U} \right)^2 \right]$$

with (M;H) = (M_1,...,M_n,H_1,...,H_n). Convergence is reached when J is less than a predefined value (dependent on the number of points).

5.4 Results

We present a test case with n = 30 planned flight tests. The parameter choice is specified in the following. The flight envelope bounds are

$[M_L, M_U] = [0.1,0.8]$;
$[H_L, H_U] = [0,3x10^4]$;

the weights are

$W_M = 1$; $K_M = 0.95$;
$W_H = 50$; $K_H = 100$;
$W_V = 500$; $K_V = 0.8$;

and the constants in formula (4) are

$a = 1116.46$; $b = 6.87x10^{-6}$; $c = 2.62$

Results for a thirty test points location problem are shown in Figure 89.

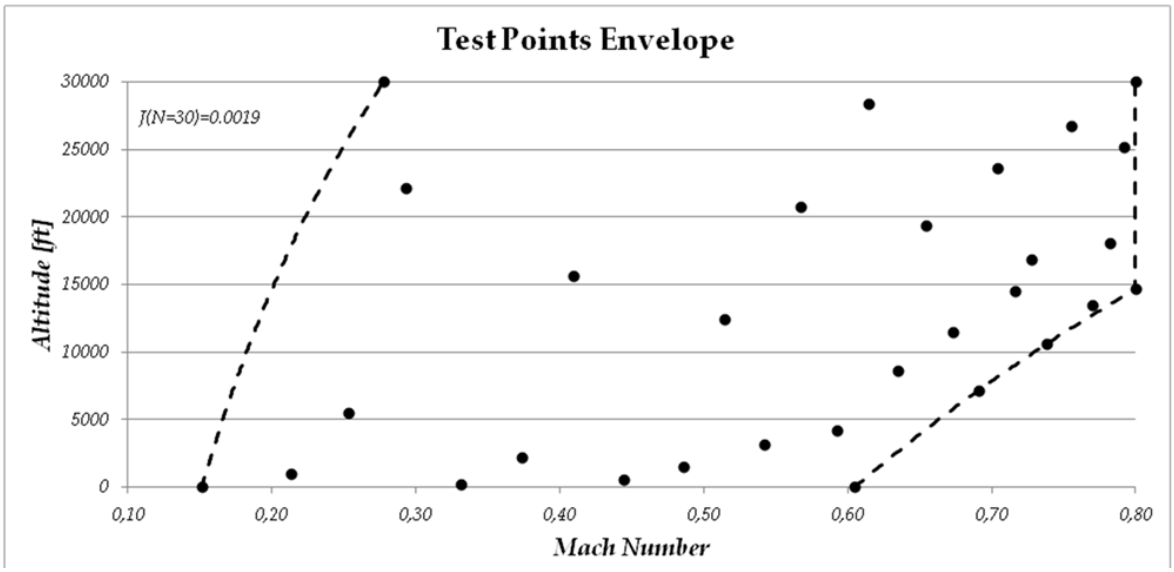

Figure 89: Test points distribution n = 30.

The test points are numbered in chronological order, in accordance with the criterion described previously. The blue points are assumed to be performed at a given stage of the test program, while the red ones are the remaining points which will be subject to a revision, due to a growth of the allocated budget and to a requirement for a more cautious approach to the most severe boundaries of the flight envelope.

As anticipated in subparagraph 5.2.1, consider that after 25 points have been performed, the test management decides to increase the number of remaining points (for an overall number of thirty five points). This problem could be defined as a sub-optimal distribution and can be solved with the same algorithm with the differences illustrated in 5.2.1.

Results for the relocation problem are presented in Figure 90, where black points represent the already performed test points, while white points (5 white points in Figure 90) are the outcome of the new optimization.

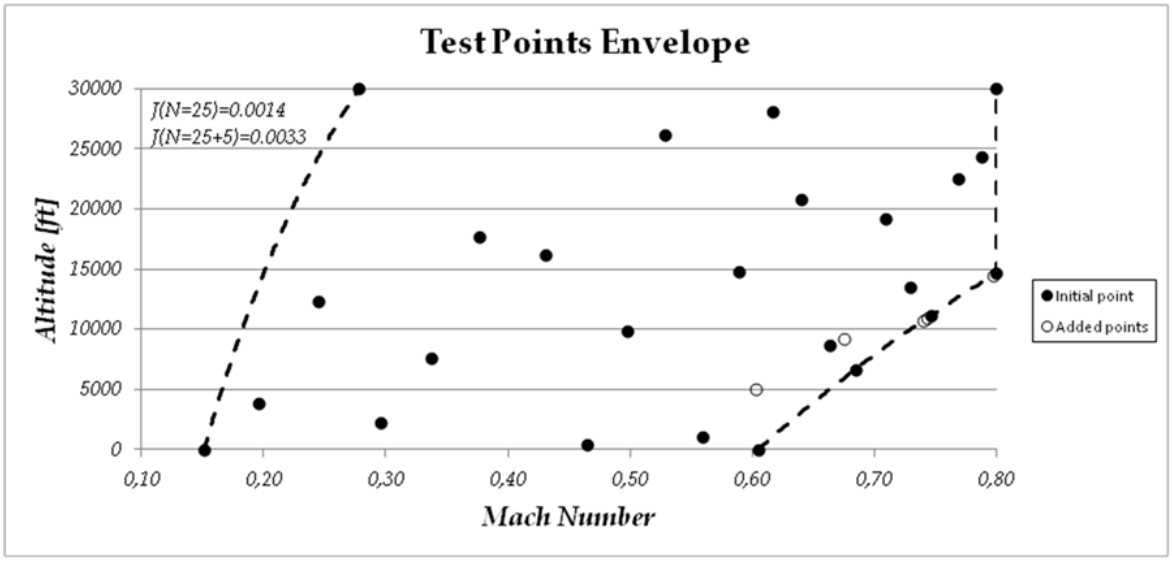

Figure 90: Test points relocation
(25 already performed test points – 5 added points).

5.5 Conclusions

An optimization method based on the concept of fields is proposed for the identification of a two-dimensional test matrix. The experimental test point distribution is optimized according to tuneable soft constraints and hard constraints. The method has been tested against a practical case: the simultaneous evaluation of aero-elastic and environmental characteristics of an aircraft. The method proved effective and computationally efficient: all the configurations tested came to a convergence in short time and the outcome was satisfactory. The method was extended to the additional problem of relocating part of the test points after the execution of an initial subset of experiments and following the decision of the test management to change the number of experiments. The results were satisfactory also for this additional task.

The proposed technique allows for an easy accomplishment of the task with minor modifications to the algorithm. A large degree of flexibility in the algorithm is allowed to tune the relative weights to attribute to the different requirements. The method proved effective and computationally efficient, exhibiting satisfactory results in both the test matrix design task and the dynamic relocation task.

CONCLUSIONS

Simulation has been an integral part of flight testing since 1950's. For decades, the science of simulation was essentially stagnant until the revolution in the computer industry began in the 1970's. Since then, simulation has become an increasingly important piece of the flight test picture.

Simulation is a key tool in flight testing. However, this is only as good as the models that comprise it. Verification and Validation of the models is an important step that must be done accomplished with rigor. Without proper validation, the flight test engineer may not be able to use the simulation to support flight testing.

As the use of simulation become more prevalent, there is a push to substantially reduce or eliminate the need to do any flight testing at all, and to just rely upon simulation to clear the flight envelope of the test aircraft. This is a dangerous trend that must be examined closely before proceeding too far down the path, but this represent the future of flight testing. The models that comprise the simulations are only as good as the data that has been used to develop them. There are still regions of the flight envelopes that require assumptions when building the models. The high AOA region is an example of this.

Wind tunnels technology is improving and so is Computational Fluid Dynamics methods. But these technologies are unable to fully predict what is going to happen when an airplane is flying at very high angles of attack. Besides modelling deficiencies, the value of having the pilot fly the aircraft and get the cues from inside the cockpit can never be duplicated no matter how complex the simulation.

However, using simulation can provide a lot of advantages to flight testing like cost savings or safety increasing. Because of cost savings can be elusive to document, and often hard to prove, this lack of firm proof will often lead an airplane development manager to question the cost of a high-fidelity simulation. But the prevention of an accident in flight test often justifies the costs of a simulation. Moreover, also the substantial delay in being able to sell the aircraft has a direct impact on profit. Simulation can not only permit to save money but also to give better value to it being able to test more complex systems.

By far the most significant benefit from using simulation to support flight testing is increased flight safety. Improving flight safety has always been the main object of simulation. Simulation allows the flight envelope to be investigated and understood prior to flight testing. Early use of simulation, even in the design stages can highlight safety concerns that can be designed out. Predictions of aircraft characteristics are gathered prior to testing and then used as a basis for comparison during actual testing.

Overall, increasing safety is one of the primary uses of flight test simulation. In the rush of getting the test program done, spending time on simulation often becomes a second priority. Yet the time and money invested are well spent if an accident or an incident can be avoided. The use of simulation to increase safety should be a part of every test program's safety reviews and safety planning.

In the future, simulation will continue to be a tool used to support flight testing and should not be used as a substitute for flight testing, but can help this in order to optimize the test activity, reduce costs and increase safety.

REFERENCES

[1] Simulation in Support of Flight Testing, RTO-AG-300 Vol.19, September 2000.

[2] Boeing Commercial Airplane Company, 777-200 Fact Sheet, February 1997.

[3] Arnold R.J.; Epstein C.S. (1986), Store Separation Flight Testing, AGARD-AG-300 Vol.5.

[4] Aircraft/Stores Compatibility, Integration and Separation Testing, STO-AG-300 Vol.29, September 2014.

[5] Aerodynamics of Store Integration and Separation, AGARD-CP-570, April 1995.

[6] Cenko A. (2010), Store Separation lessons learned during the last 30 years, 27th International Congress of the Aeronautical Sciences.

[7] Natale N., d'Argenio A., De Paolis P., de Nicola C. (2013), CFD in Support of Flight Testing for Aircraft/Stores Integration, International CAE Conference, Pacengo del Garda.

[8] Ping Fu (2008), Reverse Engineering, an Industrial Perspective, Edited by: Vinesh Raja, Kiran J. Fernandes, Springer.

[9] Chung-Lung Chen, Ching-Mao Hung (1992), Numerical study of juncture flows, AIAA Journal, Vol.30, No. 7.

[10] Sepe A.M. (2012), Integration of a underwing store on a fighter type aircraft: CAD drawing of a rockets launcher for CFD analysis, Tesi di Laurea in Ingegneria Aerospaziale.

[11] Basar T. and Olsder G.J. (1999), Dynamic noncooperative game theory, Reprint of the second (1995) edition. Classics in Applied Mathematics, 23. Society for Industrial and Applied Mathematics (SIAM), Philadelphia, PA.

[12] Drezner, Z. (1995) Facility Location: a Survey of Applications and Methods, Springer Verlag New York.

[13] Fudenberg, D. and Tirole, J. (1993) Game theory. The MIT Press, Cambridge, Massachusetts.

[14] Hansen, P., Peeters, D., Richard, D. and Thisse, J.-F. (1985) The minisum and minimax location problems revisited Operation Research vol. 33, pp. 1251-1265.

[15] Hotelling, H. (1929) Stability in Competition Economic Journal vol. 39, pp. 41-57.

[16] Mallozzi, L. (2007) Noncooperative facility location games, Operation Research Letters vol. 35, pp. 151-154.

[17] Mallozzi, L. (2013) An application of Optimization Theory to the study of equilibria for games: a survey, Central European Journal of Operations Research vol. 21, Issue 3, pp. 523-539.

[18] Monderer, D. and Shapley, L.S. (1996) Potential games, Games and Economic Behavior vol. 14, pp. 124-143.

[19] Mallozzi L., d'Argenio A., Di Francesco G, De Paolis P. (2015), Computational results for flight test points distribution in the flight envelope, Advances in Evolutionary and Deterministic Methods for Design, Optimization and Control in Engineering and Sciences, Edited by: D. Greiner, B. Galván, J. Periaux, N. Gauger, K. Giannakoglou, G. Winter, Computational Methods in Applied Sciences Series, Springer.

[20] d'Argenio A., de Nicola C, De Paolis P., Di Francesco G., Mallozzi L. (2014), Design of a Flight Test Matrix and Dynamic Relocation of Test Points, Journal of Algorithms and Optimization Vol.2, Issue 3, pp.52-60.

[21] Reina G.P., Della Sala A., Biancolini M.E., Groth C., Caridi D. (2014), Store Separation: Theoretical Investigation of Wing Aeroelastic Response, 4th Aircraft Structural Design Conference, Belfast (UK).

LIST OF FIGURES

LIST OF TABLES

SYMBOLS AND ACRONYMS

α	=	Angle of attack, deg
6-DOF	=	6 Degrees Of Freedom
AOA	=	Angle Of Attack
AOS	=	Angle Of Sideslip
ARL	=	Aircraft Rocket Launcher
C_D	=	3-D Drag coefficient
C_d	=	2-D Drag coefficient
C_L	=	3-D Lift coefficient
C_l	=	2-D Lift coefficient
C_M	=	3-D Moment coefficient
C_m	=	2-D Moment coefficient
C_P	=	Pressure coefficient
CAD	=	Computer Aided Design
CTS	=	Captive Trajectory System
CFD	=	Computational Fluid Dynamics
DoE		Design of Experiments
FCS	=	Flight Control System
FEM	=	Finite Element Method
FSI	=	Fluid Structure Interaction
GVT	=	Ground Vibration Testing
H	=	Altitude
HITL	=	Hardware-in-the-Loop
LCO	=	Limit Cycle Oscillations
M_∞	=	Asymptotic Mach number
M&S	=	Modeling and Simulation
MITL	=	Man-in-the-Loop
NURBS	=	Non Uniform Rational Basis-Splines
PC	=	Personal Computer
PIO	=	Pilot Involved Oscillations
RE	=	Reverse Engineering

$\mathbf{Re_D}$	=	Diameter based Reynolds number
RSV	=	Reparto Sperimentale Volo
$\mathbf{y_+}$	=	Dimensionless wall distance